University of Bath

UNIVERSITY OF
BATH

PHD

Electrical Capacitance Tomography For Real-Time Monitoring Of Process Pipelines

Al Hosani, Esra

Link to publication

ELECTRICAL CAPACITANCE TOMOGRAPHY FOR REAL-TIME MONITORING OF PROCESS PIPELINES

By

ESRA ALHOSANI

A thesis submitted for the degree of Doctor of Philosophy

University of Bath
Department of Electronic & Electrical Engineering

August 2016

To my grandmother, my mother, and myself

ABSTRACT

The process industry is concerned with the processing of crude resources into other products. Such crudes consist of multiphase components that introduce major challenges to the operators; hence the need for efficient instrumentations that address such challenges is highly desirable. One major need is an early deposit detection system that detects deposit before it builds-up in a pipeline or equipment to prevent any possible hazard. Another critical requirement is the need to continuously monitor the flow and deduce the flow rate of every individual phase in order to study and analyse the produced product. Hence, in order to ensure safety, increase profits, optimize production and ensure production quality, the multiphase flow must be adequately monitored and controlled. This thesis demonstrated the efficiency of novel ECT algorithms for early deposit detection and multiphase flow measurement in order to measure the flow rate of all separate phases. This thesis focuses on developments in ECT image reconstruction specifically the inverse solutions and is divided into three main studies where they all build up to complete each other. In the first study, ECT is used for the first time with a narrowband pass filter to focus on targeted locations in a pipe where dielectric contaminants are expected to deposit in order to enhance the resolution of the produced images. The experimental results showed that different deposit regimes and accumulated fine deposits could be detected with high resolution. The second study allowed a better understanding of how conductive material could be imaged using a conventional ECT device and how state of the art algorithms such as iterative total variation regularisation method and the level set method could enhance this application. Also, absolute ECT imaging is presented for the first time where the level set algorithm uses only one set of ECT measurement data. This study gives a novel solution for detecting conductive deposits as well as paves the way to use the new level set algorithm for multiphase flow measurement. In the third study, the novel narrowband level set algorithm was modified to image multiphase media in order to correctly determine the number, location and concentration of the present phases. The innovative absolute ECT imaging using level set method is tested with high contrast and low contrast multiphase data, which adds more to the challenge.

ACKNOWLEDGEMENT

List of Principal Symbols

M	Number of capacitance measurements
N	Number of electrodes
i	Source electrode
j	Receiving electrode
C	Capacitance value
Ω	Process domain
$\partial\Omega$	Boundary of the process domain
ε	Permittivity
ε_o	Free space permittivity
ϕ	Electrical potential distributions
Γ	Spatial location
V	Voltage
Q	Number of nodes in FEM mesh
P	Number of pixels
ΔC	Linearized capacitance measurement
$\Delta\varepsilon$	Linearized permittivity
λ	Linearized and normalized capacitance vector
g	Linearized and normalized permittivity vector
S	Sensitivity distribution matrix of λ with respect to g
σ	Singular values
α	Positive regularisation parameter
e	Error vector of the capacitance measurement
$\lVert . \rVert$	Euclidean norm
$\hat{g}$	Regularised solution
$\bar{g}$	Estimated solution
J	Objective functional
L	Regularisation matrix
I	Identity matrix
β	Relaxation factor
δ	Conductivity
ψ	Level set function
ξ	Step size parameter
B	Narrowband Jacobian matrix
K	Discretized form of the mapping of the level sets and the permittivity distribution
χ	Indicator function of a small narrowband of half width an FEM element

Table of Contents

LIST OF FIGURES

LIST OF TABLES

Chapter I

1   INTRODUCTION TO THE STUDY

Multiphase flows that appear in many industries (i.e. oil and gas, aerospace, chemicals, etc.) are considered complex and unpredictable, hence multiphase flow monitoring/measurement is considered a critical issue in the process industry. A multiphase medium or a flow may consist of two or more different phases in terms of their chemical/physical characteristics. Sometimes, a multiphase flow is associated with undesirable deposits or dirt (which are considered as another phase) that disturb the system and cause instrumentation faults. In order to ensure safety and increase profits, the multiphase flow must be adequately controlled and measured. In order to do so, analysis of the multiphase flow is required to determine some of the flow features/properties, such as the flow regime, number of phases, concentration of each phase, etc.

One of the major challenges related to multiphase flows in the process industry is the unattained deposit that might build-up in a pipeline or equipment and disturbs the flow causing serious problems downstream. Another multiphase flow challenge is the need to monitor different phases in a flow in order to either measure the flow rate of all separate phases or one particular phase. This study focuses on pipeline problems related to multiphase flow such as pipeline/equipment deposit monitoring and multiphase flow monitoring/measurement. The motivation, aim and objectives of the study are stated in this chapter.

1.1   MOTIVATION OF THE STUDY

Currently, multiphase flows are analysed by means of Multi-Phase Flow Meters (MPFMs) to get the flow rate of each phase, however, multiphase flow measurement using MPFMs is considered a challenging topic because multiple variables related to the fluid properties play a role in the analysis, hence, one limitation of MPFMs used today is the higher measurement uncertainties compared to single-phase metering systems. This is because of the fact that they measure more complex flows than what is measured by single-phase measurement systems. Therefore, continuous calibration and verification is always necessary for such MPFMs. Furthermore, MPFMs usually do not accommodate for contaminations in the flow, which will further affect the accuracy of the meter, and hence they are not designed to measure the

flow rate of contaminants.

In light of the limitations of the current MPFMs available in the marker, process tomography techniques have emerged to offer alternative solutions for multiphase flow measurement and deposit detection, however they are still in the stage of research. The idea of this study comes from the fact that a subsurface image of the pipe's cross section will surely help analysing the flow in terms of the flow phases and deposits. This will help to monitor and possibly automate the process for multiphase flow analysis/measurement and deposit detection, allowing quality assurance, single well surveillance/monitoring/testing and production optimization, thus increasing productivity, efficiency and safety. There are various techniques available for process tomography for imaging the subsurface properties of materials. A comprehensive review of the different process tomography techniques was conducted by [11]. For a particular application, some techniques can be useful yet others may not be.

Besides being non-intrusive and non-invasive technique, ECT technique offers the combined advantages of being fast, compact, safe, easy to interpret and cost effective. Thus, ECT is considered in this study to image the internal cross section of pipelines. The other motivation of using ECT technology comes from the fact that different constituents of a flow have different permittivity. Hence, by knowing the capacitance of each of these constituents, a proper analysis of the permittivity distribution would lead to a good estimation of their concentration and can be used to reconstruct an image of the process.

1.2   THE AIM OF THE STUDY

Despite its appealing advantages, ECT has the prominent drawback of offering low-resolution images since the ECT system is limited to few measurements per one measurement cycle, making the image reconstruction problem ill-posed and underdetermined. This *soft field* nature of the ECT system makes the implementation of ECT system a challenge. In ECT, various image reconstruction techniques have been implemented, in which some of them are better suited for one application than others.

The aim of this study is to make use of the advantages offered by ECT systems and overcome their challenges to construct high-resolution images of multiphase media. Areas of research in ECT can be classified as sensor design, hardware electronics, and image reconstruction. This thesis focuses on the image reconstruction aspect, in particular the inverse problem of a typical ECT problem and attempts to adapt conventional ECT system to:

1. **High resolution early deposit detection:** due to the limited measurements per one measurement cycle of the ECT system, the produced images are usually low in resolution making it hard to detect small amount of deposits in a medium.
2. **Monitor conductive deposits:** deposits can be conductive such as metal for which it is not clear how ECT works in such case. Metal detection using ECT is not really addressed in the literature despite the industry need for it.
3. **Low contrast multiphase imaging and measurement:** distinguishing different phases using ECT is considered a challenge since the produced images using the traditional ECT reconstruction techniques usually give enough information about the existence and location of different enclosures without distinguishing the different phases in a medium.
4. **High contrast multiphase imaging and measurement:** distinguishing different phases using ECT becomes even more challenging when a high contrast phase is present in the medium since it will dominate the domain making it hard to detect the other phases.

1.3   OBJECTIVES

The aim of the study is to be accomplished through the realization of the following objectives:

1. To review different image reconstruction techniques for ECT in order to understand the problem and the possible solutions, also to arrive at the best technique to adopt and modify.
2. To implement a high resolution ECT algorithm for early monitoring of deposits in piplines.
3. To adopt conventional ECT systems for imaging possible conductive deposits such as metal.
4. To implement a low contrast multiphase imaging algorithm to distinguish all phases in a medium.
5. To implement a high contrast multiphase imaging algorithm to distinguish all phases in a medium in the presence of a dominating phase.
6. To extract concentration information about each phase in a multiphase medium.

1.4   THESIS STRUCTURE

This study is divided into nine chapters in which Chapter 2 gives a brief introduction to the critical issues related to multiphase flow measurement and deposit detection, in order to justify the motivation and the importance of this study. Chapter 3 presents an overview of the ECT system and its potential for online process monitoring. Chapter 4 depicts the formulation of the forward problem, the linearization of the ECT forward model and the normalization of the ECT data. Chapter 5 gives a review of different image reconstruction methods for solving the inverse problem. Chapter 6 presents some novel experimental results achieved in order to investigate the capabilities of ECT for early detection of deposits in high resolution. Chapter 7 shows for the first time how ECT can be adopted for metal detection. Chapter 8 presents an innovative method for low and high contrast multiphase imaging and measurement. Finally, Chapter 9 states some limitations and challenges of the study and offers some future suggestions to take this study further to the next level of online applications.

Chapter II

2 MULTIPHASE FLOW MONITORING AND MEASUREMENT

Multiphase flow is a general term describes multiple components in a flowing stream generally appears in pipelines or vessels. In a multiphase flow, all components must be physically distinct, immiscible and have phase boundaries. In the oil and gas industry, such components are typically oil, water, gas and solid contaminants, however oil and water are sometimes considered as one phase, namely liquid. For more detailed description of multiphase flows refer to [10, 96, 112, 126, 128, 129, 132, 133].

The objective of this chapter is to provide a background to the work presented in this thesis in which novel image reconstruction techniques for ECT are developed to investigate multiphase media. The background of the work generates from the process industry especially the oil and gas. In an attempt to address two of the major issues faced in oil and gas operations, this chapter starts with a description of the two major scenarios that will be addressed in this thesis, namely deposit detection and multiphase flow measurement. Also, the current state of the art technologies in deposit detection and multiphase flow measurement are described along with their advantages and disadvantages.

2.1 DEPOSIT DETECTION

Solid deposit in oil/gas pipelines is a worldwide problem facing the process industry affecting all phases of production, transmission and distribution, causing problems to the pipeline operations up to the customer delivery point. Therefore, monitoring the propagation and deposition of such contaminants at different points of the pipeline network or at a critical equipment will help in taking more adequate preventive actions. Different forms of deposits continue to be present in the pipelines of many modern process industries. The type of contaminants depends on the pipeline material, the composition of the flow and the extraction process.

Today, in the oil and gas industry in particular, operators use three techniques to avoid blockage caused by deposits depending on their location and their physical properties, 1-chemical injection in the pipeline flow, which is costly and not very effective, 2- periodic pigging of the pipeline, which disturbs the production and/or 3- separation techniques (e.g., filters and cyclones), which disturb the flow. Examples of pipeline deposits include:

- **Hydrates:** Under high pressure and low temperature conditions in gas or oil wells, free water and natural gas combine to form ice-like solids called natural gas hydrates (Figure 2.1). Currently, hydrate inhibitors such as methanol and glycol are used as hydrate inhibitors to prevent the formation of hydrates.

- **Mineral Scales:** The accumulation of inorganic chemical deposits that coat the interior of pipelines and other production facilities such as casing, perforation valves and pumps (Figure 2.2). Mixing seawater and produced water or mixing water from multiple wells is the primary cause of mineral scale. Basically, water is the primary cause of scale formation right from the reservoir up to the delivery point. As mineral scale is difficult to remove and requires strong acids, prevention is usually preferred over inhibitors treatment. [1]

- **Waxes:** Many types of crude contain dissolved wax molecules, and at sufficiently low production temperatures, they can precipitate and deposit forming wax particles. The formation of wax can build up in pipelines and critical equipments causing restriction to the flow and creating bigger problems (Figure 2.3) [2-3]. Sometimes, heat-tracing technique is used to keep the temperature adequately high in order to prevent the formation of wax.

- **Asphaltenes:** Present in most petroleum materials. They are dark solids that start forming depending on the operating temperature, pressure and multiphase composition (Figure 2.4). Unlike wax and hydrates, asphaltenes do not melt with heat.

- **Sand:** It can be either loose sand or takes the form of sandstones. Sand is very likely to flow out of wells with the crude oil or gas.

- **Black powder:** A general term for contaminants in gas pipelines; it comprises of numerous forms of iron sulfide, iron oxide and/or iron carbonate. Sometimes these main components are mixed with other contaminants in the gas pipeline such as rouge, asphaltenes, sand, liquid hydrocarbons, metal debris and/or salt. The combinations of these contaminants appear in black dry powder, liquid or sludge suspension, depending on the pipeline condition; however the term "powder" is general (Figure 2.5). Though up to this date the source of black powder is considered to be vague, several studies have considered iron oxides and iron sulfides to be formed by either chemical or microbial processes inside the gas pipeline, mill scale, flash rust from hydro-test water corrosion or carryover from gas gathering systems. Black powder is reported to shatter inside the pipelines into very fine particles (about

one micron or less), making it easier to transport inside the pipelines and harder to filter out, causing problems not only to the pipeline operations but also to the customer equipments. Sometimes, such sub-micron sized particles accumulate forming larger particles. [4-9].
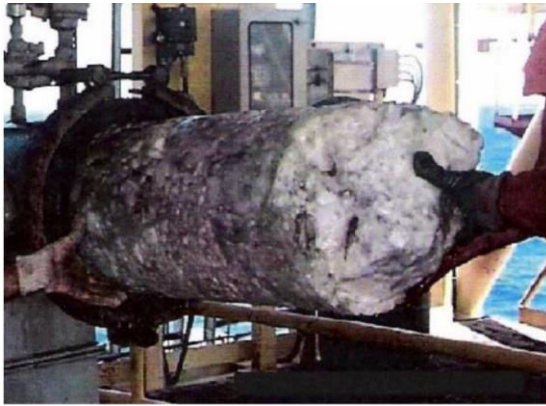
Figure 2.1. Hydrate formation in a gas pipeline [142].   Figure 2.2. Mineral scale in a pipeline [127].

Figure 2.3. Wax formation in an oil pipeline [143].

Figure 2.4. Asphaltenes formation in pipelines.   Figure 2.5. Black powder in a 508 mm pipeline [95].

2.1.1   Problems Caused by Pipeline Contaminants

Contaminants affect all stages of production, from the producing well up to the costumer delivery point. Examples of problems caused by pipeline contaminants include:

- **Fouling of filters,** which can shorten the filter life and increase the cost for maintenance and cartridges replacement (Figure 2.6).
- **Obstructing the orifice meters,** which causes inaccurate measurements of the flow rate. This can affect downstream processes and lead to revenue losses (Figure 2.7).
- **Fire hazard:** In some cases, black powder can be made up of primarily pyrrhotite ($Fe_{1-x}S$ (x = 0 to 0.2)). This material exhibits pyrophoric properties that can burn when dried out, making the process of disposing filter cartridges and bulk solids dangerous (Figure 2.8).
- **Fouling of instruments and valves,** which can cause poor measurements and adds to the cleaning and replacement costs (Figure 2.9).
- **Failure of the pipeline:** Severe and unattained corrosion caused by fast flowing contaminants such as black powder or sand can cause pipeline failure (Figure 2.10.a).
- **Wear of instruments:** Fast flowing contaminants can erode instruments. Once a component is eroded there is no treatment other than replacing it (Figure 2.10.b).
- **Fouling of compressors,** which requires expensive maintenance and replacement parts (Figure 2.11).
- **Increasing the interior pipe wall surface roughness,** which creates a flow restriction causing the pressure to drop and thus requires additional horsepower to achieve the same flow rate, creating is an additional operating expense (Figures 2.2, 2.3 and 2.4).
- **Costs of the removal process,** which include labour, chemical and waste disposal costs.
- **Fouling of equipment:** Deposition of contaminants in equipment such as boilers, separators and heat exchangers, decrease their performance.

Such critical problems can cause critical environmental impact, safety concerns, and added costs for clean up, maintenance and unscheduled production shutdown.

Figure 2.6. Filter coated with black powder [145].

Figure 2.7. Wet black powder in orifice plate [145].

Figure 2.8. Pyrophoric iron sulfide fire [145].
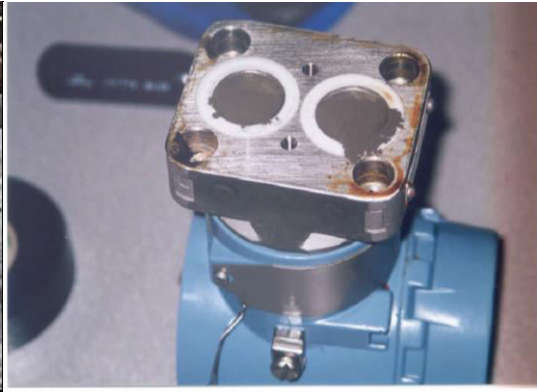
Figure 2.9 Black powder in pressure transmitter [6].

(a)
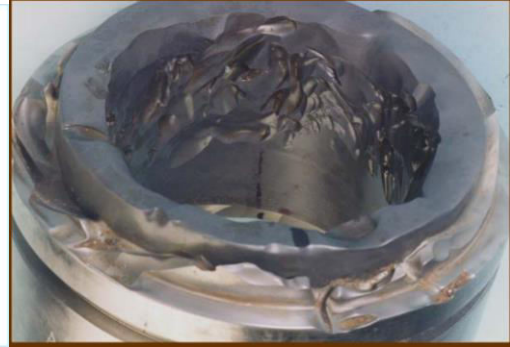
(b)

Figure 2.10. Erosion caused by sand particles to (a) a 50 mm bend pipe and (b) a choke valve [144].

Figure 2.11. Compressor valve with black powder coating [145].

2.1.2 Current Methods for Deposit Detection

A specific review of all state of the art inspection technologies for condition assessment of pipelines were given by [12-14]. However, not all techniques are applicable for deposit detection, especially hydrocarbon deposit, which often presents in oil refineries or polymer production plants. Thus, in the process industry, most commercial technologies such as radiographic, ultrasonic or electromagnetic are used for pipe inspection purposes where pits, cracks and damages in metallic pipelines are the primary concern.

Table 2.1 gives a comparison between the most popular techniques used for inspecting pipelines non-destructively for deposits, namely visual inspection, ultrasonic, radiography and infrared thermography. Table 2.1 summarizes the principle of operation of each technique, their commercial availability, their advantages and disadvantages. All of the compared techniques in Table 2.1 share the advantages of being non-invasive and non-intrusive. However, their individual advantages should be weighed carefully against their disadvantages before choosing the proper technique for a particular application. For instance, some of the eminent techniques used in the process industry for non-destructive testing such as ultrasonic, radiography and thermography techniques are mostly suitable for metallic pipes. Also most of the techniques are relatively slow and requires a trained operator to set up the test and interpret the results properly.

2.2 MULTIPHASE FLOW MEASUREMENT

Crude flowing in oil and gas pipelines usually consists of more than one phase, for instance oil/gas, oil/gas/water or gas/water. Sometimes such multiphase flows are also accompanied by solid contaminants, which are considered as another phase. Multiphase flow monitoring and measurement is highly desired in the process industry in order to ensure safety and increase profit.

2.2.1 Current Techniques for Multiphase Flow Measurement

Due to the criticality of the issue and its high demand, numerous efforts have been made to develop techniques to measure or image multiphase flows. Currently there are two ways to measure multiphase flows, separation methods and inline methods. Good reviews of methods used for multiphase flow measurement are given in [111-116] more than a decade ago. Since then, advances in this area have been slow, and mostly, the same technologies are still used today.

Table 2.1. Common non-destructive techniques used for inspecting deposits in pipelines.

Imaging method	Principle of operation	Commercial availability	Advantages	Disadvantages
Visual inspection	A CCTV camera and lighting device (or laser) attached on a mechanical or electronic carrier.	Different types are commercially available for research and process applications, e.g., pan and tilt and Side scanning evaluation technology (SSET).	• High definition video of the inspection can be achieved. • The survey can be done online or off-line. • The operator has full control of the inspection (pan, tilt or zoom the camera). • Easy interpretation of the images.	• The speed of the carrier is relatively slow (15-30 cm/s) to capture an analysable video. • The carrier must stop at multiple adjacent locations for inspection. • Only large pipes that can accommodate the carrier and the camera can be inspected. • The inspection requires the process to be stopped and the pipe to be emptied.
Ultrasonic [15]	High frequency sound waves are applied at the exterior of the pipe. The sound waves will travel through the pipe and then reflect back to their source when encountering a boundary with another medium (any fluid inside the pipe). The reflected sound waves are used to determine the thickness of the pipe.	Different types are commercially available for research and process applications i.e. contact technique (requires a couplant) and Non-contact techniques (Laser and Electro Magnetic Acoustic Transducers (EMAT) [16]).	• Good resolution. • Access to only one side of the pipe is required when the pulse-echo technique is used. • Deep penetration into the pipe, which permits detecting deep flaws and deposits. • High sensitivity, which allows the detection of small deposits and flaws. • Can cover high range of the inspected pipe. • No need to shut down the pipeline for the inspection.	• Requires a trained operator in order to set up the test and interpret the results properly. • Complex pipe geometries are more challenging to inspect. • Calibration with respect to the pipe material is required prior to the inspection. • Generally requires contact medium (couplant). • Deposits different than the pipe's material may cause errors in the reading.
Radiography	A source of radiation emits photons/neutrons through the pipe and onto a photographic film or a digital camera that record the absorbed radiation, which is used to reconstruct an image.	Different types are commercially available for research and process applications e.g., Gamma rays and X-rays.	• High resolution images can be achieved. • Ability to inspect complex pipe geometries. • High sensitivity to changes in the pipe density.	• Potential health hazards associated with the inspection. • Relatively expensive. • Relatively slow. • Sensitive to the flow orientation.
Infrared Thermography	According to the black body radiation law, all objects above absolute zero kelvin emit thermal infrared radiation. Consequently, thermographic cameras are used to detect radiation in the thermal infrared range of the electromagnetic spectrum (900–14,000 nm) and produce corresponding images. Since the amount of radiation emitted by an object increases with temperature (warm bodies stand out against cooler backgrounds), an external heat source is usually used to heat the inspected pipe (active thermography).	Different types are commercially available for research and process applications e.g., pulse thermography, lock-in thermography, stepped heating thermography, and vibro-thermography.	• Non-contact technique. • Easy interpretation of the images given that they are accurate. This is because it is only able to detect direct surface temperature and from external images the interior of a pipe can be predicted [17] (wall loss caused by corrosion will emit more heat). • Large areas can be scanned at once. • Performing thermographic inspections does not require a certified or licensed operator, however, a trained operator is essential to operate the device and interpret the results.	• Relatively expensive. • In active thermography, the pipe is heated first before inspection, which makes the process slower. • The operating condition that must be considered is somewhat drastic i.e. wind speed, cloud cover, solar radiation, dust etc. • Accuracy depends on several factors i.e. emissivity value, compensation of the reflected temperature, ambient temperature, distance, angle of view etc. • Not efficient for concrete and poly pipes [12].

2.2.1.1 Separation methods

Separation methods rely on a complete or partial separation of the multiphase flow, followed by in-line measuring instruments for each phase. One type of the separation methods is the test separator where all three phases (i.e. oil, water and gas) are separated and measured separately using dedicated meters for each phase. Typical one phase flow instrument for the gas phase is an orifice plate while for the liquid phase turbine, coriolis or ultrasonic meters are usually used. Separation between the gas and liquid phases happens due to the difference in their densities while separation between the different liquids (e.g., oil and water) happens due to their immiscibility in addition to the difference in their densities and viscosities. Another type is the two-phase separator (i.e. gas/liquid) where liquids are considered as one phase (i.e. oil and water) and then gas and liquid are separated by means of partial separation techniques such as cyclone. Afterwards the gas and liquid are measured using a gas flow meter and a liquid flow meter respectively. To extract the water cut from the liquid flow, a water-cut meter is used such as microwave water-cut meter (Figure 2.12).
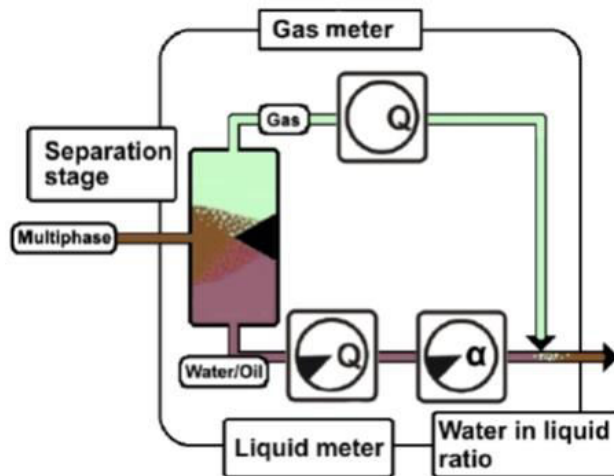
Figure 2.12. Partial separation type of MPFMs [146].

2.2.1.2 Inline MPFMs

Inline MPFMs do not require full nor partial separation of the flow; instead, the individual phases are measured directly in the pipeline carrying the multiphase flow. Inline MPFMs can also be through a bypass sample line rather than the main pipeline, where the sample flow can be either separated into gas and liquid, then measured separately, or the sample can be measured directly using inline methods. Bypass separation requires a homogenous flow where the sample flow can be considered representative.

Inline MPFMs are considered somewhat new technology compared to separators. Nearly all inline MPFMs in the market measure the total flow rate of the multiphase mixture, calculate the fraction of each phase, and then use these to calculate the flow rates of the individual phases. Some of the measuring techniques and technologies that are commonly used for inline multiphase flow measurement are:

- **Differential Pressure (DP) meters:** DP meters can be used to either calculate the flow rate of the multiphase mixture or the density of the mixture (if the flow rate is already known). There are numerous types of DP meters that are frequently used for flow measurement such as venturi, v-cone or other types of restriction; however, MPFMs usually rely on the use of a venturi.

- **Cross-correlation:** Cross correlation technique can use different technologies such as densitometers, pressure gauges, electrical sensors or electromagnetic, radioactive, or ultrasound signals. Each technology uses two sensors separated by a known distance to calculate flow velocities. The most common sensors are electrical sensors (capacitance and/or inductance). However, cross correlation does not work efficiently in homogenous flows when there is an emulsion. This is because there is nothing to cross-correlate with, since the signal-processing search for correlated signals such as flow turbulences or irregularities (e.g., slugs or bubbles).

- **Electrical properties:** Electrodes can be used to determine the phase fractions of the multiphase mixture by measuring the electrical impedance (i.e. capacitance/conductance) across a pipe and accordingly determine the electrical properties (i.e. permittivity/conductivity) of a multiphase mixture. Electrical capacitance and impedance sensors are used to measure the permittivity and the conductivity of a multiphase mixture, respectively, which both change depending on the phase fractions of the multiphase mixture. Capacitance sensors perform best in oil-continuous flow while conductivity sensors perform best in water-continuous flow.

- **Microwave technology:** Measures multiphase mixtures either by resonance or absorption techniques. Just like electrical capacitance based measurement, microwaves use the difference in permittivity of the multiphase components in order to determine the individual phase fractions.

- **Gamma ray attenuation:** The most common nuclear sources used in multiphase flow measurement are Barium 133, Caesium 137 and Americium 241 [10]. The nuclear source is mounted at one side of the pipe while a detector is placed on the opposite side. The

principle of measurement comes from the fact that the number of gamma rays that are detected is dependent on the composition of the multiphase flow, e.g., water is a strong absorber of gamma rays while gas is a weak absorber. This technology can measure the gas and liquid phases by using single energy attenuation, where the nuclear source emits high-energy gamma ray to distinguish the gas from the liquid. The liquid phase can be further analysed by using dual-energy gamma ray attenuation, where the source additionally emits low energy gamma ray to distinguish the oil from water. However gamma rays are considered hazardous and expensive.

One technique is certainly not enough to gather all unknowns in order to calculate all individual flow rates; hence, a fitting combination of two or more technologies is usually used in current MPFMs. Although inline MPFMs offer significant economic and operating advantages over separation-based flow meters, it is still widely acknowledged that no inline MPFM available in the market can meet all the requirements of multiphase metering, e.g., they can handle a certain percentage of gas or liquid. Hence, separation based MPFMs still offer better accuracy than inline MPFMs.

2.3   CURRENT LIMITATIONS OF MULTIPHASE FLOW MEASUREMENT

While MPFMs are commercially available, they still face some challenges and limitations in addition to the well-known challenges of single-phase meters [117], such as:

- **Retention time:** Despite being the most common and traditional methods in measuring multiphase flows, separation methods lack the advantage of continuous monitoring, and require some retention time, which can be up to minutes (i.e. amount of time the liquid has to stay in a vessel to assure that the liquid and gas reach equilibrium and separate).

- **Dependant reliability:** In separation methods the entire measuring system depends on the reliability of the separator, for instance, if the separator is not sized properly the single-phase instrumentations will be affected by the gas carry under or the liquid carry over. Also foams, deposits and emulsions are hard to separate and hence affect the accuracy of the instrumentations.

- **Flow disturbance:** Separation/partial separation based MPFMs disturb the flow and reduce the pressure which then requires more horsepower to pump the fluid back again to the transmission pressure.

- **Flow complexity:** Multiphase flows are hard to understand, predict or model. Therefore, typical single-phase characteristics such as flow regime, velocity profile, turbulence and

boundary layers are unsuitable for describing multiphase flows. For example, the different known horizontal and vertical flow regimes (e.g., bubbly, slug, churn, annular, plug, stratified, wavy, etc.), which are out of the control of the designer or the operator, are defined for only two phase flows (i.e. only one liquid and one gas). However in more than two-phase flow it is hard to determine the flow regime especially in a horizontal flow, hence most flow meters require vertical orientation. Some flow regimes, such as stratified or slug, induce a slip (difference in velocities between phases) between two liquids or between liquid and gas, which makes the phase fraction calculation even harder. In order to simplify their process, some MPFMs claim that adding a static mixer or installing the meter in a specific orientation (e.g., U or L configuration) will insure a homogenous flow, however, a perfect mixing can never be established in real life especially if the flow is lower than 2 ft/s.

- **Too many variables:** Usually in inline MPFMs, the volume flow rate of each individual phase is given by the phase area fraction (i.e. the cross-sectional area locally occupied by the phase divided by the cross-sectional area of the entire region) multiplied by the velocity of each phase. Hence, this approach is considered more complicated than the separation method, as for say a three-phase system, a minimum of 6 parameters must be measured or estimated (i.e. 3 phase area fractions and 3 velocities). However, each parameter depends on other parameters that are subject to continuous change as well. For example, the velocity itself is a function of fluid properties, particle shape, density, and pipe diameter [95]. In order to reduce the unknowns, either more instruments are added, which increases the complexity and the cost of the system, or a homogenous flow is induced in order to assume all phases have the same velocities, which is hard to achieve.

- **Uncertainty:** Because the multiphase flow is considered much more complex than a single flow, the uncertainty of the measurement for MPFMs is much higher than for a single-phase meter.

- **Sensitivity:** The phase-fraction measurements are sensitive to changes in the fluid properties (e.g., salinity, viscosity, density, dielectric constant, electrical conductivity, etc.), characteristics (e.g., slip, flow regime, etc.), and flow condition (e.g., pressure loss, cavitation, contamination, chemical injection additives, vibrations. etc.). Although most of these variables are given as *a priori* information to the MPFM system, such information must be regularly updated to reflect the dynamic changes of the flow.

- **Representative sample:** It is difficult to capture a representative sample of a multiphase flow, which makes it hard to accurately measure the flow and calibrate/verify the system.

- **Maintenance:** MPFMs require well-trained personnel to operate, calibrate and verify the meter. Furthermore, separators require continuous maintenance and personnel intervention.

- **Cost:** Because of the MPFMs big size (especially separation type) and high cost, they are not considered practical to install for each well for production optimization and well testing.

- **Non-tolerant to contaminants:** There is no available meter to measure contaminants. Instead, MPFMs get either fouled by contaminants or their accuracy gets negatively affected.

- **Non-robust:** Sometimes one MPFM is not enough to test all wells wanted as the composition of each well might differ and each MPFM is calibrated to handle a specific composition only. Hence several MPFMs might be required with different measurement ranges to cover all tested wells.

Because of the aforementioned limitations of the MPFMs, process tomography methods introduce alternative means to arrive at the desired measurements of a multiphase flow, or sometimes are combined with current MPFMs for assistance and enhancement.

2.4   THE IMPORTANCE OF THE STUDY

In order to control multiphase flows, an analysis is required to determine some of the flow features and properties such as the flow regime, number of phases, concentration of each phase, etc. Currently multiphase flows are being analysed by MPFMs to get the flow rate of each phase. However, MPFMs available in the market are costly, and only measure oil, gas and water contents with considerable limitations and do not accommodate for the undesirable deposits and dirt that disturb the system and defect instrumentations. So far, MPFMs cannot handle all process conditions, for instance, a meter designed to measure gassy liquid would drastically differ from a meter used to measure wet gas [133]. Process tomography has the potential to be used to get an image of the cross section of the actual pipe under any process and thus robustly measure all phases present. However, this is still in the stage of research and being constantly enhanced and modified [98].

2.4.1 Deposit Detection

Instead of waiting for a problem to occur in the pipeline system, detecting the formation of contaminants in early stages will help preventing many of the discussed problems in section 2.1.1. The monitoring can be done in critical places where deposits are more likely to exist or/and before the customer delivery point as a quality assurance procedure. ECT based early deposit detection is proposed in chapter 6, which highlights the following advantages:

- **Minimize the horsepower needed for the product transmission:** Since deposits can build up in filters and in inner pipeline walls, forming a flow restriction and dropping the production pressure, detecting it before accumulation will indeed help minimizing the cost of requiring additional horsepower to achieve the same flow rate.

- **Minimize the causes of safety hazards:** As severe and unattained erosion can cause the pipeline to fail affecting production and creating an environmental hazard.

- **Enhance pipeline inspection:** Pipeline inspection tools require a clean pipeline to properly inspect the pipeline condition, and so accumulated deposits on the interior wall of the pipeline can cause the inspection tool to trap. Also, since such devices usually use magnetic flux for leakage detection, conductive deposits, such as some forms of black powder, can be attracted to the device causing expensive misrun and inaccurate inspection.

- **Enhance the process of choosing the right separation equipment:** Prior to applying a separation technique to the pipeline system, a comprehensive study of the nature of the problem should be conducted to know what type of separation technique should be used and where exactly in the pipeline system should it be located. Hence, determining the critical locations where contaminants mostly is formed will sure help in deciding the proper location to adjust the chosen separation device.

- **Quality assurance:** Deposits monitoring before costumer delivery points (e.g., when gas suppliers send gas to electricity companies) assures good quality product with no contamination, which can badly affect their equipments. Also, when deposits accumulate in the separation equipment before the costumer delivery point, they cause the pressure to drop and thus the product delivered will not meet the costumer pressure requirements. Hence, detecting and eliminating deposits in early stages before reaching the separation equipment will hinder the plugging of the separation equipment maintaining better flow rate as requested.

- **Minimize filter maintenance costs:** The more particles accumulate in the filter; the more the pressure drops and the cartridges of the filter get fouled. Changing the filter cartridges is considered filthy, expensive and perhaps dangerous. Hence, monitoring deposits in the cartridges will help in determining when to change them.

- **Pigging frequency:** Continuously monitoring gas pipelines will help the pigging specialists to decide upon the frequency of pigging required for each pipeline. Some pigging operations have documented 500 – 5,000 kg of black powder removed from scraped pipelines per run [5], while others reported none.

2.4.2   Multiphase Flow Measurement

Multiphase flow measurement is an on-going research area, trying to improve the robustness of the online measurement of unprocessed flows. MPFMs available in the market so far are considered costly for continuous online measurement along the pipeline system. For example, the cost of an MPFM today is in the range of 100,000-500,000 USD with installation cost goes up to 25% of the hardware cost plus associated operation cost which can go up to 40,000 USD. Thus, so far one MPFM is used to analyse several wells one at a time. In the oil and gas industry, MPFM installation for each well can only be feasible if the cost falls to around 40,000-60,000 USD [118]. A compact, efficient and cost effective ECT system that is capable of accurately measuring all phases presented in an unprocessed flow is proposed in chapter 8, which can achieve the following advantages:

- **Eliminate the need of test separators,** which are costly and require heavy maintenance.

- **Improve production optimization:** For artificial lift wells (i.e. gas lift, water lift) it is important to continuously monitor and optimize the lifting process and injection rate, as the amount of gas or water required to lift has to be adjusted to specific standards to optimize the production. Most MPFM available in the market cannot handle such situations, as the gas volume fraction of the flow increases. Similar optimisation is preferably required for chemical injection, reservoir injection, water breakthrough detection, etc.

- **Enhance flow assurance,** especially before transferring the product to the costumer.

- **Allow single well surveillance:** Using a MPFM at each well will increase the time resolution of the gathered information compared to alternating well testing using test separator and therefore minimize the total uncertainty in well data. Such information is crucial when taking decisions like shutting down of wells, introducing artificial lift to the

well, drilling new wells, etc. Single well testing will also help in better control instable wells (e.g., gas lift wells), as continuous monitoring is important in such cases before and after connecting them to the main production lines as they are unpredictable.

- **Allow production allocation metering:** Measuring the amount of extracted hydrocarbon produced by each source.

- **Improve fiscal or custody transfer measurement:** This critical measurement happens when ownership of oil or gas transfers from one party to another, e.g., between two companies or between a company and the government. This measurement requires high accuracy, which is subject to national regulations for petroleum measurement set by the government authorities.

Continuous monitoring methods for pipelines are in the stage of research and this study is one step further to provide a solution to this problem. Process tomography promises a brighter future for multiphase flow measurement for industrial applications handling multicomponent mixtures. In order to address the importance of this study, Section 3.3 states the advantages of employing ECT to overcome the challenges listed in Section 2.3, while Chapter 8 presents an ECT based MPFM that demonstrates such advantages.

Chapter III

3 THE ECT MEASUREMENT SYSTEM

Process tomography techniques image the cross section of the pipe/vessel being monitored to get the required information. Each tomography method has its own limitations and is being constantly enhanced and modified. Process tomography techniques can estimate the material distribution of a process without disturbing the process itself. Such techniques work by using several sensors mounted around the process of interest in order to capture the data required to analyse and reconstruct an image of the process. Different techniques use different types of sensors depending on the characteristics used to create an image, i.e. ECT uses permittivity, Electrical Impedance Tomography (EIT) uses conductivity, Electrical Resistivity Tomography (ERT) uses resistivity, optical tomography uses absorption and scattering characteristics. In this thesis, ECT was used, however all proposed algorithms could be adapted for other tomographic techniques.

A distribution of different materials with different permittivity inside a pipe or a vessel leads to a random distribution of their permittivity. ECT measures the external capacitance of the enclosed objects to determine the internal permittivity distribution. By measuring the capacitance of the media in a specific region, the permittivity distribution can be found, which then is used to reconstruct an image representing the same region. ECT was first developed in the late 1980's to image a two-phase flow [18]. Afterwards, ECT systems were used successfully in numerous research investigations for industrial multi-phase processes including gas/solid distribution in pneumatic conveyors [19], fluidized beds [20-22, 137], flame combustion [23-25], gas/liquid flows [26], water/oil/gas separation process [27-28, 98, 138], water hammer [29], and many others [30]. For more than 20 years, tomographic techniques have promised great potential in multiphase flow measurement. However, ECT systems are mainly used to image a non-conductive media. ECT is still in the stage of research with numerous systems being developed and tested at companies and universities laboratories; still, better results are required to take it to the stage of commercialization.

3.1 THE HARDWARE DESIGN

Figure 3.1 illustrates a typical ECT system, which consists mainly of three subsystems; the capacitance sensor, the data acquisition unit and the computer unit.

3.1.1 The Capacitance Sensor

The capacitance sensor consists of the following main parts:

1. The electrodes.
2. An insulating pipe (or vessel).
3. Axial, end, and radial guards.
4. Screen.
5. Screen-electrode insulator.
6. Coaxial cables and connectors.

Typically, several electrodes are mounted equidistantly on the periphery of a non-conductive process pipe or vessel. It has been found that the thickness of the non-conductive pipe has an effect on the quality of measurement [31]. In general, reducing the thickness gives better measurements. The electrodes are separated from each other by a small gab called the axial guard. The electrodes are covered by a screen (conductive or non-conductive) to reduce external electrical noise, eliminate the effects of external grounded objects and protect the electrodes from damage. In case of a conductive pipe/vessel, the sensor must be mounted internally, using the conductive internal wall of the pipe/vessel as a screen. An insulating material must fill the gap between the electrodes and the screen. The thickness of the screen-electrode material should be carefully chosen, this is because the less the thickness is, the less the standard capacitances of the sensor become (the capacitance when the pipe is full of low permittivity only) [31], which means that the capacitances might get too small to measure. The sensor also includes radial guards in order to reduce the standard capacitance between adjoining electrode pairs. Numerous combinations of different configurations of the radial and axial guards were suggested to improve the system performance [134]. The screen and the radial guards are always maintained at earth potential. Figure 3.2 illustrates a cross-sectional view of the typical 12-electrode ECT sensor. Other shapes of ECT sensors have been used, however, circular sensors are the most common.

In an ECT system, the electrodes must be sufficiently large to provide a measureable change in capacitance. This is considered a challenge in this type of tomography, since only few electrodes can be used (usually 8 or 12), which results in limited independent measurements. This makes the image reconstruction process more challenging to produce high-resolution images.
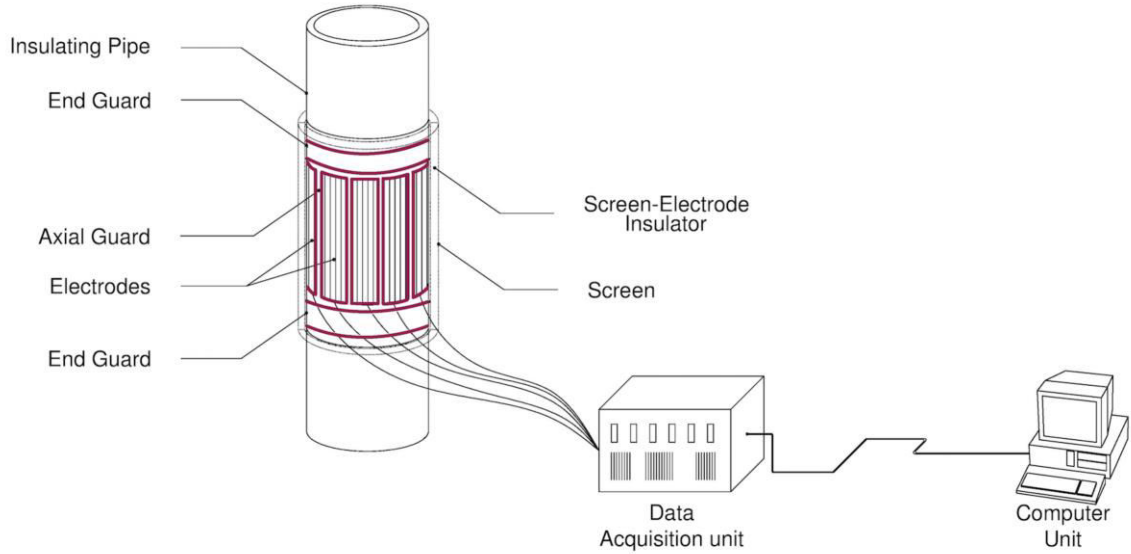
Figure 3.1. A typical ECT system

For an N electrode system, various measurement protocols can be used. However, in a typical ECT system, electrodes 1 to N are used successively as source electrodes, and the capacitance values between all single electrodes combinations are measured. Hence, for one measurement cycle, electrode 1 is first excited with a fixed positive voltage making it the source electrode while electrodes 2 to 12 are held at earth potential (zero) by 11 capacitance transducers making them the receiving electrodes. Then the capacitances between 1-2, 1-3, …, 1-12 are measured simultaneously using the transducers. Next, electrode 2 is selected as the source electrode and electrodes 3 to 12 as the detecting electrodes, while electrode 1 is connected to earth making it inactive because of reciprocity (measurement 2-1 is same as 1-2). This process continues until, electrode 11 is selected as the source electrode and electrode 12 as the detecting electrode, while electrodes 1 to 10 are held inactive. Due to the capacitance reciprocity, the mutual capacitances for a certain pair of electrodes are always equal. Generally, the number of independent capacitance measurements is the number of N-electrode combinations, taking 2 at a time as:

$$M = \binom{N}{2} = \frac{N!}{2!(N-2)!} = \frac{N(N-1)}{2}, \tag{3.1}$$

The capacitance measurements are dependent on the permittivity distribution of the medium. Hence, these measurements can be used to deduce the permittivity distribution of the medium, which is then used to produce the image.

32
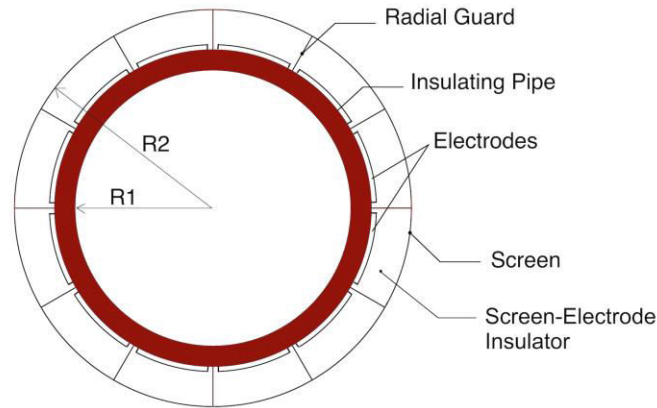
Figure 3.2. A cross-sectional view of a typical 12-electrode ECT sensor.

3.1.2 The Data Acquisition Unit

The data acquisition unit works according to the following sequence events:

1. Apply a fixed voltage, V_c, to the source electrode to excite it while keeping the rest of the detecting electrode at zero potential.
2. Measure the induced current in the receiving electrodes.
3. Deduce the capacitance measurement values C, from the given potential difference V_c, and the measured current (charge) Q, according to $C = \frac{Q}{V_c}$.
4. Convert the capacitance measurement values into voltage signals using a type of capacitance to voltage converter.
5. Condition (amplify, filter, multiplex…etc.) and digitalize the voltage signals.
6. Send the conditioned and digitalized voltage signals to a computer for processing and display.

3.1.3 The Computer Unit

The computer unit is used for hardware control and data processing, which can produce qualitative outputs (i.e image reconstruction) or/and quantitative outputs (e.g., flow rate, concentration,…etc.). The received voltage signals (from the data acquisition unit) are interpreted into capacitance measurements in the computer unit in order to use them in the image reconstruction algorithm to deduce the permittivity distribution (i.e. the image). The measured capacitance values C between a source electrode i and a receiving electrode j can be arranged in a symmetric matrix (the capacitance matrix) as:

33

$$C_{i,j} = \begin{bmatrix} C_{1,2} & C_{1,3} & \cdots & C_{1,N} \\ & C_{2,3} & \cdots & C_{2,N} \\ & & \ddots & \vdots \\ & & & C_{N-1,N} \end{bmatrix}, \quad for \begin{pmatrix} i = 1, \ldots, N-1 \\ j = i+1, \ldots, N \end{pmatrix}, \qquad (3.2)$$

Some of the matrix properties of this capacitance matrix are related to the material properties. A full investigation can be found in [136].

3.2 ECT CHALLENGES AND ADVANTAGES

There are some challenges that make the implementation of ECT system a challenge, this include:

- **Soft field effect:** The inhomogeneous generated electric field lines in the region of interest tend to spread and are dependent on the physical electrical properties of the material of interest (the permittivity). Thus, no distinct border between the pixels can be obtained. The nature of the soft field is considered much more complex than the hard field, and requires much more analysis for the image reconstruction. Unlike hard field tomography, such as X-ray CT, MRI, PET, etc., where the source field lines do not depend on the material under investigation and pass directly through it, making the reconstruction process much easier.

- **Ill-conditioned system:** That is a small error in the input (capacitance measurements) can result in much larger errors in the solution (permittivity distribution), which leads to unstable solutions.

- **Underdetermined system:** The number of variables in the system model (number of pixels) is greater than the number of equations (number of capacitance measurements). This means that the solution will not be unique, and hence regularisation methods are often used to solve the problem. This is because the system hardware is limited to a certain number of electrodes, and thus limited number of independent measurements, which are much less than the number of pixels used to reconstruct the image.

- **Nonlinearity:** Because of the soft field nature of the system, the relationship between the measured capacitance and the permittivity distribution is considered nonlinear (Figure 4.3). Hence it is difficult to establish an analytical and explicit expression of the relationship. This means that the sensitivity distribution over the process cross-section of two (or more) different materials is inherently non-uniform. Consequently, the ECT

system has different responses to different flow regimes. Therefore, a linearized model is often used instead.

- **Conductivity:** Since the physical properties of an object depend on both the permittivity and conductivity, ECT systems are mainly used to image non-conductive media. This is because the conductivity of the material will have a great effect on the capacitance measurement sensor. Only when the conductivity of the imaged object is very low, its effect on the ECT system can be ignored. However, in theory, if the conductivity of the imaged object is high, the capacitance measuring circuit will be almost shortened by the conductivity path and a clear image cannot be produced using the standard image reconstruction approaches. This limitation stands on the way of ECT to be of more use in the process or medical industries as most of the media encountered are conductive.

Because of the above problems, the image quality of the ECT system is considered somewhat poor, and the frequently used reconstruction algorithms developed for medical tomography will not produce good images if used directly in ECT (or any other soft field tomography). However, ECT systems have other advantages that made this new technology more promising for many industries. Such advantages include:

- Very fast response of the ECT sensor.
- Inexpensive.
- Compact.
- Non-hazardous.
- Non-invasive (does not require contact between the sensor and the material under investigation).
- Non-intrusive (does not change the characteristics of the material under investigation).
- Robust against high temperature and high pressure.

Although, ECT technology is still at the stage of laboratory research, it is being rapidly developing in both the hardware design and the image reconstruction quality. This is because of the promising advantages of such technology for the process industries, which enable a non-destructive monitoring of a process that is fast, cheap, practical and efficient.

3.3   THE ECT SOLUTION FOR MULTIPHASE MEASUREMENT

In [119], the authors suggested the applicability of ECT for multiphase flow measurement in the oil industry and covered the development of one. The hardware design is considered compact and practical but the main challenges are still in the software design. Some hardware design developments integrate two or more tomography modalities mostly to get more measurements such as ECT/Ultrasonic [134], ERT/ECT/ultrasonic [135] or ECT/MIT [94]. With the hardware design always in the state of development, this thesis focuses on the software aspect of a conventional ECT system for multiphase imaging, aiming to distinguish boundaries between different components in a process, where then, information about the flow (e.g., phase fraction, flow regime, vector velocity…etc.) can be extracted from the image. The image produced can be used in order to analyse the flow in order to actuate process control strategies or to develop models that describe the process for validation or simulation. ECT promises to solve some of the multiphase measurement challenges listed in Section 2.3 by offering the following advantages:

- Other than permittivity, capacitance measurements can be considered fairly insensitive to changes in fluid properties (e.g., salinity, viscosity, density, etc.), characteristics (e.g., slip, flow regime (despite water continues), etc.), or flow condition (e.g., pressure loss, cavitation, contamination, chemical injection additives, vibrations. etc).

- Minimum maintenance: no replaceable parts included, and withstand harsh environment conditions such as high pressure and high temperature.

- Tolerant to contaminants: any type of contaminants can be imaged and measured too.

- Does not disturb the flow, as it can be installed inline with no restriction orifice.

- Robust: one ECT system can cater for all required wells to test, as the composition of each well does not matter.

Chapter IV

4 FORMULATION OF THE ECT FORWARD PROBLEM

The purpose of ECT is to construct images from collected projection data taken from multiple directions. This ECT problem, like any other image reconstruction problem, can be broken down into two computational sub-problems:

1. **The forward problem,** which represents the system mathematical model (the partial differential equation representing the sensing domain). It calculates the inter-electrode capacitances C_{ij} from *a priori* information about the permittivity distribution ε. The forward problem statement can be given by:

   "Given a distribution of electrode pairs (i, j) on the boundary $\partial\Omega$ of a process domain Ω, and a distribution of permittivity ε within Ω, find the resultant measurement set C on $\partial\Omega$."

   The solution to the forward problem in two-dimensions can be expressed in the following form:

   $$C_{ij} = F(\varepsilon(x,y)) \qquad for\begin{pmatrix} i = 1, \ldots, N-1 \\ j = i+1, \ldots, N \end{pmatrix}, \tag{4.1}$$

   where F is a nonlinear forward mapping from the permittivity space into the measurements space.

2. **The inverse problem,** which finds the inverse relationship of **(4.1)** by estimating the permittivity distribution from the measured capacitance. The inverse problem statement can be given by:

   "Given a distribution of electrode pairs (i, j) and a distribution of measurement C on $\partial\Omega$, find the permittivity distribution ε within the domain Ω."

   The solution to the inverse problem can be expressed in the following form:

   $$\varepsilon(x,y) = F^{-1}(C_{ij}) \qquad for\begin{pmatrix} i = 1, \ldots, N-1 \\ j = i+1, \ldots, N \end{pmatrix}, \tag{4.2}$$

   where F^{-1} is the inverse nonlinear mapping from the measurements space to the permittivity space. However, in iterative image reconstruction techniques, the forward problem is solved implicitly within the inverse problem.

4.1 MATHEMATICAL FORMULATION OF THE SENSOR MODEL

The ECT mathematical system model can be treated as an electrostatic field problem and hence can be modelled by Poisson's equation as follow:

$$\nabla \cdot \left(\varepsilon_o \varepsilon\,(x, y)\, \nabla \phi(x, y) \right) = -\rho(x, y), \tag{4.3}$$

where ε_o is the free space permittivity, $\phi(x, y)$ and $\rho(x, y)$ are the electrical potential and the free charge density distributions, respectively. Assuming no free charges within the field, Possion's equation can be simplified to Laplace's equation:

$$\nabla \cdot \left(\varepsilon_o \varepsilon\,(x, y)\, \nabla \phi(x, y) \right) = 0. \tag{4.4}$$

To further relate the permittivity distribution to the capacitance, we use the fact that the electric field is given by:

$$E = -\nabla \phi(x, y). \tag{4.5}$$

Also, by applying Gauss law, the charge sensed by the detecting electrode j when the source electrode i is fired can be found by:

$$Q_{ij} = \int_{\Gamma_j} \varepsilon_o \varepsilon\,(x, y)\, E. \hat{n}\, d\Gamma_j, \qquad for \begin{pmatrix} i = 1, \dots, N-1 \\ j = i+1, \dots, N \end{pmatrix}, \tag{4.6}$$

where Γ_j is the surface of the receiving electrode, and $\hat{n}$ is a unit vector normal to Γ_j. Hence, the capacitance of the electrode pair (i, j) (inter electrode capacitances) can be calculated by:

$$C_{ij} = \frac{Q_{ij}}{V_{ij}}, \qquad for \begin{pmatrix} i = 1, \dots, N-1 \\ j = i+1, \dots, N \end{pmatrix}, \tag{4.7}$$

where V_{ij} is the voltage difference between detector electrode j and the source electrode i, namely $V_{ij} = V_i - V_j$, according to (4.9). As it can be noticed from (4.4) to (4.7), the measured capacitance can be linked to the permittivity distribution. Using (4.5), (4.6) and (4.7), the mutual capacitance C_{ij} for N-electrode capacitance system (when electrode i is the source and electrode j is the detector) can be found by:

$$C_{ij} = -\frac{\varepsilon_o}{V_{ij}} \int_{\Gamma_j} \varepsilon\,(x, y)\, \nabla \phi^q(x, y). \hat{n}\, d\Gamma_j, \quad for \begin{pmatrix} i = 1, \dots, N-1 \\ j = i+1, \dots, N \end{pmatrix}, \tag{4.8}$$

where ϕ^q is the electrical potential distribution of node q in the measuring electrode.

4.2 BOUNDARY CONDITION

To solve the forward problem, all capacitance measurements in **(4.8)** must be determined. To do so, **(4.4)** should be first solved to obtain the electrical potential distribution $\phi(x,y)$. First, a known distribution of the permittivity is used as *a priori* information in **(4.4)** (usually a uniform distribution is assumed), which is the permittivity distribution of the background. Then, this Laplace's equation, which is a linear second order elliptic differential equation, can be solved (e.g., using FEM) with the following Dirichlet boundary conditions:

$$\phi^q = \begin{cases} V_c & \forall (x,y) \in \Gamma_i \quad where\ (i = 1, ..., N-1) \\ 0 & \forall (x,y) \in \Gamma_k (k \neq i),\ \Gamma_{guards}\ and\ \Gamma_{screen} \end{cases}, \qquad (4.9)$$

where V_c is a fixed voltage applied to the source electrode (electrode i= 1,2,…,11 one at a time), Γ_i is the spatial location of electrode i, while Γ_{guards} and Γ_{screen} are the spatial location of the guards and screen, respectively. In other words, **(4.9)** basically states that the boundary condition is some fixed voltage, V_c, applied to the source electrode and zero to the sensing electrodes, guards and screen, as illustrated in Figure 4.1.

Other boundary conditions have been used for ECT [32,33]. For example, Dirichlet boundary conditions can be applied at the spatial location of the electrodes, as in **(4.9)**, while homogeneous zero Neumann boundary conditions are applied at the spatial location of the guards and screen, $\frac{\partial \phi}{\partial n} = 0$.

(a)   (b)
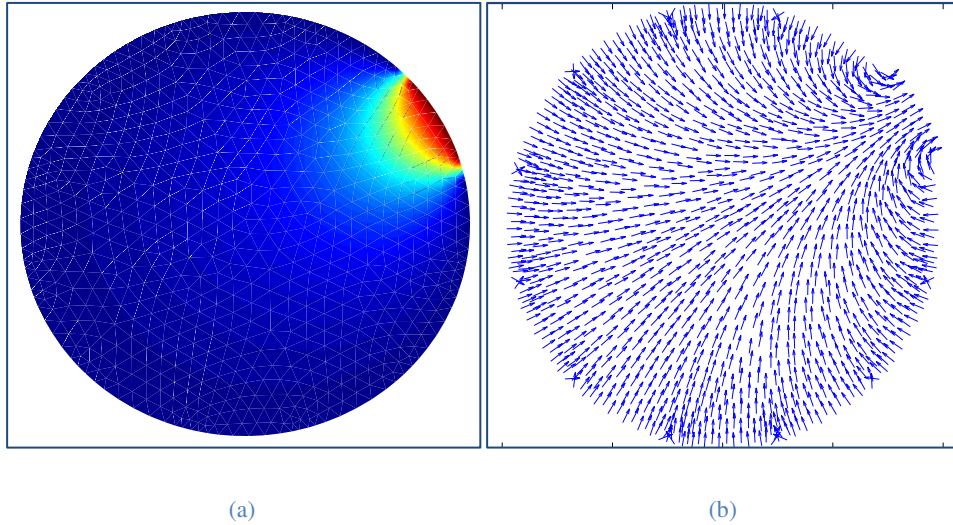
Figure 4.1. (a) Electric potential distribution of electrode 1 as a source, (b) gradient of potential with negative electric field.

39

4.3 THE FINITE ELEMENT METHOD

In general, numerical methods are used for solving a mathematical system model instead of analytical methods when:

1. Analytical solution of the mathematical system model is possible but time-consuming, and the error of approximation achieved with a numerical solution is acceptable.
2. Analytical solution for the mathematical system model is impossible, i.e. for problems that:
   a) Do not have a closed-form solution, i.e. the solution to the equations used to describe the changes in the system cannot be expressed as a mathematical analytic function.
   b) Have irregularly shaped boundaries.
   c) Have changing material properties.

As a closed form solution cannot be reached in our case, and since the permittivity distribution $\varepsilon(x, y)$ of a multiphase flow is considered asymmetric, analytical methods cannot be used to solve **(4.4)** and **(4.9)**, instead, numerical methods must be applied to find an approximate solution to the boundary value problem.

Since analytical (exact) solutions are often impossible to obtain in practice for complex systems, modern numerical methods such as Finite Element Method (FEM) do not seek exact solutions; instead they obtain approximate solutions while sustaining reasonable bounds on errors. A generated table and/or graph, rather than an exact fixed number, often represents the numerical solution of the system. The FEM is used in this thesis to calculate the potential distribution, the capacitance and the sensitivity distribution, however different numerical methods such as Boundary Element Method (BEM) [141] can be also applied.

4.3.1 Calculation of the Inter-Electrode Capacitances

As seen from **(4.8)**, it is impossible to get an explicit expression that relates the measured capacitances to the permittivity distribution of different components inside the pipe as the operator F in **(4.1)** is a nonlinear operator that cannot be separated from $\varepsilon(x, y)$ to represent a linear mapping of the model. Hence, the FEM is used to solve this equation by first discretizing (dividing) the domain of solution into a number of T elements corresponding to a number of nodes Q, creating what is it called a *mesh* (Figure 4.2.), and solving **(4.4)** with the given Dirichlet boundary condition **(4.9)** and a permittivity distribution.
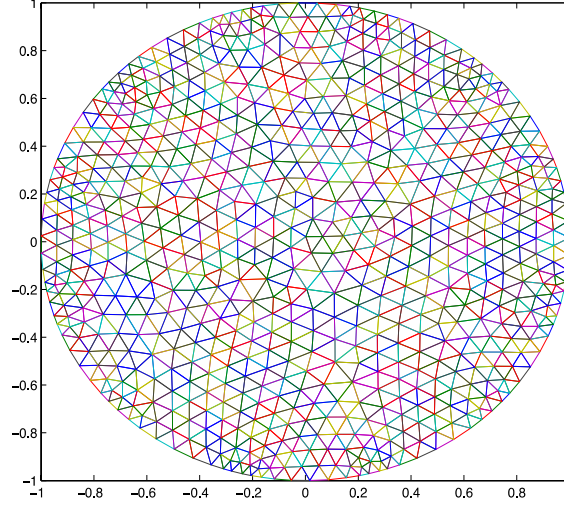
Figure 4.2 FEM mesh of 1367 three-noded rectangular elements corresponding to 739 nodes.

Equation **(4.4)** is solved for every node, q, in the mesh to get the 2D electrical potential distributions $\boldsymbol{\phi}^q(x, y)$. The resulting nodal potentials are represented in a discrete form by the vector $\boldsymbol{\phi}^q$, which is a $Q \times 1$ vector, hence the value boundary problem given by **(4.4)** and **(4.9)** can be reduced to the system of linear equations:

$$\boldsymbol{A}(\varepsilon)\boldsymbol{\phi}^q = \boldsymbol{b}^q, \tag{4.10}$$

where $\boldsymbol{A}(\varepsilon)$ is a sparse $Q \times Q$ matrix whose elements are the discrete representation of the operator $\nabla.\,\boldsymbol{\varepsilon_o}\varepsilon\nabla$, and $\boldsymbol{b}^q$ is a $Q \times 1$ vector incorporating the boundary conditions given by **(4.9)**. There are efficient methods for solving **(4.10)**, much more effective than directly inverting the matrix $\boldsymbol{A}(\varepsilon)$. Since matrix $\boldsymbol{A}(\varepsilon)$ is symmetric (i.e. $\boldsymbol{A}^T = \boldsymbol{A}$), positive-definite ($\boldsymbol{\phi}^T\boldsymbol{A}(\varepsilon)\boldsymbol{\phi} > \boldsymbol{0}$ for all non-zero vectors $\boldsymbol{\phi}^q$ in $\mathbb{R}^q$), and real, a technique based on the conjugate gradient method is preferred. For a smaller system of linear equations, sparse **LU** decompositions and Cholesky decompositions can be used to get good results. After finding the nodal potentials from **(4.10)**, the inter-electrode capacitances can be found numerically by evaluating the integral in **(4.8)**.

4.3.2   Calculation of the Field Sensitivity Model

The second task of the FEM is to calculate the field sensitivity model needed by the image reconstruction algorithm to reconstruct the image. Technically, for a two-phase medium, the field sensitivity model can be obtained by placing an object of the same permittivity as one phase inside the pipe which is filled with the second permittivity material, and keep changing

the location of the object to all different places in the sensing region inside the pipe, and measure the capacitance change as a function of position. To obtain a very accurate model, the object must be placed in every element of the FEM mesh, one at a time. However, this can be a very hectic and time-consuming process, alternatively, a sensor simulator is generally used to calculate the field sensitivity model.

In general, calculating the change of capacitance of the electrode pair (i, j) in response to a change of permittivity for each element in the FEM mesh in the sensing area, obtain the standard form of a field sensitivity model. The field sensitivity distribution of an electrode pair (i, j) for element t of the FEM mesh $S_{i,j}(t)$ is given by:

$$S_{i,j}(t) = \frac{\partial C_{ij}}{\partial \varepsilon} = - \int_{\Omega_t} \nabla \phi_i \cdot \nabla \phi_j d\Omega_t, \qquad for \begin{pmatrix} i = 1, \dots, N-1 \\ j = i+1, \dots, N \end{pmatrix}. \qquad (4.11)$$

Here ϕ_i and ϕ_j are the potential when electrodes i and j are excited, respectively, and Ω_t is the surface of element t. Because of the symmetry of the sensor model, only $\frac{N}{2}$ out of $\frac{N(N-1)}{2}$ distributions of the field sensitivity need to be calculated $(S_{1,2}, S_{1,3}, \dots, S_{1,\frac{N}{2}+1})$. The rest of the sensitivity distributions can be calculated by simple rotation transformation, reducing the computation time significantly.

Since the finite element domain has irregular elements of different areas, a linear transformation (mapping) is performed on the sensitivity distribution to transform it from the finite element domain to the image domain, which has regularly shaped square elements (pixels) of the same size. For P pixels, this transformation can be represented, for the $\frac{N}{2}$ sensitivity distributions, as:

$$S_{i,j}(p) = T\{S_{i,j}(t)\} \qquad (i = 1 \text{ and } j = 2, 3, \dots, \frac{N}{2} + 1), \qquad (4.12)$$

where $S_{i,j}(p)$ denotes the transformed field sensitivity distribution (discretized) from the finite element domain $(S(t))$ to the image domain, and $T\{.\}$, is the transformation operator. The linear transformations involves the following operations:

- **Scaling:** because the sensor geometry has different units in the two domains.
- **Translation and reflection:** applied when different co-ordinate systems are used in the two domains.
- **Interpolation/extrapolation:** of sensitivity values for each pixel p.

- **Rotation transformations:** the rest of the sensitivity distributions are obtained in the image domain by rotation transformations, where the centre of rotation is the centre of the pipe.

Alternatively, the elements in the FEM mesh can act as pixels.

4.4   LINEARIZATION

The inverse problem in ECT is an ill-posed and nonlinear problem, and therefore approximation methods based on linearization are usually used. The system model given by **(4.8)** is considered nonlinear (as the electric field, and consequently the capacitance, depend on the material present), and the integral makes it difficult to solve by a computer. This is shown in Figure 4.3, using different permittivity values (i.e 1 to 80) in a simulated region of interest inside the imaging area, and calculating the associated capacitances for each permittivity value using the forward model. Hence, it is a common practice to approximate it to represent a linear system.
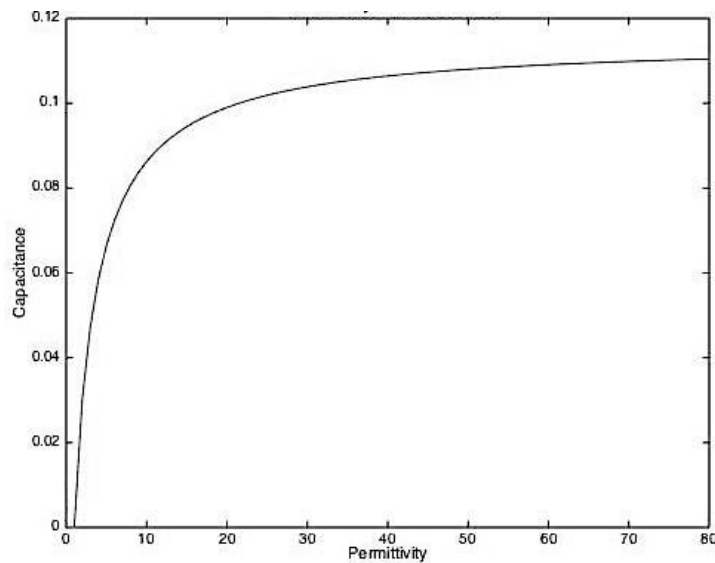
Figure 4.3. Nonlinearity of the ECT problem.

Linearization methods make it possible to employ tools for studying linear systems, in order to analyse the behaviour of a nonlinear system near a given point. In linearization, the change in capacitance measurements for a small change in permittivity, can be approximated in a linear manner. Linearization assumes that the permittivity inside each pixel is constant because of the small size of pixels (the smaller the pixel the higher the resolution). The linearization of a nonlinear function is the first order term of its Taylor expansion near the

point of interest b. Therefore, for a system defined by **(4.1)**, the linearized system can be written as:

$$C \approx F(\varepsilon_b) + \nabla F(\varepsilon_b)(\varepsilon - \varepsilon_b). \tag{4.13.a}$$

Taking
$$\Delta C = C - F(\varepsilon_b), \tag{4.13.b}$$

$$\Delta \varepsilon = (\varepsilon - \varepsilon_b), \tag{4.13.c}$$

and
$$S = \nabla F(\varepsilon_b), \tag{4.13.d}$$

equations **(4.13.a-d)** can be expressed as:

$$\Delta C = S \Delta \varepsilon. \tag{4.13.e}$$

Equation **(4.13.e)** represents the change in capacitance ΔC (linearized capacitance changes), in response to a change in permittivity $\Delta \varepsilon$ (linearized permittivity), where ε_b is the permittivity of the point of interest, and S is the Frechet derivative, which represents the sensitivity of the capacitance in response to the permittivity distribution. The Frechet derivative denotes the linear mapping.

There are M equations of the form of **(4.13.e)** corresponding to M measurements. Also, to visualize the permittivity distribution as an image in a computer, **(4.13.e)** must be discretized according to **(4.12)** into P pixels. Thus, ΔC is a $M \times 1$ vector, $\Delta \varepsilon$ is a $P \times 1$ vector and S is a $M \times P$ matrix (the jacobian), which represents the discretized sensitivity distribution of all electrode pairs.

A priori information of the permittivity distributions ε should be used as a reference to acceptably approximate the solution. Then, the inverse problem becomes a problem of finding an approximate solution to ε_b, knowing the measured capacitance C, and the reference permittivity ε. The sensitivity matrix S and the calculated capacitance $F(\varepsilon_b)$ can be obtained by solving the forward model.

In typical ECT applications, $\Delta \varepsilon$ is taken small enough in order to make the system in **(4.13.e)** stable (the difference in the permittivity of the imaged materials is small). If $\Delta \varepsilon$ is relatively small, the effect of the permittivity distribution on the sensitivity distribution can be considered insignificant. This constraint is true for low contrast cases, such as gas/oil, where both their permittivity values are close to each other, while in other cases, such as water/oil, it

is not true, and so, nonlinear methods are preferred to solve the problem, as will be demonstrated in Chapters 7 and 8.

4.5   NORMALIZATION

It is preferred to calculate the normalized capacitance and permittivity before processing the data in an image reconstruction algorithm, so it can be used universally for different pipes with different scales. This is done to reduce systematic errors and produce better results. The normalized and linearized capacitance $\lambda_{i,j}$ for each capacitance measurement, and the normalized and linearized permittivity g_p per pixel, are given by:

$$\lambda_{i,j} = \frac{C_{i,j} - C_{i,j}^{(low)}}{C_{i,j}^{(high)} - C_{i,j}^{(low)}},$$

(4.14)

$$g_p = \frac{\varepsilon_p - \varepsilon^{(low)}}{\varepsilon^{(high)} - \varepsilon^{(low)}},$$

(4.15)

where $C_{i,j}$ is the absolute capacitance measurement for electrode pair (i, j), $C_{i,j}^{(high)}$ and $C_{i,j}^{(low)}$ are the absolute capacitances when the pipe is filled with high permittivity and low permittivity, respectively, ε_p is the absolute permittivity for pixel p, while $\varepsilon^{(high)}$ and $\varepsilon^{(low)}$ are the absolute permittivity of the high permittivity and the low permittivity, respectively. The normalized form of **(4.13.e)** is given by:

$$\lambda = Sg,$$

(4.16.a)

where λ is the linearized and normalized capacitance vector, g is the linearized and normalized permittivity vector and S is the sensitivity distribution matrix of λ with respect to g. Here g represents the image that can be constructed by an image reconstruction algorithm, therefore, its normalization process is done for every pixel. The matrix **(4.16.a)** expands to a system of linear equations in the form:

$$\begin{cases} \lambda_1 = S_{11}g_1 + S_{12}g_2 + \cdots + S_{1P}g_P \\ \lambda_2 = S_{21}g_1 + S_{22}g_2 + \cdots + S_{2P}g_P \\ \quad\quad\quad\quad\quad \vdots \\ \lambda_M = S_{M1}g_1 + S_{M2}g_2 + \cdots + S_{MP}g_P \end{cases}$$

(4.16.b)

Numerous image reconstruction methods were developed and applied to solve the ECT inverse problem, where some of them are presented in the next chapter.

Chapter V

5   IMAGE RECONSTRUCTION TECHNIQUES

In general, there are three main mathematical techniques used for image reconstruction:

1. **Analytical methods:** Are based on exact mathematical solutions to the image equations and therefore are faster. However, as mentioned earlier, an explicit expression that relates the measured capacitances to the permittivity distribution of different components cannot be obtained from **(4.8)** and hence analytical methods cannot be used for ECT.

2. **Direct numerical methods:** Include one-step calculation, which makes the reconstruction faster but not very accurate. Usually such methods are combined with other iterative methods to reconstruct a better image. While sometimes they are used as a first iteration step for other iterative methods.

3. **Iterative numerical methods:** Approach a better solution to the problem by using multiple iteration steps.

As there are a variety of image reconstruction techniques, two important factors must be considered in choosing the right technique for a specific application:

1. **The availability of *a priori* information:** Some cases lack *a priori* information about the permittivity distribution of the imaged medium, e.g. the measured components are unknown.

2. **The purpose of the system:** Some applications only require the spatial location of an object inside the sensing area, others require the shape of the object, while in some applications, the concentration of a material inside the sensing area is required.

As mentioned in Section 3.2, the ECT system model is considered difficult to solve because of some major issues. First, **(4.16)** does not have a unique solution because it is considered to be underdetermined, since the number of unknown variables P in the system model (number of pixels) is greater than the number of known equations M (number of capacitance measurements). Second, **(4.16)** is sensitive to small perturbation of λ, since it is ill-conditioned. Third, the sensitivity distribution matrix S is not constant, and changes with the actual permittivity distribution. Therefore, the employed image reconstruction technique should consider such challenges in order to produce a good image. Although there is no general approach for image reconstruction, it can be categorized according to:

- **Linearity:**
  - ➢ Linear image reconstruction methods, where images are obtained by linearizing a non-linear model, and solving the inverse problem as a linear model.
  - ➢ Non-linear image reconstruction methods, where images are obtained by non-linear image reconstruction algorithms that consider the non-linear relationship between the permittivity distribution and the capacitance measurements.

- **Iteration:**
  - ➢ Non-iterative image reconstruction methods, where images are obtained by calculating the forward and inverse problems once.
  - ➢ Iterative image reconstruction methods, images are obtained by optimizing a set of *objective functional* iteratively.

Any image reconstruction algorithm is a combination of the two categories as per Table 5.1. Image reconstruction methods may be evaluated based on the image precision and the reconstruction speed; accordingly, available image reconstruction algorithms have their own advantages and disadvantages. For example; when $\Delta\boldsymbol{\varepsilon}$ is large, the linearity assumption fails, and therefore linear reconstruction methods will produce imprecise images. Different image reconstruction methods have been reviewed more than a decade ago by [34] and [35]. However, many new and more advanced techniques have been developed since then. In ECT, variations of the direct and iterative techniques have been implemented, in which the most common ones are outlined in this chapter.

Table 5.1. Categorization of image reconstruction methods

		Iteration	
		Iterative	**Non-iterative**
Linearity	**Linear**	• Forward model is linearized. • Solution is optimized iteratively.	• Forward model is linearized. • Solution is calculated once.
	Non-linear	• Forward model is not linearized. • Solution is optimized iteratively.	• Forward model is not linearized. • Solution is calculated once.

5.1 LINEAR NON- ITERATIVE METHODS

5.1.1 Linear Back-Projection (LBP)

The LBP method is one of the oldest image reconstruction methods that is still used for some medical tomography applications such as X-ray CT. This approach was also the first image reconstruction technique used for ECT [101]. Although the images produced were not highly defined, this method announced the first working prototype for ECT image reconstruction and showed its potential value for industrial applications.

Since S in **(4.16)** is non-square, it is considered non-invertible (i.e. has no direct inverse), and therefore the equation cannot be solved directly as:

$$g = S^{-1}\lambda. \tag{5.1}$$

Hence, alternative mathematical techniques should be used to calculate the inverse of S. In LBP, the image vector g can be approximated by using the transpose of the sensitivity matrix, to make the number of columns in the first matrix equal the number of rows in the second matrix, if S is an $M \times P$ matrix then S^T is a $P \times M$ matrix as:

$$\hat{g} = S^T\lambda, \tag{5.2.a}$$

where $\hat{g}$ is an approximate solution of the permittivity distribution. This approximation is based on the previous assumption that S can be considered a linear mapping from the permittivity vector space to the capacitance vector space, so its transpose S^T can be considered as an inverse mapping between the two vector space. Equation **(5.2.a)** is used to get the permittivity value at pixel p (image pixel value) according to its discrete form as follows:

$$\hat{g}(p) = \sum_{i=1}^{N-1}\sum_{j=i+1}^{N} S_{i,j}^T(p)\lambda_{i,j} \qquad for\ (p = 1, 2, \dots, P). \tag{5.2.b}$$

Although this technique is considered easy, simple and fast (i.e. involves single step vector multiplication), it produces poor images with significant artefacts as it ignores the non-linear relationship between the capacitance measurements and the permittivity distribution. Also, it cannot produce good quantitative information, but only poor qualitative images. Hence this technique is not best suited for complex systems.

5.1.2 Matrix Decomposition Based Methods

As mentioned before, the inverse of S in (4.16) cannot be found directly, however, it can be decomposed into a product of matrices (matrix factorization). There are a variety of matrix factorization techniques, though most of them are only applicable for square matrices. For non square matrices like S, singular value decomposition and QR decomposition can be applied to factorize S.

5.1.2.1 Singular Value Decomposition (SVD) method

SVD is a matrix decomposition method that has many applications including the computation of the generalized inverse (pseudoinverse). A generalized inverse of a matrix S is a matrix that retains some properties of the inverse matrix of S but not necessarily all of them. For invertible matrices the inverse and the generalized inverse are the same. However, for singular (non-invertible) matrices like S, a generalized inverse is constructed to obtain a matrix that can act as the inverse of S. The singular value decomposition of S is of the form:

$$S = U \times \Sigma \times V^*, \tag{5.3.a}$$

where

- U is an $M \times M$ unitary matrix (or simply orthogonal if U contains real numbers only) , in which its columns are made up from the eigenvectors of SS^T.
- Σ is a non-negative $M \times P$ diagonal matrix in which its singular values σ are equal to the square roots of the eigenvalues from SS^T or S^TS as:

$$\Sigma = diag[\sigma_1, \sigma_2, \dots, \sigma_P] \qquad where \quad \sigma_1 \geq \sigma_2 \geq \cdots \geq \sigma_P \geq 0. \tag{5.3.b}$$

- V is a $P \times P$ unitary matrix in which its columns are made up from the eigenvector of $S^TS.$
- V^* represents the conjugate transpose of V if it contains complex entries, or simply the transpose of V if V contains real numbers only.

Consequently, the pseudoinverse of S can be expressed as:

$$S^+ = V \times \Sigma^+ \times U^*, \tag{5.4.a}$$

where Σ^+ is the pseudoinverse of Σ, which can be constructed by replacing nonzero entries by their reciprocal as:

$$\Sigma^+ = diag \left[\frac{1}{\sigma_1}, \frac{1}{\sigma_2}, \dots, \frac{1}{\sigma_r} \right]. \tag{5.4.b}$$

Replacing S^{-1} in **(5.1)** with S^+ in **(5.4.a)** give:

$$\hat{g} = S^+ \lambda. \tag{5.5}$$

Although SVD was applied for ECT applications [36] and is considerably effective for solving inverse problems, the quality of the reconstructed images using this method is still not very satisfactory.

5.1.2.2 *Truncated Singular Value Decomposition (TSVD) method*

The idea of truncating the SVD may be treated as a problem of determining the numerical rank of the matrix S. A regularisation parameter is added to **(5.4.b)** accordingly:

$$\Sigma^+ = diag \left[\frac{w_1}{\sigma_1}, \frac{w_2}{\sigma_2}, \dots, \frac{w_r}{\sigma_r} \right], \tag{5.6.a}$$

$$w_i = \frac{\sigma_i^2}{\sigma_i^2 + \alpha} \qquad for\ (i = 1, 2, \dots, r), \tag{5.6.b}$$

where w_i can be considered as a filter and α is a positive regularisation parameter. In TSVD, all singular values smaller than some threshold value (the regularisation parameter) are treated as zeroes in order to illuminate the effect of rounding errors on these singular values. The weights w_i can be chosen accordingly:

$$w_i = \begin{cases} 1 & \forall\ \sigma_i \geq \alpha \\ 0 & \forall \sigma_i < \alpha \end{cases}. \tag{5.6.c}$$

Therefore, if $\sigma_{r_{th}}$ is the smallest singular value greater than α, then equation **(5.6.a)** can be re-written as:

$$\Sigma^+ = diag \left[\frac{1}{\sigma_1}, \frac{1}{\sigma_2}, \dots, \frac{1}{\sigma_{r_{th}}}, 0, 0, \dots, 0 \right]. \tag{5.6.d}$$

TSVD is less sensitive to high frequency noise in the measurement because of the applied filter. On the other hand, determining the truncation level is considered very challenging especially when the singular values of the coefficient matrix are descending [34].

5.1.2.3 QR decomposition

The **QR** decomposition offers an alternative way of solving a system of linear equations (**4.16.b**) without inverting the matrix **S**. the decomposition is based on taking:

$$S = QR, \tag{5.7}$$

where Q is an orthogonal matrix of size $M \times M$, and R is an upper triangular matrix of size $M \times P$. Since the matrix Q is orthogonal, its transpose is equal to its inverse, making (**4.16**) equivalent to:

$$Q^T \lambda = Rg. \tag{5.8}$$

Equation (**5.8**) is easier to solve since R is triangular.

5.1.3 Regularisation Based Methods

Although inverse problems are usually formulated based on their ill posed forward model in infinite dimensional spaces (i.e. (**4.8**)), only finite number of measurements is often obtained. Therefore, only a finite number of unknown parameters (pixels) are usually recovered. This may lead to the problems being reformed in a discrete form (i.e. (**4.16**)) making the problem ill-conditioned. In such cases, regularisation methods can be used to impose additional information (assumptions) on the solution to solve the ill-conditioned system of equations and prevent over fitting. Technically, all measurements produce some error. Considering the error, the system (**4.16**) becomes:

$$\tilde{\lambda} = \lambda + e = Sg, \tag{5.9}$$

where e is the error vector of the capacitance measurement. Ordinary linear least-squares method seeks to minimize the residual as:

$$arg\,min_g \|Sg - \tilde{\lambda}\|_2^2, \tag{5.10}$$

where $\|.\|$ is the Euclidean norm, L2 norm in this case. The *normal equation* from (**5.10**) can be written as:

$$\hat{g} = (S^T S)^{-1} S^T \tilde{\lambda}. \tag{5.11}$$

When **(4.16)** is ill posed, it might be because of either non-existence (over determined case) or non-uniqueness (underdetermined case) of g. The ordinary least-squares method is only applied for over-determined $(M \geq P)$ systems to find an approximate solution when no solution exists, provided that $(S^T S)^{-1}$ exist (**S** has full rank column). However, in case of underdetermined systems $(M < P)$, $(S^T S)^{-1}$ does not exist, and so **(5.11)** cannot be solved directly. This is because a simple least squares minimization will lead to over-fitting. Hence, in order to find a unique solution for the underdetermined system, a regularisation term is usually added to the minimization. A possible general formulation for the regularised inverse problem in the form of unconstrained optimization problem, is to find $\hat{g}$ that minimizes the following function:

$$\hat{g} \to arg\,min_g \|Sg - \tilde{\lambda}\|_2^2 + \alpha Reg(g). \tag{5.12}$$

And so, the regularised solution $\hat{g}$ is found by minimizing the objective functional:

$$arg\,min_g J(g) = \|Sg - \tilde{\lambda}\|_2^2 + \alpha Reg(g), \tag{5.13}$$

where $J(g)$ is an *objective functional*, $\alpha > 0$ is the regularisation parameter to balance the data fitting that can be tuned with different mathematical techniques, $Reg(g)$ is the regularisation term, which is an arbitrary functional that takes different form depending on the regularisation method applied, and the argument in the generalized equation can be set according to the requirement of the solution.

Obviously, the term $\|Sg - \tilde{\lambda}\|_2^2$ in **(5.13)** uses the sum of the squares to achieve numerical accuracy and precision of the solution by minimizing the discrepancy between the measured and estimated capacitances, while the regularisation term attains numerical stability of the solution by trying to keep the estimated solution close to the true one. Hence, regularisation techniques are a trade off between the accuracy and the stability of the solution. In general, any objective functional used for regularisation can be expressed in a standard form:

$$arg\,min\,J(g) = E(g) + \alpha Reg(g), \tag{5.14}$$

where $E(g)$ measures the closeness of the estimated capacitance to the measured ones, and in the standard linear regression (Tikhonov) it is given by $\|Sg - \tilde{\lambda}\|_2^2$, although this term might be modified in extended versions. $Reg(g)$ is the stabilizing function, and one common choice for it is:

$$Reg(g) = \|L_l(g - \overline{g})\|_n^n \qquad \infty \geq n \geq 1, \qquad (5.15)$$

where L_l is a regularisation matrix, which can be any kind of low-pass filters, such as weighted Fourier operator, a derivative operator of order l, a wavelet transform or a finite difference operator of the lth derivative in which its dimensions depends on the order of derivative and the boundary conditions. l can also be used for a variable order $o(g)$ in which case $L_{o(g)}$ is a banded matrix. The most common choices for n are n=1 (L1 norm regularisation) or n=2 (squared L2 norm regularisation), though other choices such as $n (g)$ can be also used. $\overline{g}$ is the estimated solution based on *a priori* information (assumed background permittivity distribution) and $\alpha\|L_l(g - \overline{g})\|_n^n$ is the constraint which seeks to keep the estimated solution close to the true one while keeping the discrepancy between the measured and estimated capacitances to minimum. Regularisation methods are used to generate a set of solutions using *a priori* constraint information, and then extract the best solution out of them. However, there is often no information available about the estimated solution, and hence $\overline{g}$ is taken as zero most of the cases.

Regularisation methods are widely used in image reconstruction and other fields, mostly because of their simplicity, as they can be considered as a simple convex optimization problem. The simplest and most common form to be applied to integral equations of underdetermined systems is Tikhonov's regularisation. Recently, non-linear regularisation methods, such as total variation regularisation, have been developed and applied to ECT, which reportedly are better reconstruction for sharp edges and jumps discontinuity in permittivity. Moreover, some linear iterative image reconstruction methods have an intrinsic regularisation property, e.g., Krylov subspace methods and Landweber, while some others regularise the solution before reconstructing the image.

5.1.3.1 *Tikhonov's regularisation*

One of the most commonly used regularisation methods for linear ill-posed inverse problems is the Tikhonov's regularisation, which has been efficiently applied in numerous fields, with satisfactory numerical performances. Tikhonov's regularisation was used by [44,45] in its simplest form, and also used by [46-49] in different hybrid forms. Tikhonov's regularisation was first used in ECT by [102].

As mentioned before, if a problem is ill-posed, the solution may be non-unique and the computing algorithm will most probably be mathematically unstable, and hence it requires to

be regularised before numerical treatment. Tikhonov's regularisation tries to balance the stability of the solution with its accuracy. In **(5.15)**, if n=2, and L_l is a finite difference operator with $l \geq 0$**,** then the regularisation is called Tikhonov's regularisation and is given by:

$$Reg(g)^{TK} = \|L_l(g - \overline{g})\|_2^2.$$

(5.16)

Consequently, using **(5.13)** and **(5.16)**, the regularised solution $\widehat{g}$ using Tikhonov's regularisation is found by minimizing the objective functional:

$$arg\,min_g J(g) = \|Sg - \tilde{\lambda}\|_2^2 + \alpha\|L_l(g - \overline{g})\|_2^2.$$

(5.17)

By solving the optimization **(5.17)**, an explicit solution, denoted by $\widehat{g}$, is given by:

$$\widehat{g} = (S^T S + \alpha L_l^T L_l)^{-1} S^T \tilde{\lambda}.$$

(5.18)

However, it was reported that Tikhonov's regularisation does not permit sharp edges when $l > 0$ and only results in smooth edges and oscillations. Therefore, the simplest yet most used form of Tikhonov's regularisation is the standard Tikhonov's regularisation, which takes $\overline{g} = 0$ and l=0, giving $L_0 = I$, where I is the identity matrix. Substituting these conditions in **(5.17)** we obtain the following normal equation:

$$(S^T S + \alpha I)\widehat{g} = S^T \tilde{\lambda}.$$

(5.19.a)

Solving for $\widehat{g}$ gives:

$$\widehat{g} = (S^T S + \alpha I)^{-1} S^T \tilde{\lambda},$$

(5.19.b)

where $(S^T S + \alpha I)^{-1}$ does always exist for $\alpha > 0$. Notice that **(5.19.b)** is a modified (regularised) version of **(5.11)** where it substitutes the non-invertible matrix $(S^T S)$ with an invertible one $(S^T S + \alpha I)$.

The quality of the solution using regularisation techniques depends highly on the choice of the regularisation parameter. An optimum α must be chosen in order to get the closest solution to the true one. Methods for tuning α include: the discrepancy principle method [37] and the Unbiased Predictive Risk Estimator (UPRE) [38], which both require *a priori* information about the noise of the measurements. Other methods that require less *a priori* information and more calculations can be also used, such as the generalized cross-validation

method [39], the L-curve method [40-41], the χ^2-curve method [42] and the Residual periodograms method [43]. Generally, the estimation of the parameter α is a very active field of research and new methods are being introduced and implemented constantly. After tuning α, **(5.18)** or **(5.19.b)** can be solved directly or by using techniques such as SVD or generalized SVD.

Although Tikhonov's method is considerably fast and suitable for online applications, it is considered difficult to control, as selecting a fitting regularisation parameter can be a challenging task. Although Tikhonov's L2-regularisation is relatively easy to solve, the reconstructed images are usually blurred and have low resolution. This is because the regularisation does not take advantage of the sparsity of the signal. Also, previous results on the use of Tikhonov's method for ECT image reconstruction showed poor quality of the images reconstructed by the algorithm due to the extreme smoothness effect. However, as it is the most classic method, it is mostly used to compare and assess the efficiency of a new technique, as this thesis will do in later chapters.

5.1.3.2 *Total Variation (TV) regularisation*

TV regularisation was first introduced by [50] and since then it has been mainly applied to digital image processing for noise removal [50] and to solve the *compressed sensing* problem (aka sparse sensing) in different applications [122]. It is based on the principle that capacitance measurements (signal) with extreme and probably false detail have high total variation. Accordingly, this regularisation works on decreasing the total variation of the estimated capacitance measurements subject to it being a close match to the measured capacitance measurements. Total variation assumes that the unknown object is piecewise constant, which allows suppressing noise while maintaining sharp edges in the reconstructed image.

In **(5.15)**, if $\bar{g} = 0$, *n=1*, and L_l is usually a discrete gradient with $l = 1$ $(L_l = \nabla)$, then the regularisation is called total variation regularisation and is given by:

$$Reg(g)^{TV} = \|\nabla g\|_1^1.$$
(5.20.a)

Equation **(5.20.a)** is equivalent of taking the integral of the absolute gradient of g over the entire sensing domain Ω:

$$Reg(g)^{TV} = \int_\Omega |\nabla g| \, d\Omega.$$
(5.20.b)

When $\bar{g} = 0$, $n=1$ and $l > 1$ then **(5.15)** is referred to as higher order TV regularisation. This regularisation technique has advantages over other smoothing techniques such as Tikhonov's regularisation, Gaussian smoothing or median filtering which reduce noise but also smoothen the edges since they cannot reconstruct the jump changes in permittivity at interfaces. By contrast, total variation regularisation removes noise, even in low signal to noise ratios, while keeping important detail such as edges especially when jump changes in permittivity are present. Also, since TV regularisation takes advantage of the sparse structure of the sensitivity matrix, it is considered faster and consumes less amount of memory than standard dense-matrix based algorithms. On the other hand, TV is only capable of restoring functions that are piecewise constant. Moreover, not all underdetermined systems of linear equations have a sparse solution, and therefore total variation cannot be applied for any underdetermined linear system. However, since the ECT sensitivity matrix is sparse in nature, TV regularisation has been applied successfully to ECT systems [51-54, 103-110, 123].

5.2   ITERATIVE RECONSTRUCTION METHODS

Due to the ill-posedness and non-linearity characteristics of the ECT problem, the quality of the reconstructed images using direct reconstruction techniques is not very satisfying. Therefore, iterative methods were later introduced and implemented for ECT to get more accurate reconstruction images. Usually, a direct method (mostly regularisation) is accompanied with an iterative scheme to produce better images. Generally, after acquiring the initial image using any direct reconstruction algorithm, the iterative reconstruction methods update the reconstructed image by:

1. **Solving the forward problem**: this involves recalculating new capacitance values in each iteration based on permittivity values of the current image vector. Also in nonlinear techniques the sensitivity matrix is recalculated in each iteration.
2. **Solving the inverse problem**: this involves finding the value of the permittivity vector by iteratively minimizing the error between the new calculated capacitance values and the measured ones.
3. **Repeating the first two steps** until convergence of a specific value is achieved for the measured and calculated capacitance values.

Determining when and how should the iterations stop is the main challenge in using iterative schemes, as the best image might be achieved somewhere between the iterations. Generally, the new image is found iteratively according to:

$$\hat{g}^{k+1} = \hat{g}^k + \beta \Delta \hat{g}, \qquad\qquad (5.21)$$

where $\hat{g}^{k+1}$ is the updated image vector, $\hat{g}^k$ is the current image and the descent direction $\Delta \hat{g}$ is the error image with a relaxation factor β, which is also called the step length, or the gain factor. β is very critical in the iterative process. Choosing it too large might diverge the solution, while choosing it too small might slow the reconstruction. $\Delta \hat{g}$ can be found using different methods, some of them are mentioned in this section. β can be chosen to be fixed in all iterations [55-56], or to be a variable [57]. The initial guess of the permittivity g^0 can be calculated using any simple algorithm, e.g., LBP.

Although iterative methods guarantee better quality images than direct methods, they are considered more time-consuming since they require more computations. However, with the rapid advance in computers speed and memory, iterative reconstruction is being more used and promise to have a wider use in the future. Also, in some cases convergence is not guaranteed hence, iterative algorithms are mostly used for offline applications. Figure 5.1 shows a flowchart of a typical nonlinear image reconstruction procedure using iterative methods. Linear iterative image reconstruction methods follow the same procedure but do not re-calculate the sensitivity matrix at every iteration.

Any non-iterative image reconstruction algorithm can be solved iteratively using **(5.21)**. In addition, other iterative algorithms of different methods have been developed so far, and some of the most common ones are mentioned briefly in this section.

5.2.1 Landweber's Iteration

The Landweber iteration was originally developed to solve ill-posed linear inverse problems, but later was extended to solve non-linear problems with constraints. The Landweber iteration was adapted for ECT applications by [55], and by [57-60,121] in other modified versions. Landweber algorithm is achieved by solving **(5.10)** using an iterative method as in **(5.21)** giving:

$$\hat{g}^{k+1} = \hat{g}^k - \beta S^T (S \hat{g}^k - \tilde{\lambda}), \qquad 0 < \beta < \frac{2}{\sigma_1^2}, \qquad (5.22.a)$$

where σ_1 is the largest singular value of **S**. Because of the relaxation parameter, β, the Landweber algorithm is considered to have an intrinsic regularisation property. If we write:

$$J(g) = \left\| S g - \tilde{\lambda} \right\|_2^2, \qquad\qquad (5.22.b)$$

then **(5.22.a)** can be expressed in terms of the gradient as:

$$\hat{g}^{k+1} = \hat{g}^k - \beta\nabla J(g^k),$$

(5.22.c)

and therefore the algorithm is considered a special case of the gradient descent.

The Landweber iteration algorithm is considered easy to implement due to its low computational complexity. However, since it is a gradient descent algorithm, the rate of convergence is relatively low and falls into a local minimum. As a result, the accuracy of the images reconstructed is not always satisfactory. One approach to improve its convergence is to adjust it to give the so-called projected Landweber iteration. When compared with other methods (LBP, Tikhonov, iterative Tikhonov and SVD), the projected Landweber iteration reportedly produced the best result [34].
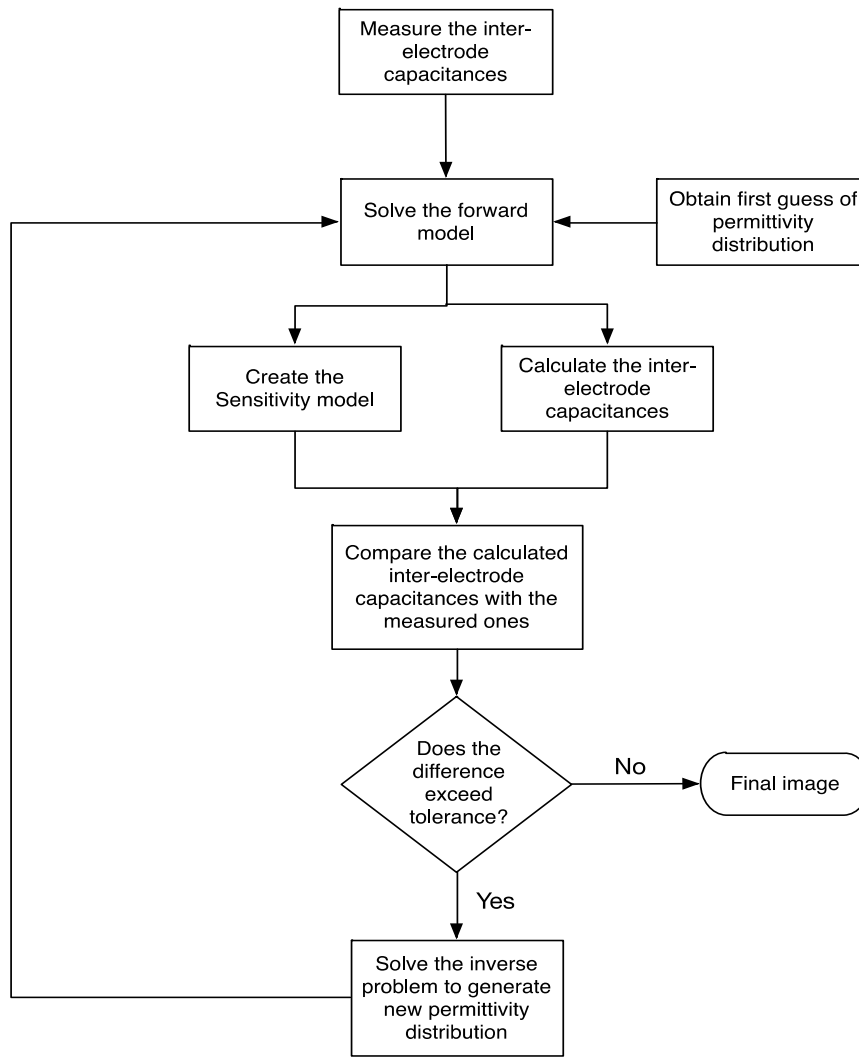
Figure 5.1. A typical nonlinear image reconstruction process of ECT.

58

5.2.2   Algebraic Reconstruction Technique (ART)

In ART, the image is improved in an iterative scheme by updating the medium permittivity distribution g as a function of the difference between the measured capacitance values $\tilde{\lambda}$ and the calculated capacitance values Sg. It does so by converging to the image vector of **(5.11)** without the need to invert the matrix $S^T S$. The updated ECT image based on **(5.21)** is described by the following expression:

$$\hat{g}^{k+1} = \hat{g}^k + \beta^k \frac{(S_i \hat{g}^k - \tilde{\lambda}_i)}{S_i S_i^T} . S_i^T \qquad (i = 1, 2, \dots, M), \tag{5.23}$$

where S_i is the ith row of the matrix S, $\tilde{\lambda}_i$ is the ith component of the vector $\tilde{\lambda}$, and β^k is a relaxation parameter, which can be neglected in simple forms of ART. The kth iteration of **(5.23)** is based on the kth row in **(4.16.b)**. This means that ART uses only one capacitance measurement in each iteration step. When the last row in **(4.16.b)** is already updated, and more iterations are still required, the first raw is used again to obtain the $(k + 1)^{th}$ iteration.

There are numerous ways for choosing the ith $\tilde{\lambda}_i$, S_i and β^k at the kth iteration, and so, different algorithms for ART have been developed. Mainly, they differ from three aspects:

1. How to choose β^k
2. How to choose $\tilde{\lambda}_i$ and S_i
3. How to update the pixels from the estimated image.

ART was first introduced by [61] for computed tomography, and later was applied to ECT in its standard form [62], and in different modified forms [63]. Although ART is considered simple, it is considerably slow and the quality of the images reconstructed by it for ECT applications was not very acceptable.

5.2.3   Simultaneous Image Reconstruction Technique (SIRT)

As mentioned earlier, ART uses only one capacitance measurement in each iteration step, and hence does not guarantee convergence if the capacitance measurements contains a substantial error. SIRT addresses this issue by including the average of the sum of all the errors between the measured and the calculated data. The updated ECT image based on the SIRT algorithm can be given as:

$$\hat{g}^{k+1} = \hat{g}^k + \beta^k \frac{1}{\sum_i S_i} \sum_i (\tilde{\lambda}_i - S_i \hat{g}^k) S_i \quad (i = 1, 2, \dots, M). \tag{5.24}$$

The above expression takes the soft field effect of ECT into account and so it is insensitive to the errors of the capacitance measurements. Although ART and SIRT are always convergent, they can only converge to a local minimum. This might not guarantee that the final version of the produced image is the best one, since the best image might occur in-between iterations. Just like ART, SIRT is still considerably slow; also it shows a smoothing effect that affects the image quality especially in interfaces. To overcome this smoothing effect, thresholding methods are usually applied. SIRT is also a descent gradient method and was first used for ECT applications by [64].

5.2.4 Newton's Method (Nonlinear)

Newton's method (aka Newton–Raphson method) can be used to find consecutively better approximations to the roots of a functional, J (i.e. **(5.17)**), defined in a Banach space. The Newton–Raphson method can be expressed as:

$$\hat{g}^{k+1} = \hat{g}^k - [J'(\hat{g}^k)]^{-1}J(\hat{g}^k). \tag{5.25.a}$$

Equation **(5.25.a)** can be expressed as gradient descent algorithm as:

$$\hat{g}^{k+1} = \hat{g}^k - [\nabla^2 J(\hat{g}^k)]^{-1}\nabla J(\hat{g}^k), \tag{5.25.b}$$

where $\nabla^2 J(.)$ and $\nabla J(.)$ are the Hessian matrix and the gradient vector of the objective function, respectively. To avoid converge to saddle points, equation **(5.25.b)** is modified by adding a relaxation parameter as:

$$\hat{g}^{k+1} = \hat{g}^k - \beta^k[\nabla^2 J(\hat{g}^k)]^{-1}\nabla J(\hat{g}^k). \tag{5.25.c}$$

The value $[\nabla^2 J(\hat{g}^k)]^{-1}\nabla J(\hat{g}^k)$ should be evaluated at each step, making it unfeasible for problems with a complex objective functional and with a large number of variables. This is because the computation of both gradient and Hessian can be very time consuming. For a simple *objective functional* given by **(5.22.b)**, **(5.25.c)** can be simplified as:

$$\hat{g}^{k+1} = \hat{g}^k - (S^{T,k}S^k)^{-1}S^{T,k}(S^k\hat{g}^k - \tilde{\lambda}). \tag{5.25.d}$$

5.2.5 Levenberg–Marquardt Algorithm (LMA) (Nonlinear)

Usually, $(S^{T,k}S^k)^{-1}$ in (5.25.d) does not exist, and thus the Newton–Raphson iterative algorithm can be modified to get the inverse as:

$$\hat{g}^{k+1} = \hat{g}^k - (S^{T,k}S^k + \alpha^k I)^{-1}S^{T,k}(S^k\hat{g}^k - \tilde{\lambda}), \qquad (5.26.a)$$

where α is a positive scalar, which can be considered as regularisation parameter. Since α^k changes in every iteration, this method is called the Levenberg–Marquardt method. If the sensitivity matrix is fixed throughout the iteration process, the expression might be called linear iterative Tikhonov's regularisation and its given by:

$$\hat{g}^{k+1} = \hat{g}^k - (S^T S + \alpha^k I)^{-1}S^T(S\hat{g}^k - \tilde{\lambda}). \qquad (5.26.b)$$

This method was successfully applied to ECT by [65-66]. A generalized Levenberg–Marquardt algorithm for an arbitrary objective functional can be given as:

$$\hat{g}^{k+1} = \hat{g}^k - \beta^k[\nabla^2 J(\hat{g}^k) + \alpha^k I]^{-1}\nabla J(\hat{g}^k). \qquad (5.26.c)$$

5.3 OTHER METHODS

Many other algorithms for ECT image reconstruction were introduced recently, some include; the total variation method, model-based reconstruction (MOR) [35], the genetic algorithm [67], the generalized vector sampled pattern matching method [68], the simulated annealing algorithm [69], robust principle component analysis method [75], the neural network algorithm [70,71], The enclosure method [76], the Offline Iteration and Online Reconstruction (OIOR) algorithm [72], the Helmholtz-type regularisation method [73], the multi-scale image reconstruction algorithm [77], the particle filter and Kalman filter methods [78], compressed sensing principle method [79], the four-dimensional reconstruction method [74] and fuzzy mathematical modelling [82,83]. Shape based reconstruction methods are also employed such as the level set method [80,81], which will be explained in Chapter 7.

Chapter VI

6   EARLY STAGE DEPOSIT DETECTION IN PIPELINES

Deposits can build up to sufficient levels on the interior wall of the pipeline creating a flow restriction. ECT technique in particular promises superior advantages for deposit monitoring as it is considered fast, compact, safe, easy to interpret, and cost effective. Thus, ECT is considered in this study to image the internal cross section of a poly pipe to detect the formation of deposits in early stages. Poly pipes are superseding their metallic and concrete counterparts and are being more popular in industries such as oil, gas and water due to their advantages of being resistant to chemical processes, cost effective, light and easy to install [84]. However, ECT has the prominent drawback of offering low-resolution images due to the ill-posedness and non-linearity of the ECT problem. Therefore, this chapter suggests the use of ECT with a new limited region tomographic image reconstruction technique using a narrowband pass filter to enhance the resolution of the produced images. The experimental results showed that different deposit regimes and fine deposits could be detected with high resolution.

6.1   LIMITED REGION TOMOGRAPHY (LRT)

Numerous inversion algorithms were suggested for ECT image reconstruction as reviewed in Chapter 5. However, due to the ill-posedness and non-linearity of the ECT problem, the quality of the reconstructed images is still under research for enhancement. In this study, the Tikhonov's regularisation method was modified to reconstruct the permittivity distribution by adding a narrowband pass filter to enhance the resolution. First, to find the initial image, standard Tikhonov's regularisation is used for minimizing the *objective functional* (**5.17**). By solving this optimization objective functional for $\overline{g} = \mathbf{0}$ and *l=0* (giving $L_0 = I,$ where I is the identity matrix), the explicit solution, denoted by $\hat{g}$, is given by (**5.19.b**).

The Tikhonov's regularisation method was successfully applied to ECT before; however, this study suggests a modification to the method taking into account prior knowledge regarding the geometry of the pipe to produce a high-resolution image. The proposed method is based on a limited region tomographic image reconstruction using a narrowband pass filter [85,86]. Figure 6.1.a shows the narrowband pass filter applied to a test pipe for deposits and scale detection. Only the "limited region" within the inner surface of the pipe will be reconstructed

to monitor the deposit condition of the pipe. The limited region is selected to be larger than the test pipe inner radius (R1) so that it can tolerate a small displacement error of the pipe from its centre. This narrowband region has a relatively uniform sensitivity due to the circular cross-section of the pipe and the equal distances from the ECT electrodes. This fact makes the limited region better conditioned compared to the traditional Full Region Tomography (FRT) where the sensitivity varies moderately throughout the imaging region (sensitivity increases closer to the electrodes and reduces towards the centre). This particular limited region is a favourable one, making it well suited for pipe detection. The principle of the LRT is to increase the accuracy by limiting the imaging area, which consequently reduces the number of unknown pixels and thus enhances the resolution as shown in Figure 6.1.b, where the Region Of Interest (ROI) is now a fraction of the whole region. Other than the better accuracy, another advantage of the LRT over FRT is the faster performance due to the reduction of pixels used in the reconstruction. Also, because of the reduced number of pixels, the inverse problem becomes better posed in the LRT, and so is considered more robust than the FRT.

FEM mesh models were designed and used for the inverse problem, where 1367 and 12184 three-nodded nonhomogeneous triangular elements corresponding to 739 and 6219 nodes were generated to create the mesh for the FRT and LRT respectively (Figures 6.2.a and 6.2.b). However, only 691 elements of the dense LRT mesh were used to construct the limited region ring as shown in Figure 6.2.c.

(a)   (b)
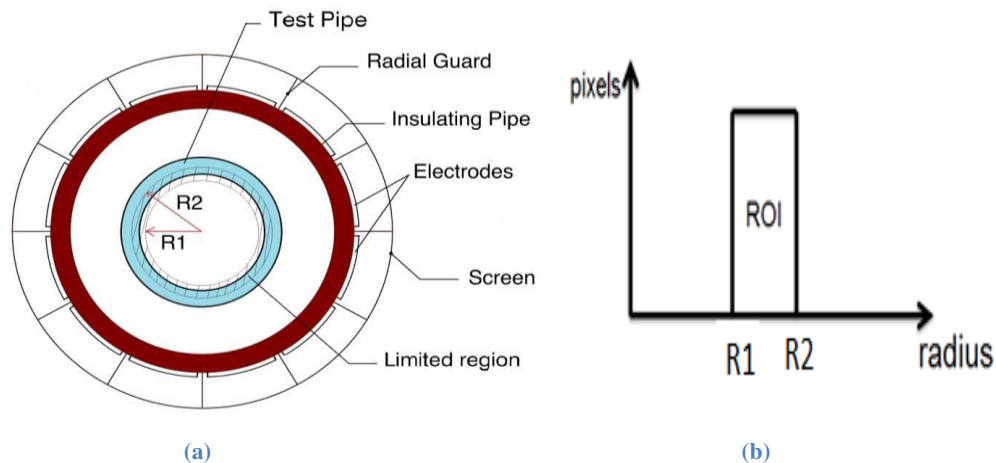
Figure 6.1. LRT for deposit detection, (a) pipe cross-section view, (b) spatial narrowband pass filter.

| (a) | (b) | (c) |
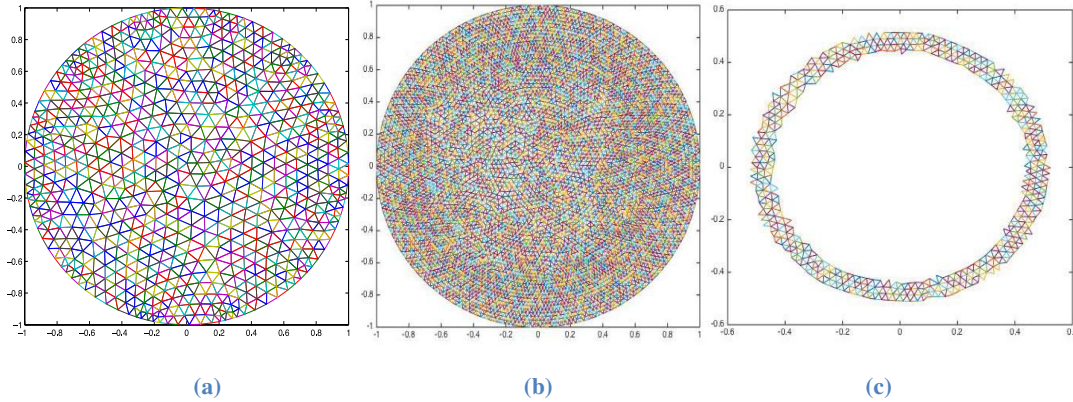
Figure 6.2. FEM mesh for a) FRT b) LRT dense mesh c) Limited region ring used for the LRT.

6.2   EXPERIMENTAL EVALUATION OF THE PIPELINE INSPECTION

The 12-electrode sensor used in the experiments is built in the University of Bath Engineering Tomography Lab (ETL) and has an inner diameter of 151mm (Figure 6.3), whereas the data acquisition unit used is a commercial PTL300E-TP-G capacitance measurement unit from Process Tomography Limited. The unit can collect sets of capacitance data at 100 frames\s with an effective resolution of 0.1 fF and measurement noise level better than 0.07 fF. Typically, samples concentration down to 1% of the upper calibration value (corresponding to the case where the sensor is filled with the higher permittivity material) can be measured. MATLAB is used for data collection, image reconstruction and processing. Two experimental models mimicking the pipeline and the deposits were prepared in the laboratory in order to simulate scale/Asphaltenes/wax and sand/black powder deposits in real processes. The test pipe is made of polyethylene, which has a relative permittivity of 2.25. The inner and external diameter of the test pipe are 77 mm and 88mm, respectively (Figure 6.4.b), and it was placed in the centre of the ECT sensor, as shown in Figure 6.4.a. This is because the sensitivity of the measurements in the middle of the imaging region is almost uniform.

64
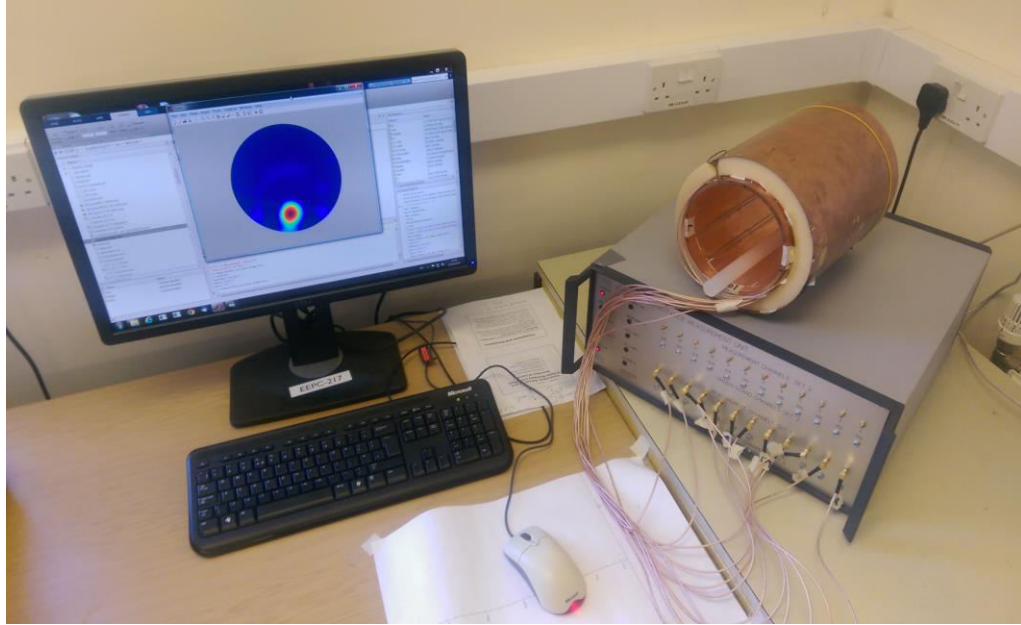
Figure 6.3. The ECT system of the University of Bath Engineering Tomography Lab.
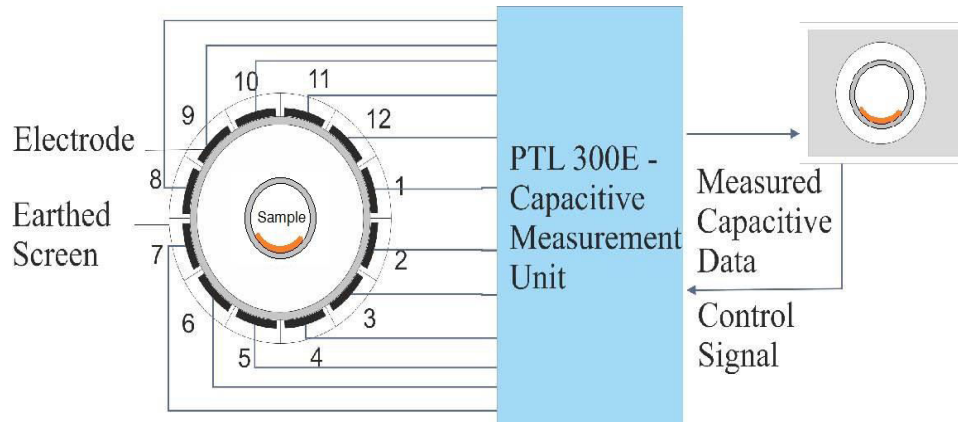
(a)
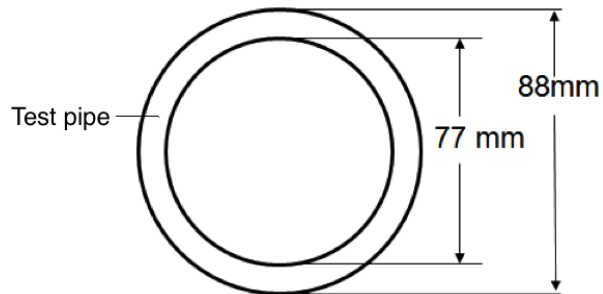
(b)

Figure 6.4. (a) Block diagram of the ECT system, (b) the dimensions of the test pipe used for deposit detection.

6.2.1   Geometric Analysis

The first part of the experiment is done in order to test the capability of the algorithm to detect the build-up of deposits inside a pipeline or an equipment (e.g. scale/Asphaltenes/wax). To simulate this case, typical printer papers with relative permittivity of 3.85 were used to investigate 4 different cases:

- **In case 1:** a pile of 24 pieces of paper ($\approx 3\ mm$ in thickness), which are 52.5mm wide and 297mm long (Figure 6.5.a), was placed internally in one side of the test pipe.

- **In case 2:** two piles of paper of the same dimensions used in case 1 were placed internally in two opposite sides of the test pipe.

- **In case 3:** 20 papers of a typical A4 size (210mm X 297mm) ($\approx 3\ mm$ in thickness) (Figure 6.5.b), were piled and rolled inside the inner surface of the test tube.

- **In case 4:** case 1 and 3 were combined by adding the pile of paper used in case 1 to the setting of case 3.

For the sake of comparison, both LRT and FRT were constructed for all cases and are shown in Figure 6.6.

<div align="center">(a)   (b)</div>
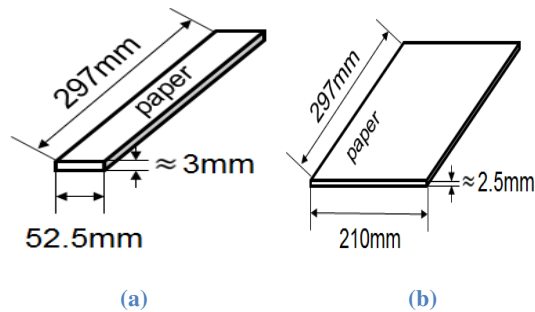
Figure 6.5. The paper-folds and their dimensions.

6.2.2   Resolution Analysis

The second part of the experiment is done to assess the resolution of the algorithm in term of the smallest amount of deposits it can detect. In an attempt to simulate deposits in pipelines, very fine sand (0.0625 to 0.125 mm diameter) with relative permittivity of 2.5 to 3.5 was used. Six Different layers of sand with varying thicknesses, namely, 0.5, 1, 2, 3, 4 and 5 mm were investigated and shown in Figure 6.7. As it can be seen in Figure 6.7, all locations of the deposits have been identified in both sets of images from LRT and FRT, however the LRT

provides superior results in identifying the level of deposit. We decided not to show the thersholded images of the deposit in LRT as it can be subjective, but the scale of reconstructed value shows that when thersholded with the same level will produce information about the level of deposit.

Experimental setting   **Full Region Tomography (FRT)**   **Limited Region Tomography (LRT)**
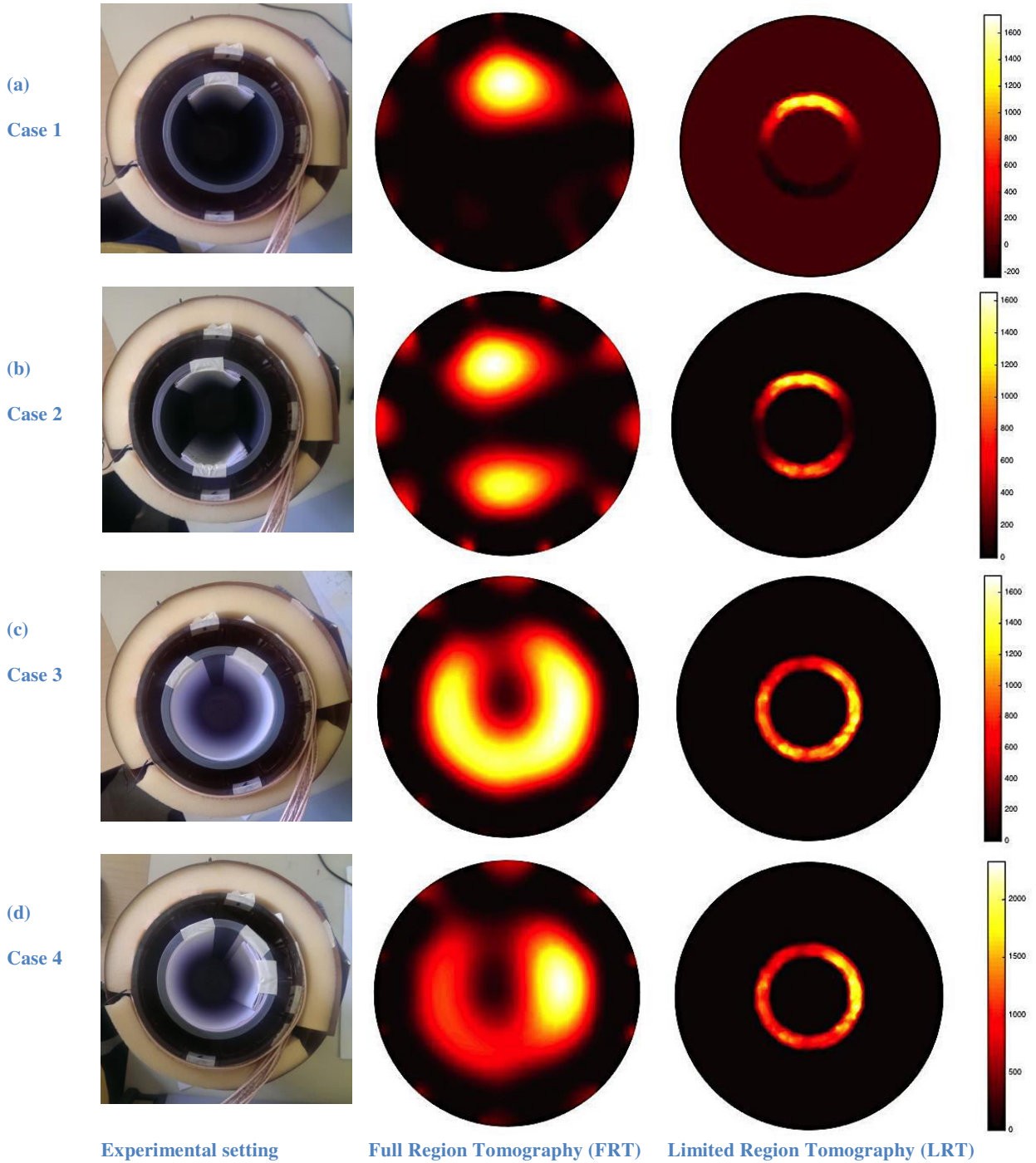
Figure 6.6. Reconstruction of paper samples as models of scale, Asphaltenes or wax deposits (a) case 1, (b) case 2, (c) case 3, and (d) case 4.

	(a) 0.5 mm	(b) 1 mm	(c) 2 mm	(d) 3 mm	(e) 4 mm	(f) 5 mm

Experimental setting   **Full Region Tomography (FRT)**   **Limited Region Tomography (LRT)**
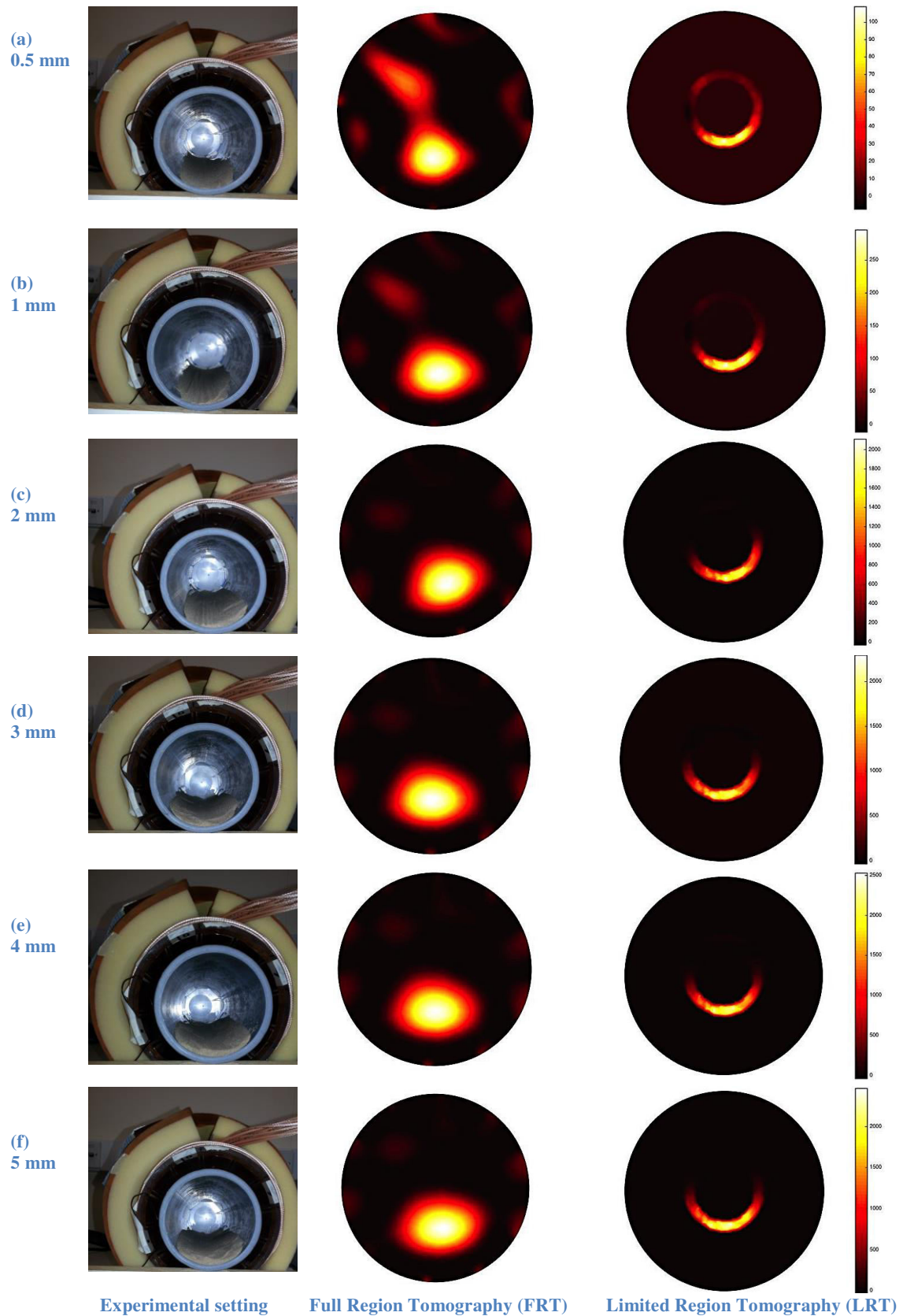
Figure 6.7. Reconstruction of various layers of sand deposits.

6.3 DISCUSSION

From Figures 6.6 and 6.7, it can be noticed that both LRT and FRT were able to detect fine deposits and give information about their location. However, the LRT generally provides a more robust solution in all experimental scenarios presented here and could remarkably detect a layer of deposit as small as 0.5 mm without noise. This indicates that the proposed LRT method allows a detection of deposit with the resolution of 0.085% of the entire imaging region, which makes the ECT a very good method for detection of deposit. The experimental results in Figure 6.6 show that different deposit regimes can be detected along the inner wall of the pipe. This conclusion is promising in terms of detecting deposit accumulation inside pipelines, which increases the interior pipe wall roughness and leads to other more serious problems. Note that due to the high resolution of the LRT technique the test pipe is almost always visible in the reconstructed images. This is because even though the test pipe is considered as a reference and subtracted from the measured data, the LRT could detect the small associated error.

As mentioned earlier the limited region chosen in the LRT, shown in Figure 6.1.a, has a relatively uniform sensitivity due to its concentric location. To illustrate the advantage of this orientation, an SVD analysis of the sensitivity matrix for the LRT and FRT was carried out, normalized and then compared, as shown in Figure 6.9. In order to visualize the superiority of this technique, a new limited region was created according to Figure 6.8 where the region of interest is now a shifted circle to the right. According to the Picard condition, the number of singular values above the noise level of the measurements represents the amount of information that can be extracted from the inverse model. It can be seen from Figure 6.9 that only 29 singular values for the circle orientation (Figure 6.8) were above the noise level, while both the LRT and FRT had 57 and 52 singular values above the noise level, respectively.

Concluding from the results, the ECT system with the proposed LRT algorithm provides a non-invasive inspection method for non-conductive pipes. This inspection can help improve the accuracy of flow meters and allow early detection then early removal of deposits. ECT sensors can be designed in almost any geometrical form, so the proposed method could be extended to other geometries allowing inspection of deposit inside tanks and other types of vessels. This technique is not necessarily applied for static cases. The same concept can be easily adapted to assess real live processes. For example, the process flow is known to be

homogenous in particular locations in the pipeline (i.e. after a static mixer or after a particular orientation of the pipeline). In such locations this technique can be applied in such a way to image only a small portion of the pipe's cross-section. This small portion will be representative of the whole cross section and such information can be updated to reflect the entire area.
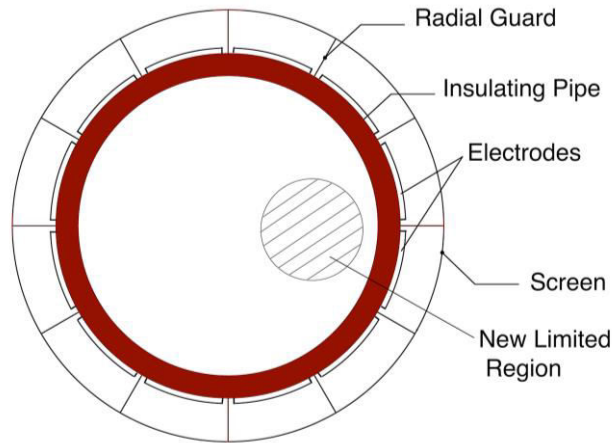
Figure 6.8. New limited region, an example of a circle in the corner, created for the sake of comparison with the proposed LRT.
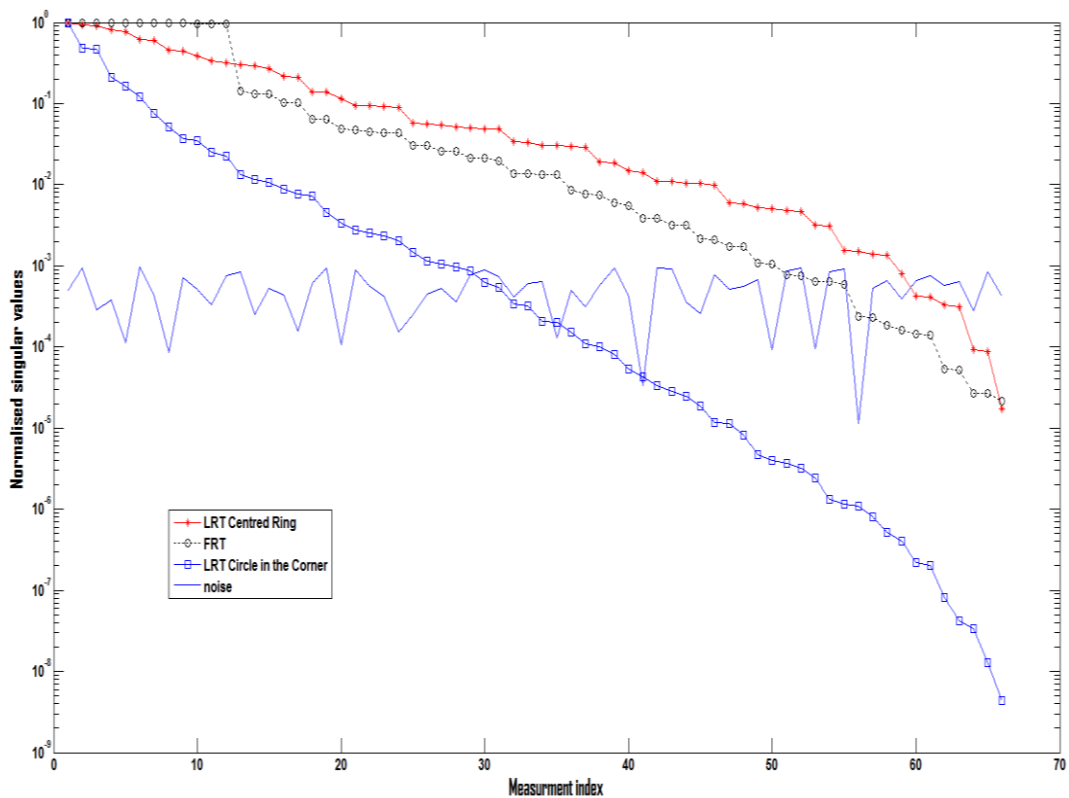
Figure 6.9. SVD analysis of the Jacobian matrix for the LRT, FRT and new LRT.

Chapter VII

7   METAL DETECTION USING ABSOLUTE VALUE ECT DATA

Most studies for process ECT employ classical iterative reconstruction techniques, where the inverse problem is solved iteratively by updating the estimated model, thus improving the match between the measured and the calculated capacitance. However, such iterative techniques require stabilization, and thus a least-squares functional is usually augmented by some additional regularisation term. Such regularisation may lead to 'over-smoothing' the reconstructed images, which makes the characterization of all the different phases in terms of size and contrast a major challenge, especially when one of the phases has low concentration or has relatively higher permittivity. This is because the linearity assumption fails when $\Delta\varepsilon$ given by **(4.13.c)** is large, and therefore linear reconstruction methods will produce poor images. Thus, so far, the ECT system has mainly been used to image low-contrast non-conductive media, not taking into consideration the more complicated scenarios of multiphase media. This is because if the conductivity of the imaged object is high, the capacitance measuring circuit will be almost shortened by the conductivity path and a clear image cannot be produced using the standard image reconstruction approaches. This chapter challenges this limitation by attempting to adapt conventional ECT systems to image metallic objects (i.e. highly conductive) with high resolution.

Different from dielectric specimen whose conductivity is negligibly low, metallic material normally is of high conductivity ($\delta > 10^8$ S/m). Any electric field applied through a conductor will force the inner free charges to move until the net electric field is zero inside the conductor, i.e. the electric potential is the same on any point of the conductor. In ECT, the electrostatic equilibrium on metallic materials will create an increment on the measured capacitances. This chapter sets out to allow a better understanding of how metallic deposits could be imaged using conventional ECT device and how state of the art algorithms could enhance this application. This application is particularly important for the oil and gas industry, as some of the contaminants such as black powder may be conductive in early stages. This chapter offers new findings about the ECT behaviour towards metal deposits, as this is not really addressed in the literature despite the industry need for it.

Also studying the ability of ECT systems to image conductive material will help develop more robust algorithms that caters for all multiphase flow scenarios such as when water is

involved. Level set method [92] was employed in this study to image metal objects by using absolute ECT measurements. The results were compared to two reportedly powerful techniques, namely, linear single step Tikhonov's regularisation method (already explained in Section 5.1.3.1) and linear iterative total variation regularisation method (already explained in Section 5.1.3.2) with the split Bregman iteration introduced by [124], which both use two sets of ECT data to reconstruct the image in time difference mode. The results indicate that the applications of conventional ECT systems can be extended to metal samples using the suggested algorithms and forward model, and so other techniques are expected to behave accordingly.

7.1   FORWARD MODELLING OF METAL SAMPLES

When a source electrode is energised, the free charge inside the metal start moving by the force of electric field. The metal will reach the electrostatic equilibrium in a very short time ($\sim 10^{-19}$s) [125], making the electric potential the same everywhere within the metal region:

$$\phi^a = \phi^b \qquad for \ a, b \in \Omega_{metal}. \tag{7.1}$$

It is clear from **(4.8)** that the measured capacitance is the surface integration of electric displacement of the sensing electrode. The metal performs like a void of electric field/displacement, shortening the distance between the source and detector electrodes, i.e. the capacitance will be increased.

This section studies the ability of ECT to image conductive materials by creating a model of an inclusion of high permittivity to simulate the scenario of conductive objects. In [120], the authors proposed a 1-dimensional (1D) ECT model (shown in Figure 7.1) to demonstrate the increase in capacitance due to conductive objects by introducing a dielectric inclusion of permittivity $\varepsilon = \varepsilon_x . \varepsilon_0$, where ε_x is its relative permittivity. To match the capacitance of the metal standing between the two electrodes (Figure 7.1.a), the inclusion must be of the size of $D_x = \frac{\varepsilon_r}{\varepsilon_x - 1} . D$, where D is the size of the metal (Figure 7.1.b). The 1D analysis implies that the metal in ECT can be potentially imaged as a dielectric sample. To make the size of the dielectric inclusion close to the metal, $\frac{\varepsilon_x}{\varepsilon_x - 1}$ must be close to 1, i.e. ε_x is a big value. This study extends this ECT metallic evaluation model from 1D to 2-Dimensional (2D). To validate the implication above, a squared metal of the side length of 0.6 unit length (the external radius of the insulation wall is 1 unit length) is presented in Figure 7.2.
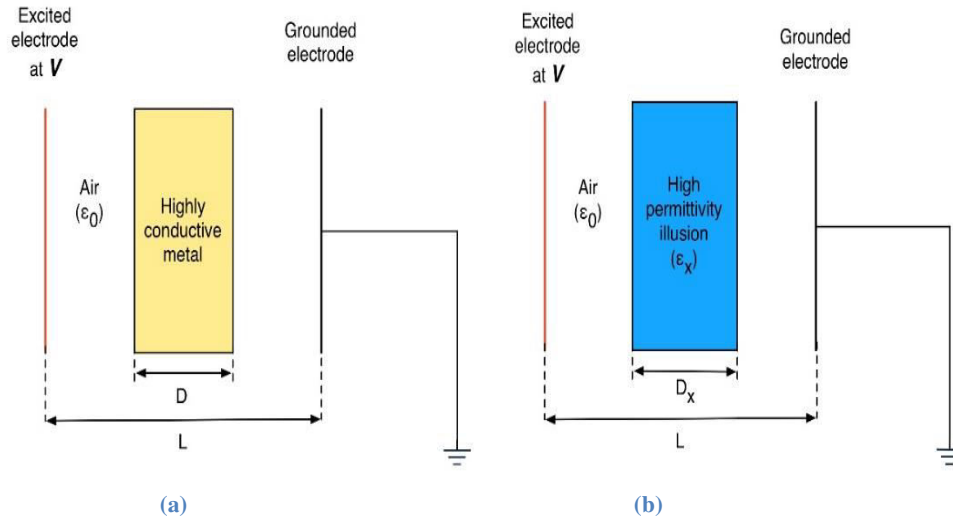
Figure 7.1. 1D analysis of the same capacitances from two different inclusions between one pair of electrodes (a) a metallic sample of the size D (b) a dielectric sample of permittivity ε_x and size D_x.
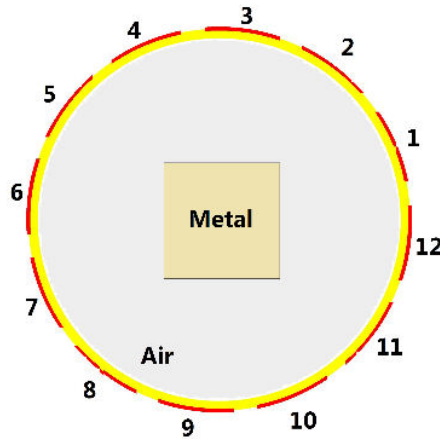
Figure 7.2. A square metallic sample in a 2D ECT sensor with 12 electrodes.

In the first test, the equal potential (ep) model, all the points in the region of metal are set to be equal in potential which follows the real scenario within the sensor when a metal object is imaged. Then in the second test, high permittivity (hp) model, the metal is replaced by a dielectric material where its relative permittivity is set to ε_x =1000, so the dimension is almost the same as the metal, as $\frac{\varepsilon_x}{\varepsilon_x - 1} = 1.001$. The simulation results based on FEM are presented in Figure 7.3. When electrode 12 is excited, the two sets of electric potential distribution, ϕ_{ep} and ϕ_{hp}, from ep and hp models are plotted in Figure 7.3.a and Figure 7.3.c respectively. By energising the electrodes in turn, the two sets of 66 mutual capacitances, C_{ep} and C_{hp}, are obtained and plotted in Figures 7.3.b and 7.3.d respectively.

	Electric potential distribution (electrode 12 is energised)	Mutual capacitances (*M*=66)
Equal potential model	(a) ϕ_{ep}	(b) C_{ep}
High permittivity model	(c) ϕ_{hp}	(d) C_{hp}
The difference between two models	(e) $\phi_{ep} - \phi_{hp}$	(f) $C_{ep} - C_{hp}$
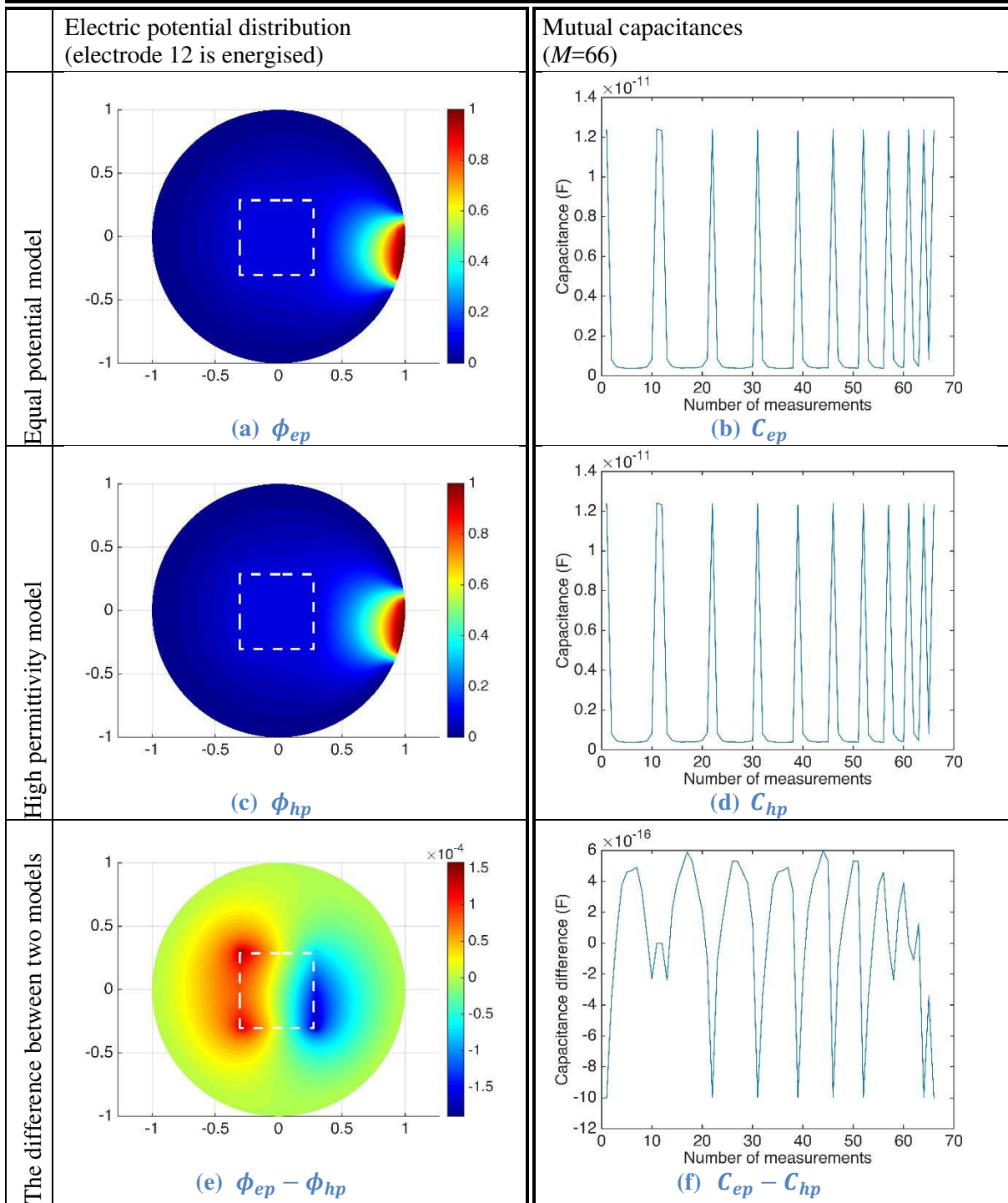
Figure 7.3. Electric potential distribution of a square metal in ECT (marked by the white dashed lines) and the mutual capacitances for the ep model, hp model and the difference between them.

In Figure 7.3.e, the colour bar indicates that the difference between the potential distributions of these two models, $\phi_{ep} - \phi_{hp}$, which appears to be very small. The points of minimum (blue) and maximum (red) electrical potential are located in the two edges of metal, which are the closest and farthest from the energised electrode 12. This shows that the electrical potential in the high permittivity region is decreasing but in a very small rate, while there is no potential change in the same region of the ep model. In Figure 7.3.f, the difference in the mutual capacitances, $C_{ep} - C_{hp}$ is 5 orders less in magnitude than the C_{ep} and C_{hp}, which is at noise level for a real measurement. This means that capacitance measurements cannot tell the difference between the metal and the dielectric of high permittivity of the same size.

Since ECT imaging is to reconstruct the permittivity distribution within the sensing region, the mutual capacitances are the key input for the process of the inverse solver. However, the capacitance measurements are not affected by the permittivity of the metallic material under test, but by the electrostatic equilibrium of the highly conductive material. The hp model is an approximate model to compensate for the zero electric field on that region of metal; meanwhile this approximation converts the problem of imaging metal to dielectrics of high permittivity. Therefore, applying the inverse solvers for high contrast problems will result in a promising reconstruction for the metallic material. To bridge the changes in permittivity distribution and the changes in capacitance measurements, a sensitivity matrix $\mathbf{S}$ is built according to **(4.11)**.

7.2   LEVEL SET (LS) METHOD

Osher and Sethian first developed the level set method in the 1980s for modelling the front propagation of surfaces under curvature [87]. Since then, it has been used in many disciplines, such as image processing, fluid mechanics, optimal design, computer graphics, computational geometry and inverse problems. Santosa [88] was the first to develop two computational approaches for solving inverse problems based on the level set method in which the desired unknown is a region in $\mathbb{R}^2$ or $\mathbb{R}^3$. The first approach results in a Hamilton-Jacobi equation, which is nonlinear time-dependent partial differential equation for the level set function whose evolution minimizes the residual in the data fit. Whereas the second approach is based on an optimization method (i.e. Gauss-Newton) that generates a sequence of level set functions that reduces the residual. For electrical and electromagnetic tomography in particular, some initial studies were conducted using different types of level set techniques for shape reconstruction [90,91].

In the level set method, the constructed shapes are given as the zero level set of one or more higher dimensional function called the "level set functions". By updating this function the constructed shapes can move accordingly, and thus the topological changes can be performed automatically. Hence, instead of finding the internal permittivity of the unknown shape, $\mathcal{E}_{int}$, the level set technique is able to represent boundaries of different shapes by the zero level set of a predefined level set function ψ. For a 2-dimensional problem, suppose D is the characteristic set of interest. Then the boundary of the inclusion ∂D is the interface between the two materials and is given by the zero level set of the function ψ as:

$$\partial D = \{r : \psi(r) = 0\}. \tag{7.2}$$

Thus, the image parameter at each point r, $\varepsilon(r)$ can be represented in terms of a level set function as:

$$\varepsilon(r) = \begin{cases} \mathcal{E}_{int} \ for \ \{r : \psi(r) < 0\}, \\ \mathcal{E}_{ext} \ for \ \{r : \psi(r) > 0\}. \end{cases} \tag{7.3}$$

Accordingly, the capacitance data can be described as a function of a level set function $C = F(\psi(\varepsilon(r)))$. Equation (7.3) represents the mapping that assigns to a given level set function the corresponding permittivity distribution. This can be denoted as $\varepsilon = \varphi(\psi(\mathbf{r}))$. Representing the $\boldsymbol{\varepsilon}(\mathbf{r})$ through a level set function $\psi(\mathbf{r})$ instead of representing it in terms of D makes the image reconstruction process simpler, as no *a priori* assumption about the topology (i.e. spatial location) or the nature (i.e. shape and size) of D is needed. On the other hand, due to the nonlinear dependence of $\boldsymbol{\varepsilon}$ on ψ, this approach will lead to a nonlinear inverse problem even if the forward problem was linearized. Notice that in this inverse problem statement, $\boldsymbol{\varepsilon}(\mathbf{r})$ is not the unknown, instead it only performs as an intermediate parameter to arrive at the real unknown, which is the level set function $\psi(\mathbf{r})$.

In order to facilitate the dependence of the forward map on small changes in the shape, we look at the variation of ε caused by a variation in ψ. Let $\mathbf{r}$ be a point on the boundary of D, which is represented by (7.2). Suppose $\psi(r)$ and $\mathbf{r}$ are perturbed by a small variation giving $\psi'(\mathbf{r}) = \psi(\mathbf{r}) + \delta\psi(\mathbf{r})$ and $r' = r + \delta r$, respectively. This will result in changing the region D to be a new region denoted by D'. Accordingly, ε will vary to $\varepsilon' = \varepsilon + \delta\varepsilon$. In Figure 7.4 notice that r which was on the boundary of D and on $\psi(\mathbf{r}) = 0$ now belongs to $\mathcal{E}_{int}$ of $\psi(\mathbf{r})$ and the boundary of D' ($\psi'(\mathbf{r}) = 0$) according to (7.3). Figure 7.4 shows how updating the level set function will change the status of each point r to belong to either $\boldsymbol{\mathcal{E}_{int}}$ or $\boldsymbol{\mathcal{E}_{ext}}$ of the

updated level set function $\psi'(\mathbf{r})$.
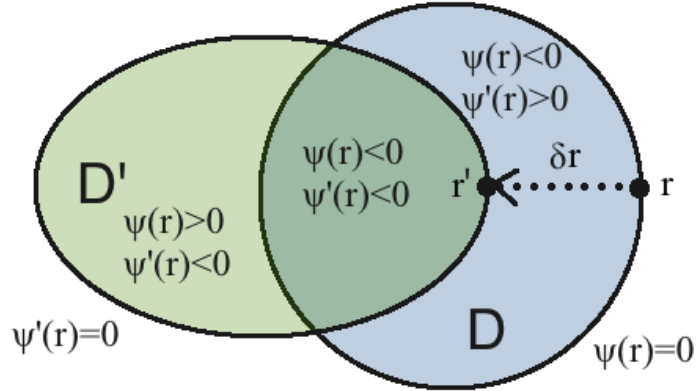
Figure 7.4. The geometry of the variation of the point r under a variation of the level set function.

This level set function ψ is given as *a priori* assumption at first and then updated in such a way that moves the boundaries accordingly. Such updates are chosen in a way that reduces a given cost function. One of the first employed techniques for updating moving boundaries is based on a time evolution approach leading to a Hamilton-Jacobi equation. However, another approach for shape reconstruction using level set is the use of optimization methods as an alternative to shape evolution, which was first suggested by Santosa [88]. To find the update of the level set, different optimization techniques can be employed. This study employs a modified optimization approach based on the Gauss-Newton method to derive the updates for the level set function.

In the optimization approach, a sequence of surfaces $\psi_k(\mathbf{r})$ such that $D_k \to D$ where $\partial D_k = \{\mathbf{r} : \psi(\mathbf{r}) = 0\}$ is generated. To solve the inverse problem in a least-squares sense, the minimizer of the objective *functional* $J(\psi(\varepsilon))$ is found as:

$$arg\ min_\psi J(\psi(\varepsilon)) = \|F(\psi(\varepsilon(\mathbf{r}))) - C\|_2^2 + \alpha Reg(\psi(\varepsilon(\mathbf{r})), \qquad (7.4)$$

where $\alpha>0$ is the regularisation parameter that can be tuned with different mathematical techniques and $Reg(\psi(\varepsilon(\mathbf{r}))$ is the regularisation term, which is an arbitrary functional that takes different forms depending on the regularisation method applied, and the argument in the generalized equation can be set according to the requirements of the solution. Different regularisation methods have been used to enhance the level set method such as curve shortening [89,92,93]. The regularisation term has much less effect on the problem when using a level set method, which makes the problem better posed. Using a modified Gauss-Newton approach for minimizing the nonlinear regularised least-squares functional $J(\psi)$ in

(7.4) we arrive at the following equation for the level set evolution:

$$\psi\,(\varepsilon)^{k+1} = \psi\,(\varepsilon)^{k} + \xi^{k}(\boldsymbol{B}^{T,k}\boldsymbol{B}^{k}+\alpha^{k}\boldsymbol{L}^{T}\boldsymbol{L})^{-1}\boldsymbol{B}^{T,k}(F(\psi\,(\varepsilon)^{k}) - \boldsymbol{C}), \qquad (7.5)$$

with $\boldsymbol{B} = \boldsymbol{SK}$, and $\boldsymbol{K} = c\chi$, where

- ➤ $\boldsymbol{L}$ is the regularisation matrix. In this study we considered $\boldsymbol{L}^{T}\boldsymbol{L} = \boldsymbol{I}$, alternatively other regularisation matrices can also be used such as the Laplacian,
- ➤ ξ is the step size (relaxation) parameter, which is the magnitude of change in shape in every update. The step size can stay constant for all alterations or can be changed with the iterations. For this study the step size was chosen by trial and error and was held constant for all iterations,
- ➤ $\boldsymbol{B}$ is the narrowband Jacobian matrix, which represents the sensitivity values of only those few elements surrounding ∂D of all different regions,
- ➤ $\boldsymbol{S}$ is the sensitivity matrix for all elements of the FEM mesh, and
- ➤ $\boldsymbol{K}$ is the discretised form of $\varepsilon = \varphi\,(\psi(\boldsymbol{r}))$, which includes the indicator function χ of a small narrowband of half width an FEM element centred at ∂D and a constant c as a normalization factor.

As it can be noticed from **(7.5)**, the inverse problem of the interfaces between two different materials is solved using a narrow-band method where only the surrounding pixels are inverted. This technique tends to improve the computational cost and the condition number of the discrete inverse problem by decreasing the number of unknowns compared to the traditional pixel based image reconstruction.

Both the regularisation parameter α and the step size parameter ξ need to be tuned in order to arrive at their optimal choices, which depend on the mesh density, the permittivity contrast and the initial guess of the permittivity values. In general, the larger α is chosen, the smoother the updates will be and the harder for the scheme to perform splitting of the topological changes. In this study, α was manually tuned for each case. However, other techniques can be applied to make the reconstruction process more automatic. The initial guess of the level set functions can be any kind of function, however, the most common choice is a distance function $\psi^{k} = -dist(\partial\text{D})$. In this paper, we choose a circular inclusion to be the initial guess for the level set function as:

$$\psi^k = (X - X_0)^2 + (Y - Y_0)^2 - \vartheta^2, \tag{7.6}$$

where (X_0, Y_0) are the cartesian coordinate of the centre and ϑ is the radius of the circular inclusion. This nonlinear level set algorithm can work with one capacitance data (i.e. absolute capacitance data). In this case the background data of free space is used for a simple scaling calibration of the forward model.

7.3   EVALUATION OF METAL MONITORING USING CONVENTIONAL ECT

The capacitance measurement unit used was PTL300E, which is a commercial product from process tomography LTD [28]. The signal frequency of the measurement system is 1.25 MHz, i.e. the period of switching is 0.8μs. This means that it provides enough time for the conductor to reach the electrostatic equilibrium [125]. The effective range of capacitance measurement is from 0.1 fF to 2.0 pF. The sensor consists of 12 electrodes. The internal radius of the tank is R1=9.5cm the external is R2=10cm. Each electrode in the width of 4.5cm is evenly distributed on the periphery. MATLAB was used for data collection, image reconstruction and processing. FEM mesh models were designed and used for the inverse problem, where 1367 three-node nonhomogeneous triangular elements (i.e. pixels) corresponding to 739 nodes were generated to create the mesh.

Two types of sample are used in this experiment: sample 1 is a rectangular metal of size 8.2cm x7.5cm while sample 2 is a cylindrical pipe with an external diameter of 6.3cm. In test 1 the rectangular metal is placed in the centre of the ECT sensor while in test 2 the rectangular metal was slightly shifted clockwise. In tests 3, 4 and 5, one then two then three cylindrical pipes were placed in the centre of the ECT sensor.

The proposed LS algorithm was used to reconstruct the images and the results are shown in Figure 7.5 along with the linear single step Tikhonov's regularisation method and the linear iterative total variation regularisation with the split Bregman iteration. Regularisation parameter of 10^{-5} was selected for all Tikhonov and LS results, while 10 and 12 iterations were used for the split Bregman and the level set minimisations respectively to get the produced imaged. This number represents the least number of required iterations to produce an acceptable image). The norms of the error between the measured and calculated capacitances of tests 3, 4 and 5 for all iterations are shown in Figure 7.6. The level set reconstructed images shown in Figure 7.5.d are based on the minimum residual norm.
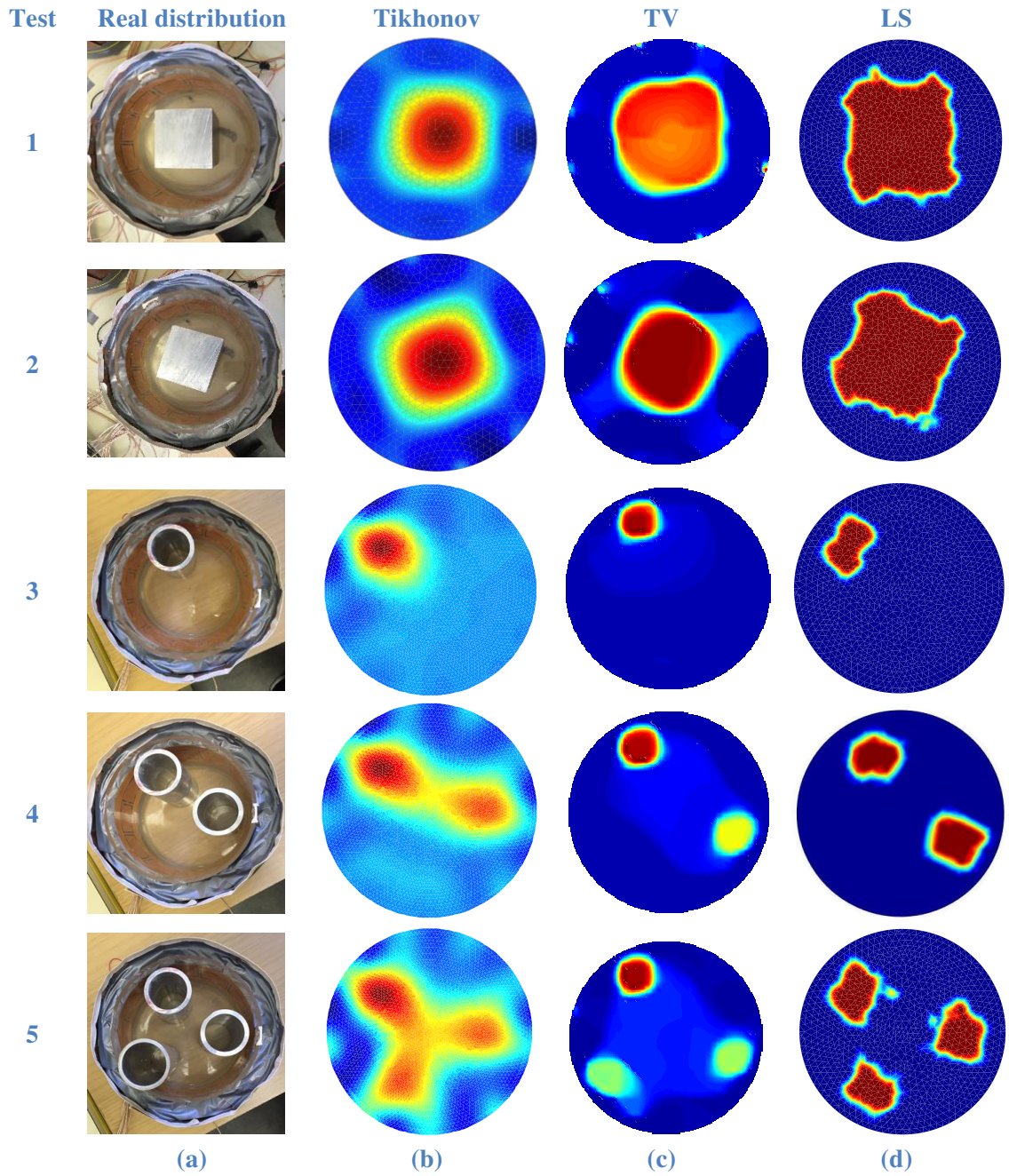
Figure 7.5 Reconstructed images: (a) the experimental setup, (b) the reconstructed shape using the standard Tikhonov's regularisation method, (c) the reconstructed shape using linear total variation method, (d) the reconstructed shape using the level set method.
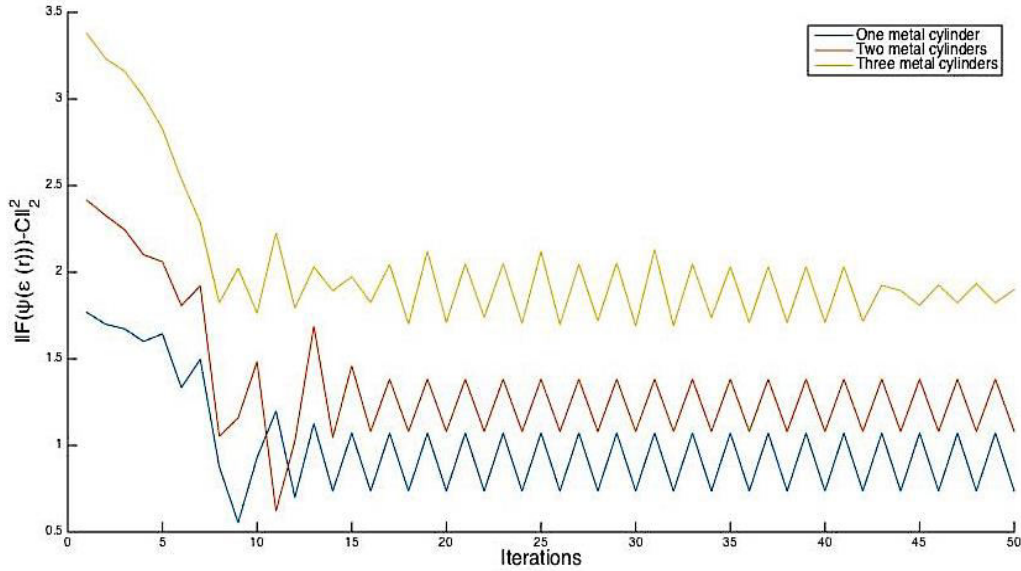
Figure 7.6. The norms of the error between the measured and calculated capacitances for 50 iterations of the level set method for one metal cylinder, two metal cylinders, and three metal cylinders.

7.4 DISCUSSION

The objective of this study was to demonstrate the possibility to adopt conventional ECT systems to image conductive materials such as metal or water. Initially the ECT forward model was verified, concluding that a very large permittivity can be used to represent the metallic samples. From Figure 7.5, it can be seen that this objective can be better achieved by the LS method, which preserves the edges of images better than the TV or Tikhonov's regularisation methods. In terms of resolving different objects within the reconstructed images, LS method also was the most effective. Although TV showed good results compared to the traditional Tikhonov's regularisation method in term of identifying all objects, it gives fails information about the detected objects as it can be seen from the colour scales of test 4 and 5 (which gives the assumption that two different materials are included).

Although LS method depends on the choice of permittivity values for the background and inclusion, this is not a problem for metallic sample imaging as any high permittivity value will be a good representation of metallic samples (e.g., 4 or above). In the LS method, the high-contrast inclusions are incorporated explicitly in the LS model without them dominating the entire domain. This makes the LS method more suitable for high-contrast image reconstruction with sharp boundaries than traditional regularisation-based methods, which have the limitation of over-smoothing the reconstructed image particularly when a high-contrast inclusion is present. Furthermore, LS method can recover the geometry of the

81

unknown interface despite any previous knowledge except for the permittivity value of the metal, which can be any arbitrary high value. This can be seen from our choice of the initial guess (i.e. a circle in the centre of the domain), which does not nearly represent the true shape. Still, an accurate image was retrieved even though the initial guess was far away from the true shape.

Another advantage of the suggested level set method is its ability to improve the computational cost and the condition number of the discrete inverse problem by reducing the number of unknowns compared to other traditional pixel based image reconstruction methods. This can be observed from **(7.5)** where the inverse problem is solved by using a narrow-band method in which only the adjacent pixels are inverted. Furthermore, since the level set method requires only absolute ECT data without any reference data, it is considered more robust for real-life applications. Based on the proposed forward model there is an infinite large change in permittivity, which is a suitable scenario for a binary reconstruction such as LS.

The computational time for a single step Tikhonov's algorithm is 1.1 sec, while iterative TV has computational time of 2.1 sec for 10 iterations and nonlinear level set method took 5.3 sec for 12 nonlinear iterations. These are all done in a mesh of 2064 elements. The computational time is indicated for comparison purposes, for real time imaging this can be optimised. The computation time was not the only limitation of the LS method, but also the instability of the method shown in Figure 7.6. Such behaviour could be attribute to the choice of the tuning parameters and it is worth further investigations. On the other hand, since the regularisation parameters were chosen empirically the results in Figure 7.5 are considered somewhat subjective. However, the results highlighted the superiority of TV and LS methods for this application (i.e. imaging conductive material using conventional ECT system) and paved the way for adapting the LS method for imaging multiphase media with a dominating phase (i.e. a higher permittivity phase). Also, since TV method showed promising results, perhaps curved based regularisation could be investigated in the future enabling better shape recovery for LS reconstruction.

Chapter VIII

8   MULTI-PHASE IMAGING USING ABSOLUTE VALUE ECT DATA

Multiphase flow measurement is a vital topic in the process industries especially the oil and gas exploration & production due to the critical need for measuring the individual phases of oil, gas and water in crude production. In this chapter, a multiphase shape reconstruction based on the level set method for ECT is presented, where the multiphase framework for image segmentation developed by [89] and the narrowband level set formulation developed by [92] are modified and employed to tackle this non-linear problem. Both high and low contrast cases of a multiphase reconstruction are studied. In this approach, the permittivity values of all different phases are approximated and assumed to be known while their size, shape, and location are recovered from the data. The aim of our reconstruction is to correctly determine the location of the present phases and their concentration. This is done by estimating the size and contrast of every phase without an emphasis on the exact shape of the phases but rather an estimated one. The multiphase level set shape reconstruction results shown in this chapter are some of the first ones using experimental data of ECT. Such information has the potential to be used for multiphase flow metering.

8.1   MULTIPHASE LEVEL SET BASED INVERSE PROBLEM

Equation **(7.3)** is suitable for two-phase reconstruction; however, it can be extended to cover multiple phases as several authors have suggested. One of the earliest and most common methods for multiphase image reconstruction is based on the colour level set technique, which was first proposed by Vese and Chan [89] for image segmentation. In this technique, the evolution of up to 2^W different phases can be described using W level set functions. However, in this study, a modification of the colour level set method suggested by [93] was employed for the ECT reconstruction. In this approach, m different phases are described by using $W=m$-1 level set functions. Therefore, three level set functions ($\psi_1(\mathbf{r})$, $\psi_2(\mathbf{r})$ and $\psi_3(\mathbf{r})$) are used to represent four phases (Figure 8.1) where each of the four phases is allowed to have any complex topology. Accordingly **(7.3)** can be extended to be:

$$\varepsilon(\mathbf{r}) = \begin{cases} \mathcal{E}_1 & for\ \{\mathbf{r}:\ \psi_1(\mathbf{r}) \leq 0\}, \\ \mathcal{E}_2 & for\ \{\mathbf{r}:\ \psi_1(\mathbf{r}) > 0\ and\ \psi_2(\mathbf{r}) \leq 0\}, \\ \mathcal{E}_3 & for\ \{\mathbf{r}:\ \psi_1(\mathbf{r}) > 0\ and\ \psi_2(\mathbf{r}) > 0\ and\ \psi_3(\mathbf{r}) \leq 0\}, \\ \mathcal{E}_4 & for\ \{\mathbf{r}:\ \psi_1(\mathbf{r}) > 0\ and\ \psi_2(\mathbf{r}) > 0\ and\ \psi_3(\mathbf{r}) > 0\}. \end{cases} \tag{8.1}$$
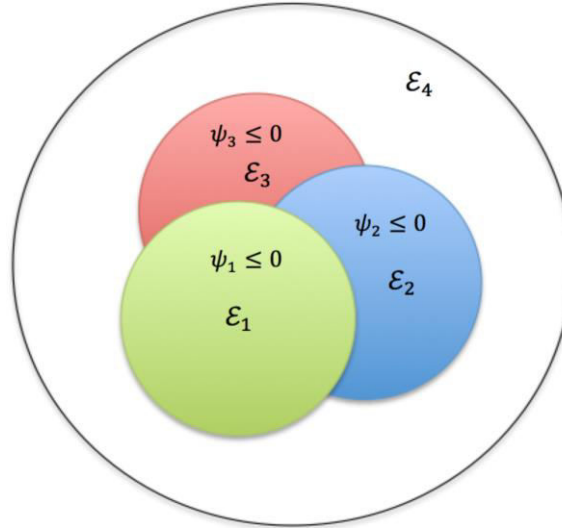
Figure 8.1. Employed level set representation of four different phases (i.e. $\mathcal{E}_1, \mathcal{E}_2, \mathcal{E}_3$ and $\mathcal{E}_4$) by three level set functions (ψ_1, ψ_2, ψ_3 and ψ_4).

The rest of the theory is similar to what was explained in Chapter 7.2 but developed for three level set functions instead of one. For the initial guess of the level set functions, 3 separated circular inclusions were chosen to be the initial guesses for the three level set functions according to **(7.6)**. Absolute capacitance measurement was employed as explained earlier. Figure 8.2 shows a flowchart of the level set ECT image reconstruction algorithm developed for this study.

8.2   EVALUATION OF MULTIPHASE MONITORING USING LEVEL SET METHOD

To demonstrate the power of this algorithm for multiphase monitoring simulated and experimental results of low contrast and high contrast cases are shown and discussed. For the low contrast case, more than two different phases, which all have low permittivity values are imaged and analysed. This case can be related to real life scenarios such as when a pipeline is carrying $\mathcal{E}_1 = gas$, $\mathcal{E}_2 = oil$ and $\mathcal{E}_3 = low\ permittivity\ deposits$. On the other hand, for the high contrast case, a combination of low permittivity and high permittivity phases are imaged and analysed. This case can be related to real life scenarios such as when a pipeline is carrying $\mathcal{E}_1 = gas$, $\mathcal{E}_2 = oil$, $\mathcal{E}_3 = deposits$ and $\mathcal{E}_4 = water$. This case is relatively harder to image using traditional pixel based methods as the inverse problem becomes highly nonlinear when a high permittivity component is introduced as it dominates the region. FEM mesh models were designed and used for the inverse problem, where 1367 three-nod nonhomogeneous triangular elements (i.e. pixels) corresponding to 739 nodes were generated to create the mesh.
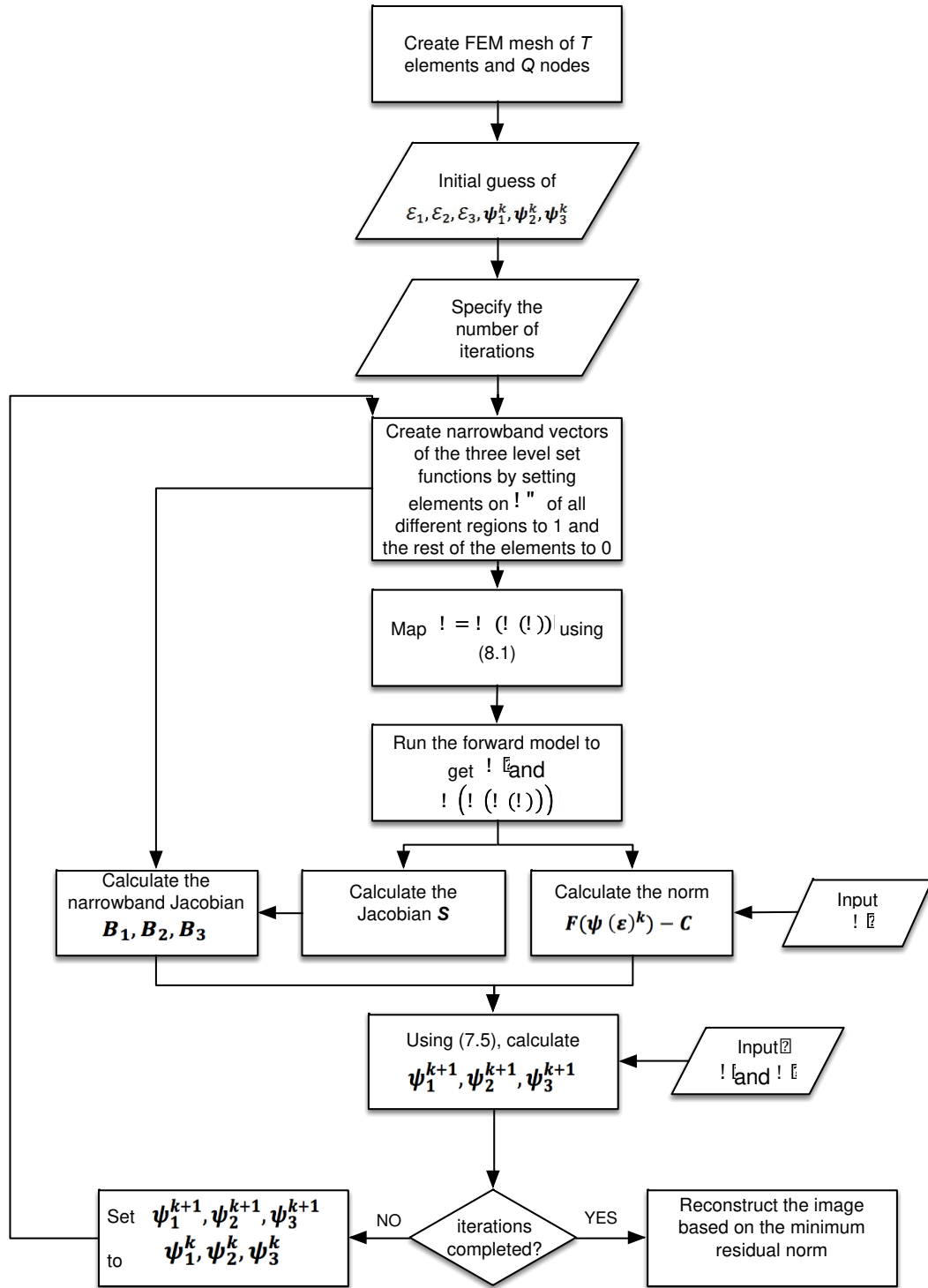
Figure 8.2. Flowchart of the level set ECT image reconstruction algorithm developed for this study.

8.2.1 Simulation Results

For the sake of comparison, the traditional Tikhonov's regularisation image reconstruction simulation results for both cases are shown and discussed to illustrate the advantage of the shape based reconstruction methods over the classical pixel based methods.

8.2.1.1 Case 1: low contrast simulation

A 4-phase low contrast simulation was conducted and the results for both the level set method and the standard Tikhonov's regularisation image reconstruction method are shown in Figure 8.3 along with the true shape for the sake of comparison. The permittivity values used in the simulation were $\mathcal{E}_1 = 4$, $\mathcal{E}_2 = 3$, $\mathcal{E}_3 = 2$ and $\mathcal{E}_4 = 1$. In order to construct the level set image, 250 iterations were used and the norms of the error between the simulated and calculated capacitances for all iterations are shown in Figure 8.4. The level set reconstructed image shown in Figure 8.3.b is based on the minimum residual norm, which in this case appeared in iteration 155. This shows that the best result might not occur in the latest iteration, rather somewhere in the iteration process. Accordingly, the algorithm might just terminate at the minimum residual iteration to reduce the computation cost.

(a) (b) (c)
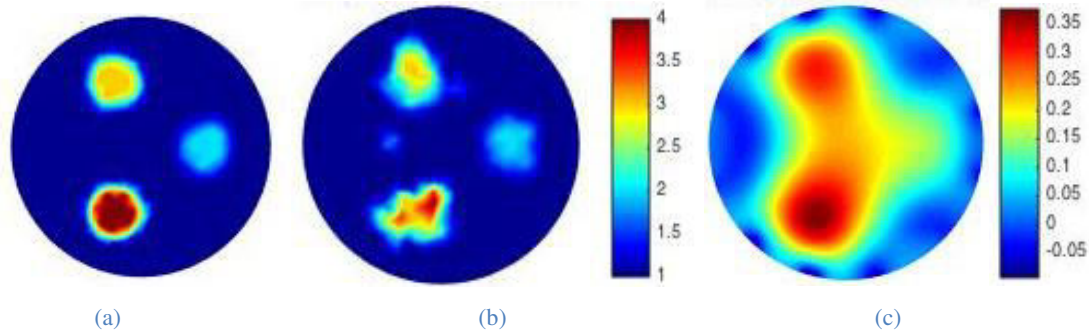
Figure 8.3. Simulation results for case 1 (a) the true shape of the simulation (b) the reconstructed shape using level set method (c) the reconstructed shape using standard Tikhonov's regularisation image reconstruction method.

Figure 8.5 shows the histograms of the permittivity distribution per pixel (FEM element) for the true shape, the level set reconstruction and the standard Tikhonov's regularisation image reconstruction. The obvious similarity between the true shape and the level set reconstruction histograms demonstrate the superiority of the level set method over the traditional Tikhonov's regularisation image reconstruction. The histogram of the level set method shown in Figure 8.5.b shows only 4 phases and each pixel strictly belongs to one and only one of the 4 possible phases. On the other hand the histogram of the standard Tikhonov's regularisation

86

image reconstruction method shown in Figure 8.5.c shows a large range of permittivity values, which makes such methods harder to threshold and hence information about the individual phases are harder to obtain.

Figure 8.4. The norms of the error between the simulated and calculated capacitances for 250 iterations of the level set method for case 1.

(a)

(b)

(c)

Figure 8.5. The histograms of the permittivity distribution per pixel for case 1 (a) true shape, (b) the level set reconstruction, (c) the standard Tikhonov's regularisation image reconstruction.

87

8.2.1.2 Case 2: high contrast simulation

A 4-phase high contrast simulation was conducted and the results for both the level set method and the standard Tikhonov's reconstruction method are shown in Figure 8.6 along with the true shape for the sake of comparison. The permittivity values used for the 4-phase simulation were $\mathcal{E}_1 = 80$, $\mathcal{E}_2 = 3$, $\mathcal{E}_3 = 2$ and $\mathcal{E}_4 = 1$. In order to construct the level set image, 250 iterations were used and the norms of the error between the simulated and calculated capacitances for all iterations are shown in Figure 8.7. The level set reconstructed image shown in Figure 8.6.b is based on the minimum residual norm, which in this case appeared in iteration 172. Figure 8.8 shows the histograms of the permittivity distribution per pixel for the true shape, the level set reconstruction and the Tikhonov's regularisation image reconstruction.

(a)   (b)   (c)
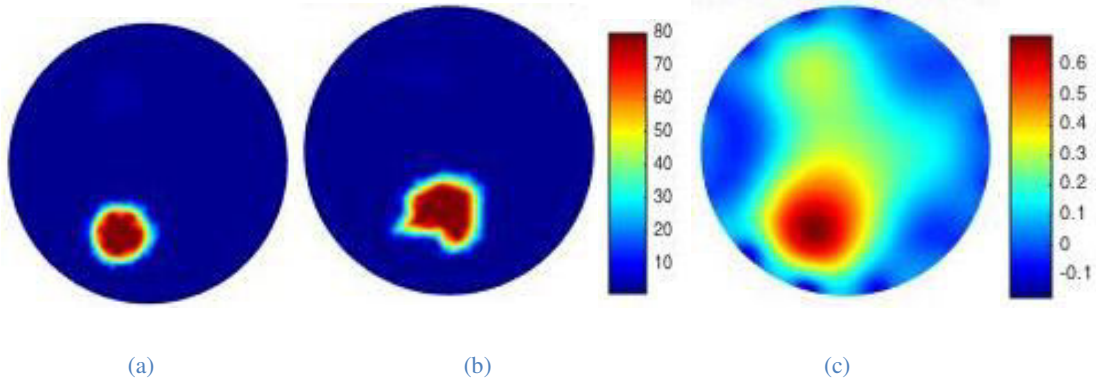
Figure 8.6. Simulation results for case 2 (a) the true shape of the simulation (b) the reconstructed shape using level set method (c) the reconstructed shape using standard Tikhonov's regularisation image reconstruction method.

From Figures 8.6.a and 8.6.b, it can be seen that the high permittivity phase of water is dominating the region and thus it is hard to see with the bare eye the lower permittivity phases. However, all phases do exist in the data and this is evident by the histograms of the permittivity distribution per pixel shown in Figures 8.8.a and 8.8.b. Also, the number of reconstructed pixels per phase was extracted to calculate the phase volume fraction and it is shown in Table.3.

Figure 8.7. The norms of the error between the simulated and calculated capacitances for 250 iterations of the level set method for case 2.

(a)

(b)

(c)
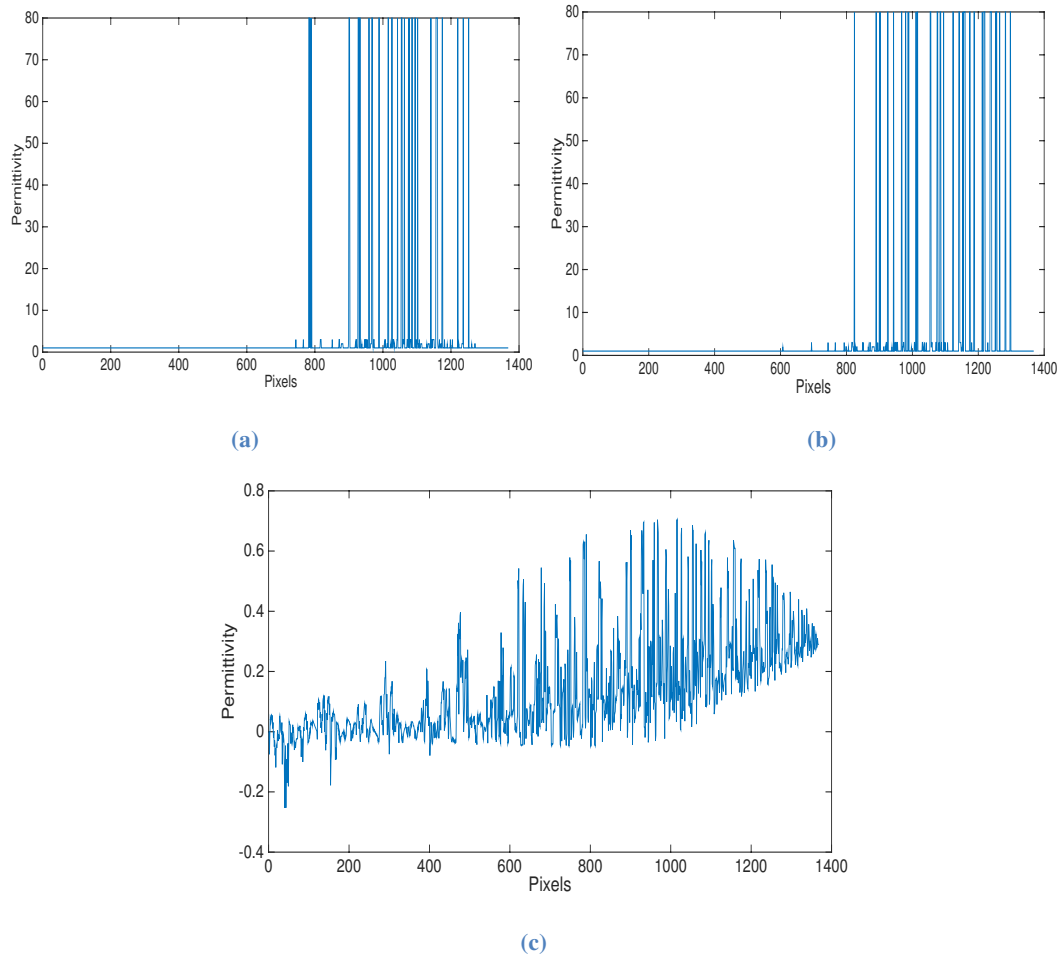
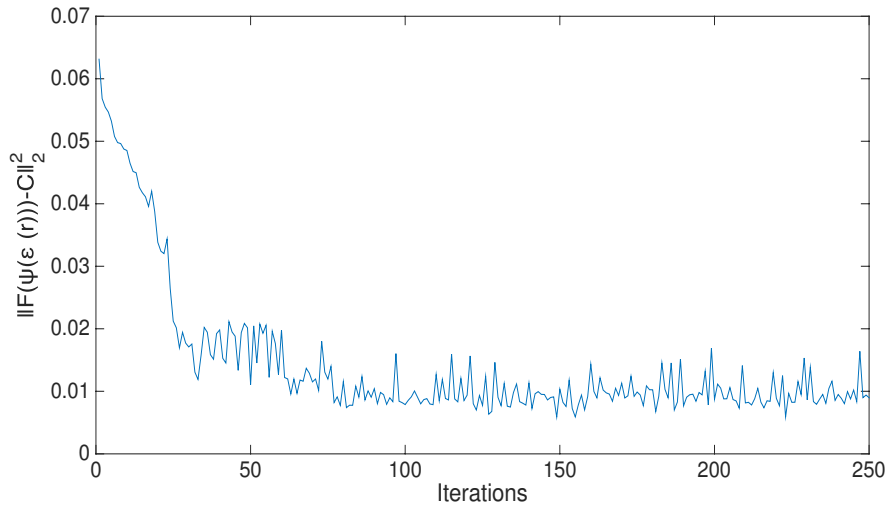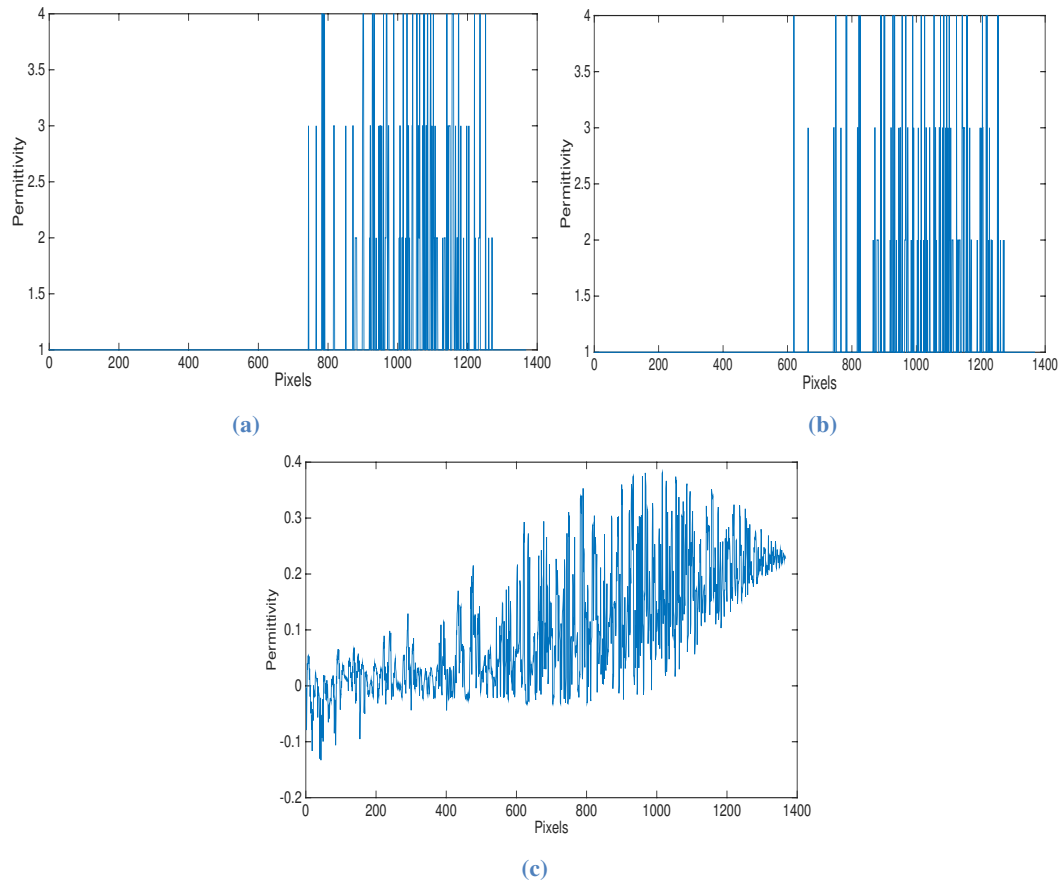**Figure 8.8. The histograms of the permittivity distribution per pixel for case 2 (a) true shape, (b) the level set reconstruction, (c) the standard Tikhonov's regularisation image reconstruction.**

8.2.2 Simulated Phase Area Fraction

By definition, the phase area fraction is the cross-sectional area locally occupied by the phase of a multiphase region, divided by the cross-sectional area of the entire region (e.g., pipe) at the same local point. This can be translated digitally by dividing the number of pixels per phase over the total number of pixels. Consequently, the area fractions of all phases were calculated according to the below equation and given in Table 8.1.

$$\text{Phase area fraction} = \frac{number\ of\ pixels\ per\ phase}{total\ number\ of\ pixels}. \tag{8.2}$$

Table 8.1. A comparison between the true shape and the level set reconstruction in terms of the area fraction per phase for the simulated cases.

	Area Fraction							
	True shape				Level Set reconstruction			
Phase Permittivity	$\mathcal{E}_1$	$\mathcal{E}_2$	$\mathcal{E}_3$	$\mathcal{E}_4$	$\mathcal{E}_1$	$\mathcal{E}_2$	$\mathcal{E}_3$	$\mathcal{E}_4$
Case 1:low contrast	0.034	0.033	0.032	0.901	0.027	0.031	0.034	0.909
Case 2:high contrast	0.034	0.033	0.032	0.901	0.044	0.032	0.021	0.903

Calculating the phase area fraction demonstrates the ability to extract quantitative information using ECT by the level set method. The phase fraction is a key parameter for determining other important parameters such as density, viscosity, average velocity, pressure drop, and heat transfer.

1.1.1 Experimental Results

For the experimental evaluation, a 12-electrode sensor was used, which was built in the University of Bath Engineering Tomography Lab (ETL). The sensor has an inner diameter of 151mm whereas the data acquisition unit used is a commercial PTL300E-TP-G capacitance measurement unit from Process Tomography Limited (Figure 6.3). The unit can collect sets of capacitance data at 100 frames\s with an effective resolution of 0.1 fF and measurement noise level better than 0.07 fF. MATLAB was used for data collection, image reconstruction and processing. Four different experimental models were prepared in the laboratory in order to examine the ability of the algorithm to detect and distinguish different phases.

The experimental results for the low contrast case for the level set method is shown in Figure 8.9 along with the experimental setups for the sake of comparison. Two experimental setups were investigated:

- Setup 1: is a 3-phase setup where two wooden rods of permittivity $\mathcal{E}_1 = 2.3$ and a plastic rod of permittivity $\mathcal{E}_2 = 3$ were reconstructed against an air background of permittivity $\mathcal{E}_3 = 1$.

- Setup 2: is a 4-phase setup where a plastic rod of permittivity $\mathcal{E}_1 = 3$ and a wooden rod of permittivity $\mathcal{E}_2 = 2.3$ were divided by a book of permittivity $\mathcal{E}_3 = 3.85$ and reconstructed against an air background of permittivity $\mathcal{E}_4 = 1$. This setup is more challenging since all phases are close in permittivity values and are closely located to each other.

In this case 250 iterations were used to construct the level set image and the norms of the error between the measured and calculated capacitances for all iterations are shown in Figure 8.10. The level set reconstructed images shown in Figure 8.9 are based on the minimum residual norm. Standard Tikhonov's reconstruction was not produced for the experiment data because absolute capacitance data was used to generate the level set images where only one measured data set was used without the need of a reference data set. Whereas standard Tikhonov's reconstruction needs a reference data set to produce good results. Hence, using standard Tikhonov's reconstruction when absolute data is used could not generate meaningful images.

Figure 8.11 shows the histograms of the permittivity distribution per pixel. Comparison between the true shape and the level set reconstruction histograms is hard to achieve for experimental setups, however these histogram demonstrate the superiority of the level set method over the traditional Tikhonov's reconstruction. This can be seen in the constant permittivity values of the level set method (each constant represents one phase).

Figure 8.9 Level set experimental results for case 3 (a) experimental setup 1, (b) experimental setup 2.
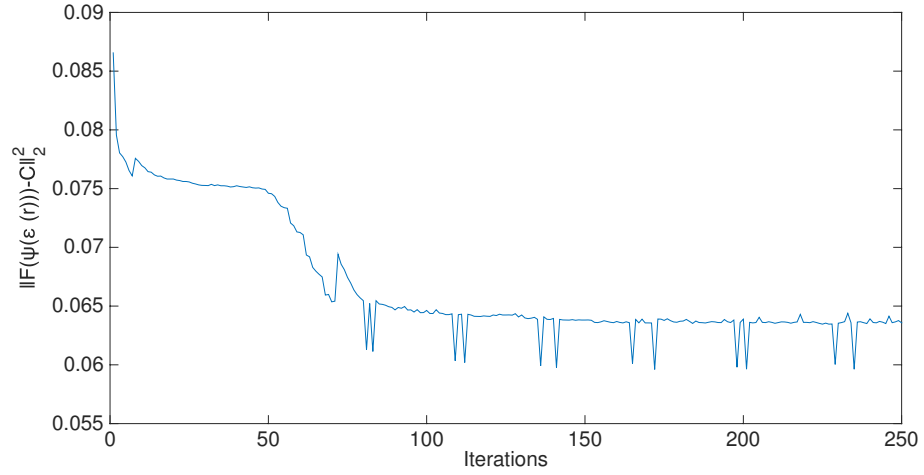

(a)

(b)

**Figure 8.10. The norms of the error between the measured and calculated capacitances for 250 iterations of the level set method for case 3 (a) experimental setup 1, (b) setup 2.**

8.2.2.2   Case 4: high contrast experiment

The experimental results for the high contrast case for the level set method are shown in Figure 8.12 along with the experimental setups for the sake of comparison. Two setups were investigated:

- Setup 3: is a 3-phase setup where water of permittivity $\mathcal{E}_1 = 80$ (ignoring the plastic bottle) and two wooden rods of permittivity $\mathcal{E}_2 = 2.3$ were reconstructed against an air background of permittivity $\mathcal{E}_3 = 1$.
- Setup 4: is a 4-phase setup where water of permittivity $\mathcal{E}_1 = 80$, a plastic rod of permittivity $\mathcal{E}_2 = 3$ and two wooden rods of permittivity $\mathcal{E}_3 = 2.3$ were reconstructed against an air background of permittivity $\mathcal{E}_4 = 1$. This setup is more challenging since wood and plastic are close in permittivity values and are closely located to each other.

In this case 250 iterations were used to construct the level set images and the norms of the error between the measured and calculated capacitance for all iterations are shown in Figure 8.13. The level set reconstructed images shown in Figure 8.12 are based on the minimum residual norm. Since water with its high permittivity is dominating the area, it is hard to distinguish the lower permittivity phases from the reconstructed images. However, the number of pixels per phase can be extracted as seen in the histogram (Figure 8.14) of the permittivity distribution per pixel. Accordingly, the phase area fraction can be extracted and analysed as in Table 8.2.

93
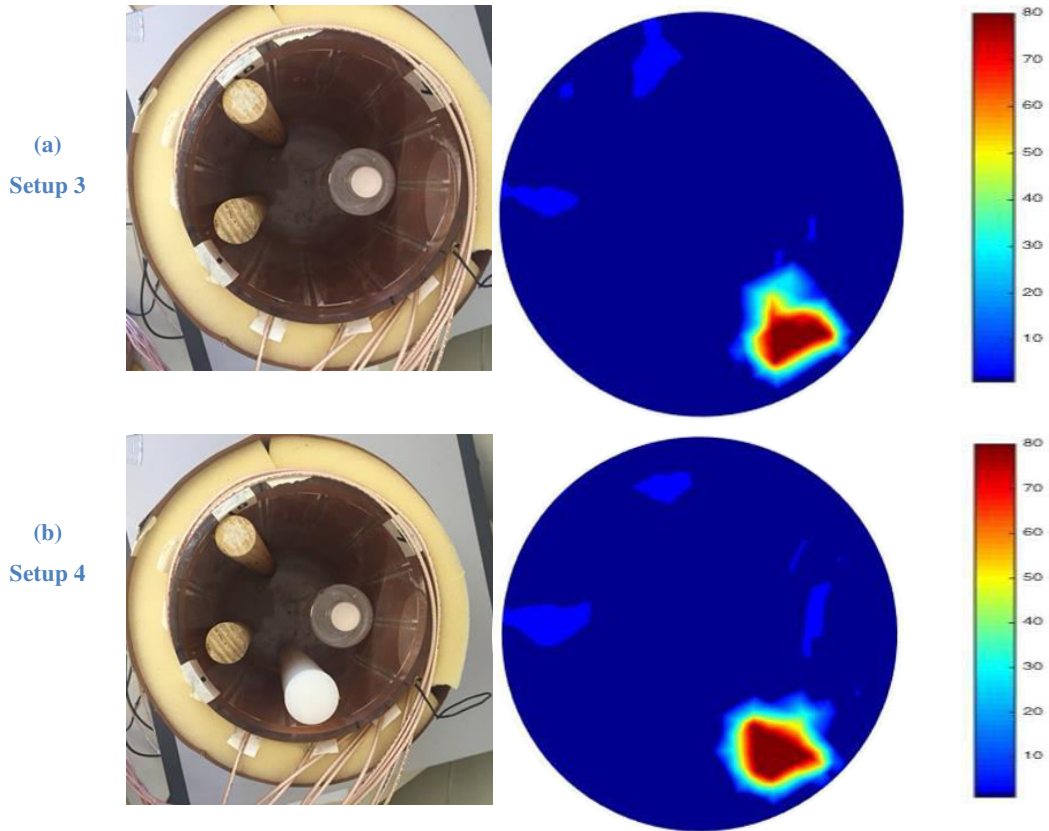
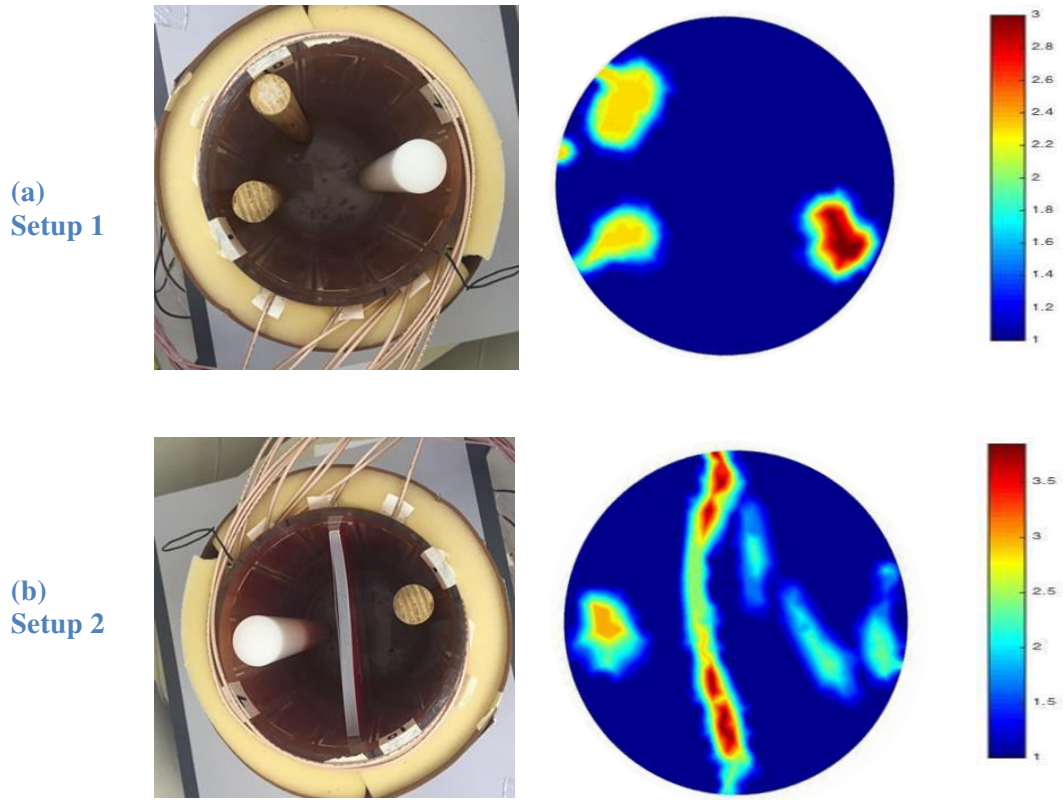**Figure 8.12. Level set experimental results for case 4 (a) experimental setup 3, (b) experimental setup 4.**

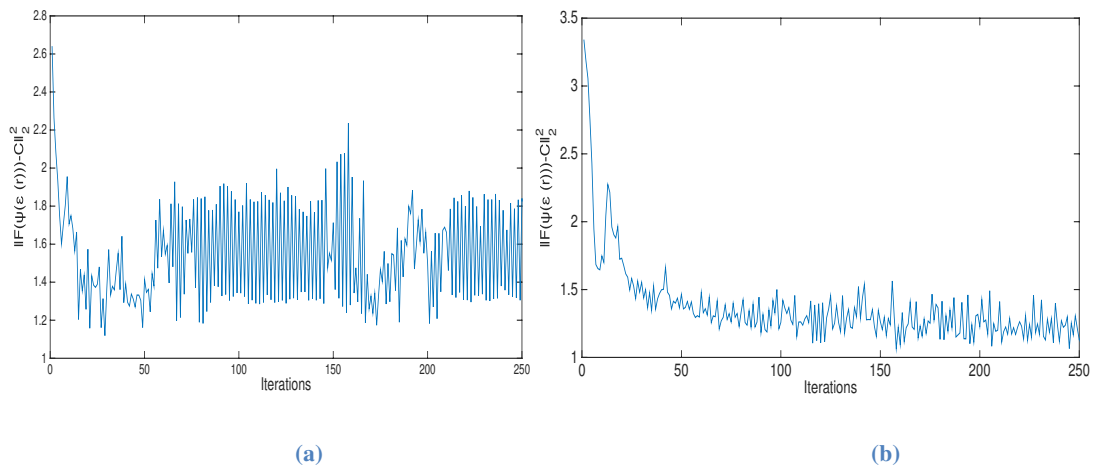(a)   (b)
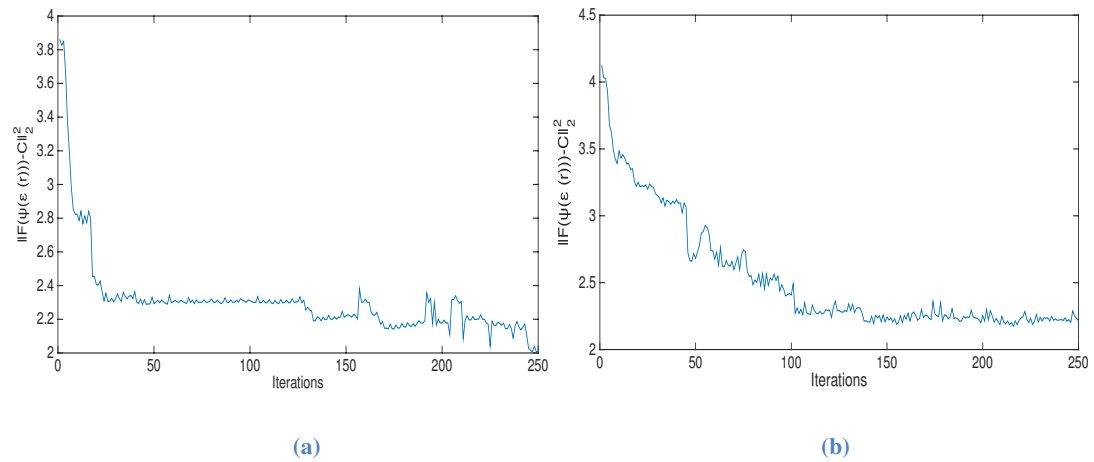
Figure 8.13. The norms of the error between the measured and calculated capacitances for 250 iterations of the level set method for case 4 (a) experimental setup 3, (b) setup 4.

(a)   (b)
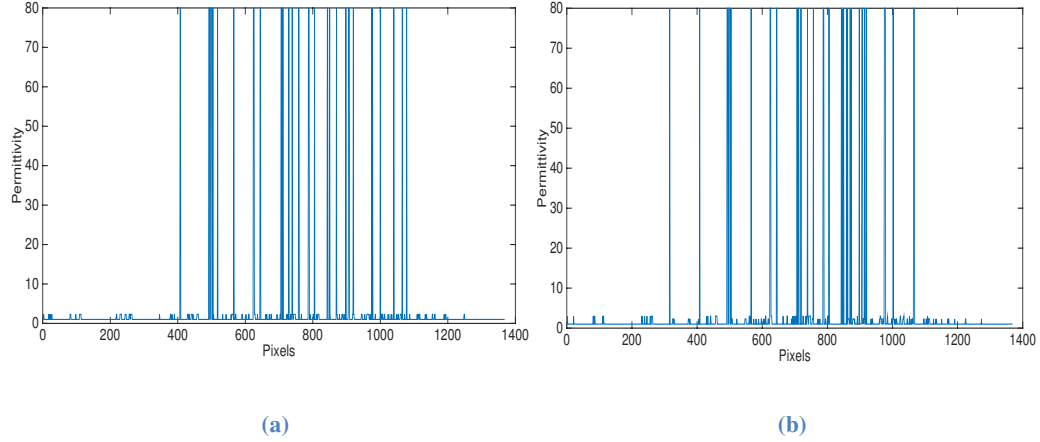
Figure 8.14. The histograms of the permittivity distribution per pixel for case 4 (a) experimental setup 3, (b) experimental setup 4.

8.2.2.3   *Experimental phase area fraction*

The area fractions of all phases for the level set reconstruction of the experimental cases were calculated according to **(8.2)** and given in Table 8.2. For the experimental setup, the   true shape area fraction was calculated according to the following equation:

$$\text{Phase area fraction (for experemental setup)} = \frac{phase\ cross\ sectional\ area}{pipe\ cross\ sectional\ area}. \qquad (8.3)$$

Table 8.2. A comparison between the true shape and the level set reconstruction in terms of the area fraction per phase for the experimental cases

| | Area Fraction | | | | | | | |
| | True shape | | | | Level Set reconstruction | | | |
Phase Permittivity	ε_1	ε_2	ε_3	ε_4	ε_1	ε_2	ε_3	ε_4
Case 3: low contrast setup 1	0.054	0.025	0.921	NA	0.084	0.032	0.884	NA
Case 3: low contrast setup 2	0.025	0.027	0.080	0.868	0.031	0.081	0.051	0.836
Case 4: high contrast setup 3	0.032	0.054	0.914	NA	0.042	0.091	0.867	NA
Case 4: high contrast setup 4	0.032	0.025	0.054	0.889	0.048	0.069	0.042	0.841

95

Such simple experimental setups is sufficient for a static study as long as they provide different phases (i.e. different permittivity values) and can be considered as a valid first step towards studying multiphase process fluids.

8.3 DISCUSSION

The objective of this study was to demonstrate the ability of the LS method to detect and quantify all phases despite any pre knowledge other than an estimated permittivity value of the phases. From the results, it can be seen that this objective can be better achieved by the LS method than traditional pixel based image reconstruction. This can be observed from the reconstructed level set images, which show similar patterns of the true patterns shown in the simulated and experimental results. Since the interaction between the capacitance measurements and the process media is nonlinearly influenced by the inhomogeneity of the flow, applying standard single step reconstruction methods that are based on regularisation tools, usually only result in low-resolution images, especially in high contrast cases where one phase has higher permittivity value compared to the other phases. This makes classical reconstruction techniques more challenging in terms of correctly distinguishing the other low permittivity phases since the high permittivity phase will dominate and make the problem highly nonlinear.

The results in this chapter demonstrate the potential and feasibility of the proposed LS technique for detecting, locating and characterizing all different phases possibly appearing in a multiphase process. The advantage of this method over traditional MPFM available in the market is that this ECT method minimizes the uncertainty of the measurements as it is non-dependant on any variable other than estimated permittivity values, and thus it minimizes the sensitivity of the measurements to changes in the fluid properties (e.g., salinity, viscosity, density, dielectric constant, electrical conductivity, etc.), characteristics (e.g., slip, flow regime, etc.), and flow condition (e.g., pressure loss, cavitation, contamination, chemical injection additives, vibrations. etc.). Moreover, not only that it is tolerant to contaminants, but also any type of contaminants can be imaged and measured too. As mentioned earlier there is no available meter to measure contaminants, at best MPFM can measure oil, gas and water only, given many *a priori* information about the flow. Instead, available MPFMs get either fouled by contaminants or the accuracy gets negatively affected.

Simulation and experimental results demonstrated that the multi-phase LS based algorithm is capable of imaging three or four phase permittivity contrasts. Such promising results can also

be extended to image more than 4 phases by adding more level set functions to the model accordingly. The nonlinear nature of the proposed algorithm as well as an estimated prior knowledge about the contrast permittivity values enabled us to recover those permittivity profiles by using one set of capacitance data. This is critically important in real life application where absolute ECT data can be used to recover multi-phase flow data without requiring a reference data. Another advantage of the level set shape reconstruction method over traditional image reconstruction methods is the ability to accurately estimate the phase volume fraction, as illustrated in Tables 8.1 and 8.2. This is because unlike traditional image reconstruction methods, the level set method can distinguish different phases in a medium.

The results shown in this chapter are designed in order to study the potential of this algorithm for multiphase imaging. The algorithm shows promising results, however it is also open for enhancement. The performance of this method and hence the accuracy can be further investigated and enhanced by refining the following features:

- Generally, the permittivity values may be known and supplied to the algorithm as *a priori* assumption, but the method can be extended where both the permittivity values and the topology are determined simultaneously [23].
- A pre-step of determining the best initial guess of the level set functions can improve the speed of convergence.
- The level set model can be improved by modifying the number/type of used level set functions and/or the mapping $\varepsilon = \varphi\left(\psi(r)\right)$ shown in **(8.1).**
- The tuning parameters (i.e. the step size, the regularisation parameter) and the regularisation matrix can be chosen differently using other methods to arrive at the best choices.
- In order to adapt this method to online monitoring, the tuning parameters can be automated.
- Applying a less dense mesh or stopping the iteration process if the residual reached a specified set point can enhance the speed of convergence.
- Applying a denser mesh or allowing further iterations may enhance the resolution of the image.
- This technique can also be extended to 3D image reconstruction.
- Other optimization techniques can be applied to arrive at the best results in terms of image resolution and computation time. One important optimization would be to implement this algorithm in high performance computing such as GPU.

In addition to the fact that the level set approach promise to make an ill-posed problem better behaved, it offers other advantages such as:

1. Performing numerical computations of a geometric object containing curves and surfaces on a fixed Cartesian grid without the need to parameterize such objects.
2. The level set method has the ability to follow shapes with changing topology (i.e. split in to multi-regions, develops holes or vice versa).
3. The level set method does not require *a priori* assumption about the topology (i.e. spatial location) nor the nature (i.e. shape and size) of the inclusion.
4. The level set method is well suited for high contrast image reconstruction with sharp boundaries. This is because the high contrast inclusion is incorporated explicitly in the level set model without it dominating the entire region and overshadowing the other low contrast inclusions. Unlike traditional pixel based techniques, which have the limitation of over smoothing the reconstructed image especially when a high contrast inclusion is dominating the region.

Because of such advantages, the level set method has a great potential for shape reconstruction applications and thus for multiphase image reconstruction. The hope is that the results of this chapter will help in better understanding and further extending the application of ECT for multi-phase flow imaging.

Chapter IX

9   CONCLUSIONS AND FUTURE DIRECTION

9.1   SUMMARY

Multiphase flow measurement is a very challenging and critical topic in industrial process tomography. Two major challenges related to multiphase flow are pipeline/equipment deposit monitoring and multiphase flow monitoring/measurement. Deposits might build-up in a pipeline or equipment and disturb the flow, causing serious problems downstream. On the other hand monitoring different phases in a crude flow is considered extremely important in order to study and analyse the produced product. Hence, in order to ensure safety, increase profits, optimize production and ensure production quality, the multiphase flow must be adequately monitored and controlled. This study demonstrated the ability and potential of ECT imaging for monitoring/measuring a multiphase flow in order to either measure the flow rate of all separate phases or one particular phase (e.g., flow deposit). To support the thesis that an economic-based ECT system can deliver significant value to the process industry for monitoring/measuring multiphase processes, the following objectives were met successfully:

1. Reviewed different image reconstruction techniques for ECT in order to understand the problem and the possible solutions.
2. Implemented a high resolution ECT algorithm for early deposit detection in pipelines.
3. Adopted ECT system for possible conductive deposits such as metal.
4. Implemented a low contrast multiphase imaging algorithm to distinguish all phases in a medium.
5. Implemented a high contrast multiphase imaging algorithm to distinguish all phases in a medium in the presence of a dominating phase.
6. Extracted concentration information about each phase in a multiphase medium.

9.2   CONCLUSIONS

Different image reconstruction techniques for ECT were reviewed and the capabilities of ECT for monitoring multiphase media were studied and discussed. Accordingly, this thesis was divided into three main studies:

9.2.1 Deposit Detection in Pipelines

In this study, ECT with a novel Limited Region Tomographic (LRT) image reconstruction using a narrowband pass filter was used to focus on targeted locations in a pipe where contaminants are expected to deposit in order to enhance the resolution of the produced images. Laboratory experiments were carried out using the suggested LRT and compared to the traditional Full Region Tomography (FRT). Results showed that both LRT and FRT were able to detect fine deposits and give information about their location. However, the LRT could remarkably detect a layer of deposit as small as *0.5 mm* without noise and generally provides a more robust solution. This indicates that the proposed LRT method allows a detection of deposit with the resolution of 0.085% of the entire imaging region, which makes the ECT a very good method for detection of deposit. This conclusion is promising in terms of detecting deposit accumulation inside pipelines, which increases the interior pipe wall roughness and leads to other more serious problems.

9.2.2 Metal Detection Using Absolute Value ECT Data

In this study, ECT was used for metallic sample imaging which represents a possible scenario of having conductive deposits. A high contrast material such as metal is considered a challenge for ECT systems as traditional image reconstruction methods become highly nonlinear. Due to the electrostatic equilibrium of metallic materials within static electric field, the capacitance measurements are increased. The efficiency of non-iterative linear methods (i.e. Tikhonov's regularisation), TV regularisation with linear measurements and iterative nonlinear methods (i.e. LS) for the image reconstruction was investigated. The results demonstrated that both TV and LS methods could be adapted to image conductive inclusions such as metal with good resolution. Nevertheless, the produced images using LS method could identify sharp interfaces and distinguish multiple metal objects better. Also, absolute ECT imaging was presented for the first time where the LS algorithm uses only one set of ECT measurement data. This study paved the way for adapting the LS method for imaging multiphase media with a dominating phase (i.e. a higher permittivity phase).

9.2.3 Multiphase Imaging Using Absolute Value ECT Data

In this study, the novel narrowband level set algorithm was modified to image multiphase media in order to correctly determine the number, location and concentration of the present phases. The innovative absolute ECT imaging using level set method was tested with high

contrast and low contrast multiphase data. Simulation and experimental results demonstrated that the multiphase LS based algorithm is capable of imaging three or four phase permittivity contrasts despite any *a priori* information except for an estimated permittivity values. The results also showed the superiority of this algorithm over classical pixel based image reconstruction methods especially in accurately estimating the phase volume fraction of all different phases in the medium.

9.3   LIMITATIONS

Despite the promising results shown in this thesis it is fair to mention some of the limitations of this work:

1. ECT can be used to image non-conductive pipelines only. However, in case of a conductive pipe, the sensor can be mounted internally, using the conductive internal wall of the pipe as a screen.

2. All of the experiments in this thesis were static and the algorithms were not tested for a dynamic flow.

3. The thesis presents a 2D ECT imaging in which the deposits to be imaged must cover the entire length of the ECT sensor, whereas in real applications, the deposits may be smaller or non-uniform especially in a case such as black powder flowing in a gas pipeline. In such cases, the proposed methods can be employed for 3D ECT, which can promise better real life solutions.

4. In an oil/water process, the flow can be either oil-continuous or water-continuous. This depends on the water liquid ratio, the density, the viscosity, the flow rate, and the presence of other chemicals. Although it is certain that ECT and the proposed algorithms are suitable for an oil-continuous case, it is not clear how they can perform in a water-continuous case, as conventional ECT system is not the best option for such scenarios.

9.4   FUTURE DIRECTION

This thesis formulated a comprehensive study for ECT potential in imaging pipelines carrying a multiphase flow. It presented a framework for new algorithms that can be used for ECT to improve resolution and efficiency to detect both low and high contrast media. It also demonstrated the benefits of developing an economic-based ECT system for monitoring multiphase media. The algorithms developed have laid a foundation for high-resolution

multiphase ECT imaging and it opens up several avenues for future work in economic-based ECT imaging for multiphase media. Although the proposed solutions showed very promising results, they are still not in the stage of real process testing and always open for enhancements. Some future direction suggestions include:

1. **Enhancing the Developed Algorithms:** The performance of the algorithms and hence the accuracy can be further investigated and enhanced by refining the tuning parameters. More suggestions for enhancing the level set algorithm were given in Section 8.3. Also, the LRT in Chapter 5 can utilizes nonlinear iterative solutions to be compared with our solution. This thesis focuses on the inverse problem aspect of image reconstruction; however, the forward problem aspect is as important and can significantly enhance the solution. Hence, further studies on enhancing the forward model can be adapted such as using Boundary Element Method (BEM) instead of FEM.

2. **Adopting the Algorithms for Online Flow Monitoring:** At this stage the suggested algorithms can be used online in real time if the system was placed on the pipeline in such a way that representative samples are being taken continuously and allowed to settle before an image is captured then returned to the flow. But because of the promising results achieved in this study, further online studies can be adapted to the algorithms to investigate their capability to image multiphase fast flows in real time inline.

3. **Employing the proposed algorithms by other electrical tomography techniques:** such as EIT, ERT, MIT or others.

4. **Phase volume fraction measurement:** The extracted phase area fraction can be further extended to measure the phase volume fraction. This can be achieved, for example, by locating two ECT systems on the pipeline separated by known distance and cross-correlate the captured images.

5. **Constructing three-dimensional capacitance images:** i.e. time and two-dimensional space image or three-dimensional space image.

6. **Enhancing the speed of convergence:** For a typical PC like the one used for this study, the nonlinear LS algorithm presented in here takes *34 s* to run the experimental data for a mesh of *1367* elements, and *65 s* for a mesh of 2064 elements. Such computation time is not ideal for online measurements, as it will not give real time measurements of the process.

7. **Enhancing the stability of the algorithms:** as it can be seen from the norms of the error between the measured and calculated capacitances in Chapters 7 and 8, the LS algorithm is instable. This makes the algorithm unsuitable for online measurement in this stage of research.

REFERENCES

[1] M. Crabtree, D. Eslinger, P. Fletcher, M. Miller, A. Johnson and G. King, "Fighting Scale–Removal and Prevention," *Oilfield Review*, pp. 30-45, 1999.

[2] L. Azevedo and A. Teixeira, "A critical review of the modeling of wax deposition mechanisms," *Petroleum Science and Technology*, 21, pp. 393-408, 2003.

[3] A. Aiyejina, D. P. Chakrabarti, A. Pilgrim and M. K. S. Sastry, "Wax formation in oil pipelines: A critical review," *Int. J. Multiphase Flow*, 37, no. 7, pp. 671–694, 2011.

[4] R. M. Baldwin, "Black powder problem will yield to understanding, planning," *Pipeline & Gas Industry*, pp. 109-112, 1999.

[5] O. Trifilieff and T. H. Wines, "Black powder removal from transmission pipelines: Diagnostics and Solutions," Pall Corp., NY, USA, Rep. FCBLACKPEN, 2009.

[6] N. A. Tsochatzidis, "Effect of black powder contaminants on gas metering equipment", *International Conference Oil & Gas Maintenance Technology*, Manama, Bahrain, 11-13 Dec., 2007.

[7] N. A. Tsochatzidis, "Methods help remove black powder from gas pipelines," *Oil & Gas Journal*, 105, pp. 52-58, March 12, 2007.

[8] A. M. Sherik, "Black powder in sales gas transmission lines" *Saudi Aramco Journal of Technology*, Fall 2007, pp. 2-10, 2007.

[9] J. Smart, "Movement of black powder in pipelines - part 1" in *PPSA newsletter*, November 2008.

[10] *Handbook of multiphase flow metering*, The Norwegian Society for Oil and Gas Measurement and The Norwegian Society of Chartered Technical and Scientific Professionals, Norway, March 2005.

[11] M. S. Beck and R. A. Williams, "Process tomography: a European innovation and its applications," *Meas. Sci. Technol.*, 7, pp. 215–224, 1996.

[12] Z. Liu and Y. Kleiner, "State of the art review of inspection technologies for condition assessment of water pipes," *Measurement*, 46, no. 1, pp. 1–15, 2013.

[13] Z. Liu and Y. Kleiner, "State-of-the-art review of technologies for pipe structural health monitoring," *IEEE Sensors J.*, 12, no.6, pp. 1987-1992, 2012.

[14] S.B. Costello, D.N. Chapman, C.D.F. Rogers and N. Metje, "Underground asset location and condition assessment technologies," *Tunnelling and Underground Space Technology*, 22, no. 5–6, pp. 524–542, 2007.

[15] *Nondestructive Testing Handbook: Ultrasonic Testing*, 7, American Society for Nondestructive Testing Inc., Columbus, OH, USA, 2007.

[16] W. Luo and J. L. Rose, "Guided wave thickness measurement with EMATs," *Insight-Non-Destructive Testing and Condition Monitoring*, 45, no. 11, pp. 1–5, 2003.

[17] G. Shen and G. Chen. "Infrared Thermography Test for High Temperature Pressure Pipe" *Insight - Non-Destructive Testing and Condition Monitoring*, 49, no. 3, pp. 151-153, 2007.

[18] S. M. Huang, A. Plaskowski, C. G. Xie and M. S. Beck, "Capacitance-based tomographic flow imaging system," *Electronics Letters*, 24, no. 7, pp. 418–419, 1988.

[19] A. J Jaworski and T. Dyakowski, "Application of electrical capacitance tomography for measurement of gas-solids flow characteristics in a pneumatic conveying system," *Meas. Sci. Technol.,* 12, no. 8, pp. 1109-1119, 2001.

[20] G. E. Fasching and N. S. Smith, "A capacitive system for three-dimensional imaging of fluidized beds," *Review of Scientific Instruments*, 62, no.9, pp. 2243-2251, 1991.

[21] S.J. Wang, T. Dyakowski, C.G. Xie, R.A. Williams and M.S. Beck, "Real-time capacitance imaging of bubble formation at the distributor of a fluidized-bed," *Chem. Eng. J. Biochem. Eng.*, 56, no. 3, pp. 95–100, 1995.

[22] S. Liu, W. Q. Yang, H. G. Wang and Y. Su, "Investigation of square fluidized beds using capacitance tomography: preliminary results" *Meas. Sci. Technol.*, 12, no. 8, pp. 1120–1125, 2001.

[23] R. He, C. M. Beck, R. C. Waterfall and M. S. Beck, "Applying capacitance tomography to combustion phenomena," in *Proc. 2nd ECAPT Conf.*, Karlsruhe, 1993 pp. 300–302.

[24] R. He, C. M. Beck, R. C. Waterfall and M. S. Beck, "Finite element modelling and experimental study of combustion phenomena using capacitance measurements," in *Proc. 3rd ECAPT Conf.*, Porto, 1994, pp. 367–376.

[25] R. C. Waterfall, R. He, N. B. White and C. B. Beck, "Combustion imaging from electrical impedance measurements," *Meas. Sci. Technol.*, 7, pp. 369–74, 1996.

[26] R. White, "Using electrical capacitance tomography to monitor gas voids in a packed bed of solids," *Meas. Sci. and Technol.*, 13, no. 12, pp. 1842–1847, 2002.

[27] Ø. Isaksen, A. S. Dico and E. A. Hammer, "A capacitance based tomography system for interface measurement in separation vessels," *Meas. Sci. Technol.*, 5, pp. 1262–1271, 1994.

[28] Z. Huang, D. Xie, H. Zhang and H. Li, "Gas–oil two-phase flow measurement using an electrical capacitance tomography system and a Venturi meter," *Flow Measurement and Instrumentation*,16, pp. 177–182, 2005.

[29] W. Q. Yang, M. S. Adam, R. Watson and M. S. Beck, "Monitoring water hammer by capacitance tomography," *Electron. Lett.*, 32, pp. 1778–1779, 1996.

[30] W. Deabes, and M. Abdelrahman, "Solution of the forward problem of electric capacitance tomography of conductive materials," in *The 13th WMSCI Conf.*, Orlando, Florida, USA, 2009.

[31] C. G. Xie, S. M. Huang, B. S. Hoyle, R. Thorn, C. Lenn, D. Snowden and M. S. Beck, "Electrical capacitance tomography for flow imaging: system model for development of image reconstruction algorithms and design of primary sensors," *IEE Proceedings G in Circuits, Devices and Systems* 139, no. 1, pp. 89-98, 1992.

[32] B. Brandstätter, G. Holler and D. Watzenig, "Reconstruction of inhomogeneities in fluids by means of capacitance tomography," *COMPEL: The International Journal for Computation and Mathematics in Electrical and Electronic Engineering*, 22, no. 3, pp. 508-519, 2003.

[33] D. Watzenig, B. Brandstatter and G. Holler, "Adaptive regularization parameter adjustment for reconstruction problems," *IEEE Transactions on Magnetics*, 40, no. 2, pp. 1116-1119, 2006.

[34] W. Q. Yang and L. Peng, "Image reconstruction algorithms for electrical capacitance tomography," *Meas. Sci. Technol.,* 14, no. 1, pp. R1–R13, 2003.

[35] Ø. Isaksen, "Areview of reconstruction techniques for capacitance tomography," *Meas. Sci. Technol.*, 7, no. 3, pp. 325–337, 1996.

[36] H. Yan, C. Liu and J. Gao, "Electrical capacitance tomography image reconstruction based on singular value decomposition," in *WCICA, Fifth World Congress on Intelligent Control and Automation*, 2004, pp. 3783-3786.

[37] H. W. Engl and H. Gfrerer, "A posteriori parameter choice for general regularization methods for solving linear ill-posed problems," *Applied Numerical Mathematics*, 4, no. 5, pp. 395–417, 1988.

[38] Y. Lin and B. Wohlberg, "Application of the UPRE method to optimal parameter selection for large scale regularization problems," *SSIAI: IEEE Southwest Symposium on Image Analysis and Interpretation*, 2008, pp. 89-92.

[39] G. Golub, M. Heath and G. Wahba, "Generalized cross-validation as a method for choosing a good ridge parameter," *Technometrics,* 21, no. 2, pp. 215–223, 1979.

[40] P. C. Hansen, *Rank-deficient and discrete ill-posed problems: numerical aspects of linear inversion*, SIAM, Philadelphia, PA, USA, 1998.

[41] P. C. Hansen, "Analysis of discrete ill-posed problems by means of the L-curve," *SIAM Rev.*, 34, no. 4, pp. 561–580, 1992.

[42] J. Mead and R. A. Renaut. "The χ^2-curve method of parameter estimation for generalized Tikhonov regularization," *Tech. Report*, 2007.

[43] B. W. Rust and D. P. O'Leary, "Residual periodograms for choosing regularization parameters for ill-posed problems," *Inverse Problems*, 24, no. 3, 034005-30, 2008.

[44] L. H. Peng, H. Merkus and B. Scarlett, "Using regularization methods for image reconstruction of electrical capacitance tomography," *Particle & Particle Systems Characterization*, 17, no. 3, pp. 96-104, 2000.

[45] W. R. B. Lionheart, "Reconstruction algorithms for permittivity and conductivity imaging," in *Proc. of the 2nd World Congress on Industrial Process Tomography*, 2001, pp. 4-11.

[46] S. Gomez, M. Ono, C. Gamio and A. Fraguela, "Reconstruction of capacitance tomography images of simulated two-phase flow regimes," *Applied Numerical Mathematic*s, 46, no. 2, pp. 197-208, 2003.

[47] H. Yan, L. J. Liu, H. Xu and F. Q. Shao, "Image reconstruction in electrical capacitance tomography using multiple linear regression and regularization," *Meas. Sci. Technol.*, 12, no. 5, pp. 575–581, 2001.

[48] Z. Huang, B. Wang and H. Li, "Application of electrical capacitance tomography to the void fraction measurement of two-phase flow," *IEEE Trans. Instrum.* Meas,, 52, no. 1, pp. 7-12, 2003.

[49] J. Lei, S. Liu, Z. Li and M. Sun, "An image reconstruction algorithm based on the extended Tikhonov regularization method for electrical capacitance tomography," *Measurement*, 42, no. 3, pp. 368-376, 2009.

[50] L. I. Rudin, S. Osher and E. Fatemi, "Nonlinear total variation based noise removal algorithms, " *Proc. of the 11th Annual International Conference of the Center for Nonlinear Studies, Physica D*, 60, 1992, pp. 259-268.

[51] M. Soleimani and W. R. B. Lionheart, "Nonlinear image reconstruction for electrical capacitance tomography using experimental data," *Meas. Sci. Technol.*, 16, pp. 1987–1996, 2005.

[52] W. Fang, "A nonlinear image reconstruction algorithm for electrical capacitance tomography," *Measurement Science and Technology*, 15, no. 10, pp. 2124-2132, 2004.

[53] H. Wang, L. Tang and Z. Cao, "An image reconstruction algorithm based on total variation with adaptive mesh refinement for ECT," *Flow Measurement and Instrumentation*, 18, no. 5, pp. 262-267, 2007.

[54] T. C. Chandrasekera, Y. Li, J. S. Dennis and D. J. Holland, "Total variation image reconstruction for electrical capacitance tomography," in *IEEE International Conference on Imaging Systems and Techniques Proceedings*, 2012, pp. 584-589.

[55] W. Q. Yang, D. M. Spink, T. A. York and H. McCann, "An image reconstruction algorithm based on Landweber iteration method for electrical capacitance tomography," *Meas. Sci. and Technol.*, 10, no. 11, pp. 1065-1069, 1999.

[56] W. Q. Yang and S. Liu, "Electrical capacitance tomography with square sensor," *Electronics Letters*, 35, no. 4, pp. 295-296, 1999.

[57] S. Liu, L. Fu and W. Q. Yang, "Optimization of an iterative image reconstruction algorithm for electrical capacitance tomography," *Meas. Sci. Technol.*, 10, no. 7, pp. L37-L39, 1999.

[58] J. D. Jang, S. H. Lee, K. Y. Kim and B. Y. Choi, "Modified iterative Landweber method in electrical capacitance tomography," *Meas. Sci. Technol.*, 17, no. 7, pp. 1909–1917, 2006.

[59] G. Lu, L. Peng, B. Zhang and Y. Liao, "Preconditioned Landweber iteration algorithm for electrical capacitance tomography," *Flow Measurement and Instrumentation*, 16, no. 2, pp. 163-167, 2005.

[60] H. Yan, L. J. Liu, D. Z. Qiang, "An Iterative Electrical Capacitance Tomography Image Reconstruction Algorithm," in *ISCID Second International Symposium on Computational Intelligence and Design*, 2009, 1, pp. 310-313.

[61] R. Gordon, R. Bender and G. T. Herman, "Algebraic reconstruction techniques (ART) for three-dimensional electron microscopy and X-ray photography," *J. Theoretical Biology*, 29, no. 3, pp. 471-481, 1970.

[62] N. Reinecke and D. Mewes, "Resolution enhancement for multi-electrode capacitance sensors," in *Reviewed Proc. 3rd ECAPT Conf.*, 1994.

[63] T. Loser, R. Wajman and D. Mewes, "Electrical capacitance tomography: image reconstruction along electrical field lines," *Meas. Sci. Technol.*, 12, no. 8, pp. 1083-1091, 2001.

[64] S. Bangliang, Z. Yiheng, P. Lihui, Y. Danya and Z. Baofen, "The use of simultaneous iterative reconstruction technique for electrical capacitance tomography," *Chemical Engineering Journal*, 77, no. 1, pp. 37-41, 2000.

[65] S. H. Lee, S. B. Lee, Y. S. Kim, J. H. Kim, B. Y. Choi and K. Y. Kim, "A filtering approach of iterative Tikhonov regularization method in ECT," *5th IEEE Conference on sensors*, Daegu, Korea, 22-25 Oct. 2006, pp. 919-922, 2006.

[66] J. Lei, S. Liu, Z. Li and M. Sun, "An image reconstruction algorithm based on the extended Tikhonov regularization method for electrical capacitance tomography," *Meas. Sci. Technol.*, 19, no. 3, pp. 368–376, 2008.

[67] C.H. Mou, L.H. Peng, D.Y. Yao and D.Y. Xiao, "Image reconstruction using a genetic algorithm for electrical capacitance tomography," *Tsinghua Science and Technology*, 10, pp. 587–592, 2005.

[68] M. Takei, "GVSPM image reconstruction for capacitance CT images of particles in a vertical pipe and comparison with the conventional method," *Meas. Sci. Technol.*, 17, pp. 2104–2112, 2006.

[69] C. Ortiz-Aleman, R. Martin and J. C. Gamio, "Reconstruction of permittivity images from capacitance tomography data by using very fast simulated annealing," *Meas. Sci. Technol.*, 15, pp. 1382–1390, 2004.

[70] Q. Marashdeh, W. Warsito, L. S. Fan and F. L. Teixeira, "Non-linear image reconstruction technique for ECT using a combined neural network approach," *Meas. Sci. Technol.*, 17, pp. 2097–2103, 2006.

[71] W. Warsito and L. S. Fan, "Neural network based multi-criterion optimization image reconstruction technique for imaging two- and three-phase flow systems using electrical capacitance tomography," *Meas. Sci. Technol.*, vol. 12, pp. 2198–2210, 2001.

[72] S. Liu, L. Fu, W.Q. Yang, H. Wang and F. Jiang, "Prior on-line iteration for image reconstruction with electrical capacitance tomography," *IEE Proceedings - Science, Measurement and Technology,* 151, no. 3, pp. 195–200, 2004.

[73] M. Soleimani, P. Yalavarthy and H. Dehghani, "Helmholtz-type regularization method for permittivity reconstruction using experimental phantom data of electrical capacitance tomography," *IEEE Trans. Instrum. Meas,*, 59, no.1, pp. 78-83, 2010.

[74] M. Soleimani, C. N. Mitchell, R. Banasiak, R. Wajman and A. Adler, "Four-dimensional electrical capacitance tomography imaging using experimental data," *Progress In Electromagnetics Research*, 90, pp. 171-186, 2009.

[75] J. Lei, S. Liu, X. Wang and Q. Liu, "An image reconstruction algorithm for electrical capacitance tomography based on robust principle component analysis," *Sensors*, 13, no. 2, pp. 2076-2092, 2013.

[76] Z. Cao and L. Xu, "Direct image reconstruction for electrical capacitance tomography by using the enclosure method," *Meas. Sci. Technol.*, 22, no. 10, 104001-8, 2011.

[77] J. Lei, S. Liu, Z. Li, M. Sun and X. Wang, "A multi-scale image reconstruction algorithm for electrical capacitance tomography," *Appl. Math. Modelling*, 35, no. 6, pp. 2585–2606, 2011.

[78] D. Watzenig, M. Brandner and G. Steiner, "A particle filter approach for tomographic imaging based on different state-space representations," *Meas. Sci. Technol.*, 18, pp. 30–40, 2007.

[79] X. Wu, G. Huang, J. Wang and C. Xu, "Image reconstruction method of electrical capacitance tomography based on compressed sensing principle," *Meas. Sci. Technol.*, 24, no. 7, 075401-7, 2013.

[80] B. Kortschak, H. Wegleiter and B. Brandstätter, "Formulation of cost functionals for different measurement principles in nonlinear capacitance tomography," *Meas. Sci. Technol.*, 18, no. 1, pp. 71–78, 2007.

[81] R. Banasiak and M. Soleimani, "Shape based reconstruction of experimental data in 3D electrical capacitance tomography," *NDT & E Int.*, 43, pp. 241–249, 2010.

[82] R. Banasiak, R. Wajman, T. Jaworski, P. Fiderek, H. Fidos, J. Nowakowski and D. Sankowski, "Study on two-phase flow regime visualization and identification using 3D electrical capacitance tomography and fuzzy-logic classification," *International Journal of Multiphase Flow*, 58, pp. 1-14, 2014.

[83] W. A. Deabes and M. A. Abdelrahman, "A nonlinear fuzzy assisted image reconstruction algorithm for electrical capacitance tomography," *ISA Transactions,* 49, no. 1, pp. 10-18, 2010.

[84] A. DeRosa, "Quenching the thirst of iron pipe," *Plastics News*, 13, no. 32, pp. 1–3, 2001.

[85] M. Evangelidis, L. Ma and M. Soleimani, "High definition electrical capacitance tomography for pipeline inspection," *Progress in Electromagnetics Research*, 141, pp. 1-15, 2013.

[86] M. Zhang, E. Al Hosani, and M. Soleimani, "A limited region electrical capacitance tomography for detection of wax deposits and scales in pipelines," in the 5th International Workshop on Process Tomography (IWPT-5), Jeju, South Korea, September 16-18, 2014.

[87] S. Osher and J. A. Sethian, "Fronts propagating with curvature dependent speed: algorithms based on Hamilton-Jacobi formulations," *J. Comput. Phys.*, 79, pp. 12-49, 1988.

[88] F. Santosa, "A level set approach for inverse problems involving obstacles," *ESAIM Control. Optim. Calc. Variat.*, 1, pp. 17–33, 1996.

[89] L. A. Vese and T. F. Chan, "A multiphase level set framework for image segmentation using the Mumford and Shah model," *Int. J. Computer Vision*, 50, no. 3, pp. 271–293, 2002.

[90] O. Dorn, E. L. Miller and C.M. Rappaport, "A shape reconstruction method for electromagnetic tomography using adjoint fields and level sets," *Inverse Problems*, 16, pp. 1119-1156, 2000.

[91] A. Litman, D. Lesselier and F. Santosa, "Reconstruction of a two-dimensional binary obstacle by controlled evolution of a level-set," *Inverse Problems*, 14, pp. 685-706, 1998.

[92] M. Soleimani, W. Lionheart and O. Dorn, "Level set reconstruction of conductivity and permittivity from boundary electrical measurements using experimental data," *Inverse Problems in Science and Engineering*, 14, no. 2, pp. 193–210, 2006.

[93] N. Irishina, D. Álvarez, O. Dorn and M. Moscoso, "Structural level set inversion for microwave breast screening," *Inverse Problems*, 26, no. 3, 035015-26, 2010.

[94] M. Zhang, L. Ma and M. Soleimani, "Dual modality ECT-MIT multi-phase flow imaging," *Flow Measurement and Instrumentation*, 46, pp. 240–254, 2015.

[95] Dr John Smart. "Keep on Moving," *World Pipelines*, December 2009.

[96] An introduction to multiphase flow measurement. Tuvnel. Glasgow, UK. [Online]. Available:
http://www.tuvnel.com/_x90lbm/An_Introduction_to_Multiphase_Flow_Measurement.pdf

[97] Y. Abdul-Wahab, R. Abdul-Rahim, M. H. Fazlul-Rahiman, H. Abdul-Rahim, S. R. Aw, J. Jamaludin and N. S. M. Fadzil, "A review of process tomography application in inspection system," *J. Teknologi*, 3, pp. 35-39, 2014.

[98] Y. Li, W. Yang, C. G. Xie, S. Huang, Z. Wu, D. Tsamakis and C. Lenn, "Gas/oil/water flow measurement by electrical capacitance tomography," *Meas. Sci. Technol.*, 24, 074001-12, 2013.

[99] W. Q. Yang, A. L. Stott, M. S. Beck and C. G. Xie, "Development of capacitance tomographic imaging systems for oil pipeline measurements," *Rev. Sci. Instrum.*, 66 pp. 4326–4332, 1995.

[100] I. Ismail, J .C. Gamio, S. F. A. Bukhari and W. Q. Yang, "Tomography for multi-phase flow measurement in oil industry," *Flow Meas. Instrum.*, 16, pp. 145–155, 2005.

[101] C. G. Xie, A. Plaskowski and M. S. Beck, "8-electrode capacitance system for two-component flow identification," *IEE Proc.*, 136, no. 4, pp. 173–183, 1989.

[102] J. C. Goble. "The three-dimensional inverse problem in electric current computed tomography." Ph.D thesis, Rensselaer Polytechnic Institute, Troy, NY, USA, 1990.

[103] A. Borsic, B. M. Graham, A. Adler and W. R. B. Lionheart, "Total variation regularization in electrical impedance tomography," *MIMS EPrint*, 2007.

[104] D. C. Dobson and F. Santosa, "An image-enhancement technique for electrical impedance tomography," *Inverse Problems*, 10, pp. 317–334, 1994.

[105] W. Fang, "A nonlinear image reconstruction algorithm for electrical capacitance tomography," *Meas. Sci. Technol.*, 15, pp. 2124–2132, 2004.

[106] H. Wang, L. Tang and Z. Cao, " An image reconstruction algorithm based on total variation with adaptive mesh refinement for ECT," *Flow Measurement and Instrumentation*, 18, no. 5–6, pp. 262–267, 2007.

[107] M. Soleimani and W. R. B. Lionheart, "Nonlinear image reconstruction for electrical capacitance tomography using experimental data," *Meas. Sci. Technol.*, 16, pp. 1987–1996, 2005.

[108] S. Osher, M. Burger, D. Goldfarb, J. Xu and W. Yin, "An iterated regularization method for total variation based image restoration," *Multiscale Modeling & Simulation*, 4, no. 2, pp. 460-489, 2005.

[109] T. C. Chandrasekera, Y. Li, J. S. Dennis and D. J. Holland, "Total variation image reconstruction for electrical capacitance tomography," in *IEEE International Conference on Imaging Systems and Techniques Proceedings*, 2012, pp. 584-589.

[110] X. Wu, G. Huang, J. Wang and C. Xu, "Image reconstruction method of electrical capacitance tomography based on compressed sensing principle," *Meas. Sci. Technol.* 24, no. 7, 075401-7, 2013.

[111] V. Bertola, "Two-phase flow measurement techniques," *Modeling and Experimentation in Two-Phase Flow*, New York, USA: Springer, 2003, pp. 281-323.

[112] E. A. Hammer, G. A. Johansen, T. Dyakowski, E. P. L. Roberts, J. C. Cullivans, R. A. Willians, Y. A. Hassan and C. S. Claiborn, "Advanced experimental techniques," *Multiphase Flow Handbook*, Crowe C.T. (eds.), Boca Raton: CRC Press, 2006.

[113] G. Oddie and J. R. A. Pearson, "Flow-rate measurement in two-phase flow," *Annual Review of Fluid Mechanics*, 36, pp. 149-172, 2004.

[114] J. Werther, "Measurement techniques in fluidized beds," *Powder Technology*, 102 pp. 15-36, 1999.

[115] Mishra R., Singh S.N., and Seshadri V, "Velocity measurement in solid-liquid flows using an impact probe," *Flow Measurement and Instrumentation*, vol. 8 pp. 157-165, 1997.

[116] A. K. Jana, T. K. Mandal, D. P. Chakrabarti, G. Das and P. K. Das, "An optical probe for liquid-liquid two-phase flows," *Meas. Sci. Technol.*, 18, pp. 1563-1575, 2007.

[117] R. C. Baker, "Flow Measurement Handbook: Industrial Designs, Operating Principles, Performance and Applications," Cambridge, UK: Cambridge University Press, 2000.

[118] L. Scheers, K. Busaidi, M. Parper, M. Halovorsen and T. Wideroe, "Multiphase Flow Metering Per Well – Can it be Justified?," *20th North Sea Flow Measurement Workshop*, St. Andrews, Scotland, 2002.

[119] I. Ismail, J. C. Gamio, S. F. A. Bukhari and W. Q. Yang, "Tomography for multi-phase flow measurement in the oil industry," *Flow Measurement and Instrumentation*, 16, no. 2, pp. 145-155, 2005.

[120] M. Zhang and M. Soleimani, "Imaging floating metals and dielectric objects using electrical capacitance tomography," *Measurement*, 74, pp. 143-149, 2015.

[121] J. Ye, H. Wang and W. Yang, "A sparsity reconstruction algorithm for electrical capacitance tomography based on modified Landweber Iteration", *Meas. Sci. Technol.*, 25, no. 11, 115402-16, 2014.

[122] P. Montesinos, J. F. P. J. Abascal, L. Cussó, J. J. Vaquero and M. Desco, "Application of the compressed sensing technique to self-gated cardiac cine sequences in small animals," *Magn. Reson. Med.,* 72, no. 2, pp. 369–380, 2013.

[123] J. F. Abascal, J. Chamorro-Servent, J. Aguirre, S. Arridge, T. Correia, J. Ripoll, J. J. Vaquero and M. Desco, "Fluorescence diffuse optical tomography using the split Bregman method," *Medical Physics*, 38, pp. 6275-6284, 2011.

[124] T. Goldstein and S. Osher, "The split Bregman method for l1-regularized problems," *SIAM J. Imaging Sci.*, 2, pp. 323-343, 2009.

[125] Z. Zushou, "The time to reach electrostatic equilibrium of a conductor," *Physics and Engineering*, 12, pp. 20-21, 2003.

[126] C. E Brennen, *Fundamentals of Multiphase Flow*. New York: Cambridge University Press, 2005.

[127] waterwellsolutions.com, "meniral scale problems and blubac," [Online]. Available: http://www.waterwellsolutions.com.au/mineral_scale_problems.html. [Accessed: 30-July- 2016].

[128] M. Wörner, *A compact introduction to the numerical modeling of multiphase flows*. Forschungszentrum Karlsruhe, Germany, 2003.

[129] A. J. Ghajar, "Non-boiling heat transfer in gas-liquid flow in pipes: a tutorial," *J. Brazilian Soc. Mech. Sci. Eng.*, 27, pp. 46-73, 2005.

[130] Y. Makogon, *Hydrates of Hydrocarbons*. Tulsa, Oklahoma: PennWell Books, 1997.

[131] E. Sloan, *Clathrate Hydrates of Natural Gases*. New York City: Marcel Dekker Inc., 1990.

[132] R. Thorn, G. A. Johansen and B. T. Hjertaker, "Three-phase flow measurement in the petroleum industry," *Meas. Sci. Technol.*, 24, 012003-19, 2012.

[133] V. S. V. Rajan, R. K. Ridley and K, G, Rafa, "Multiphase flow measurement techniques—a review," *J. Energy Resour. Technol.*, 115, no. 3, pp. 151–161, 1993.

[134] M. J. Pusppanathan, F. Yunus, N. M. N. Ayob, R. Abdul-Rahim, F. A. Phang, H. Abdul-Rahim, L. P. Ling, K. Abas, "A novel electrical capacitance sensor design for dual modality tomography multiphase measurement," *J. Teknologi (Sciences & Engineering)*, 64, no. 5, pp. 45–47, 2013.

[135] X. Jia, B. S. Hoyle, F. J. W. Podd, H. I. Schlaberg, M. Wang, R. M. West, R. A. Williams and T. A. York, "Design and application of a multi-modal process tomography system," *Meas. Sci. Technol.*, 12, pp. 1157–1165, 2001.

[136] W. Fang and E. Cumberbatch, "Matrix properties of data from electrical capacitance tomography," *J. Eng. Math.*, 51, pp. 127–146, 2005.

[137] J. S. Halow and P. Nicoletti, "Observations of fluidized bed coalescence using capacitance imaging," *Powder Technology*, 69, pp. 255–277, 1992.

[138] T. Zhao, M. Takei, K. Masaki, R. Ogiso, K. Nakao and A. Uchiura, "Sensor design and image accuracy for application of capacitance CT to the petroleum refinery process," *Flow Measurement and Instrumentation*, 18, pp. 268–276, 2007.

[139] W. Warsito, Q. Marashdeh and L. S. Fan, "Electrical capacitance volume tomography," *IEEE Sensors Journal*, 7, no. 4, pp. 525-535, 2007.

[140] D. N. Dyck, D. A. Lowther, and E. M. Freeman, "A method of computing the sensitivity of electromagnetic quantities to changes in materials and sources," *IEEE Trans. Magn.*, 30, pp. 3415-3418, 1994.

[141] T. E. Dyhoum, D. Lesnic, R. G. Aykroyd, "Solving the complete-electrode direct model of ERT using the boundary element method and the method of fundamental solutions," *Electronic Journal of Boundary Elements*, 12, no. 3, pp. 26-71, 2014.

[142] S. Zarinabadi and A. Samimi, "Problems of hydrate formation in oil and gas pipes deals," *Australian Journal of Basic and Applied Sciences*, 5, no. 12, pp. 741-745, 2011.

[143] ice-pigging.com, "Applications: oil & gas – pipe cleaning," [Online]. Available: http://www.ice-pigging.com/en/applications/3/oil-gas-pipe-cleaning. [Accessed: 29-July- 2016].

[144] J. Peters, "Erosion testing and CFD erosion modeling," NEL, UK, 2014.

[145] F. Mueller and Mark Null, "Impurities in the Gas Stream," Environmental Design, Inc., US, 2006.

[146] piping-engineering.com, "Multiphase Flow Meter- Well Fluid Analysis Meter," [Online]. Available: http://www.piping-engineering.com/multiphase-flow-meter-well-fluid-analysis-meter.html. [Accessed: 29- July- 2016].

SELECTED PUBLICATIONS

The following list of papers by the author that have already appeared or have been accepted for publication, are relevant to this thesis.

- E. Al Hosani, M. Zhang and M. Soleimani, "A limited region electrical capacitance tomography for detection of deposits in pipelines," *IEEE Sensors Journal*, 15, no. 11, pp. 6089-6099, 2015.

- E. Al Hosani and M. Soleimani, "Multi-phase permittivity imaging using absolute value electrical capacitance tomography data and a level set algorithm," *Proceedings of the Royal Society A: Mathematical, Physical and Engineering Sciences,* 374, no. 2070, 20150332-18, 2016.

- E. Al Hosani, M. Zhang, J. F. P. J. Abascal and M. Soleimani. "Imaging metallic samples using electrical capacitance tomography: forward modelling and reconstruction algorithms," *Meas. Sci. Technol.*, 27, no. 11, 115402-10, 2016.

- E Al Hosani and M Soleimani. "Absolute multiphase electrical capacitance tomography reconstruction using a level set algorithm." In: The Abu Dhabi International Petroleum Exhibition and Conference (ADIPEC), 7-10 November 2016, Abu Dhabi, UAE.

- M. Zhang, E. Al Hosani and M. Soleimani, "A limited region electrical capacitance tomography for detection of wax deposits and scales in pipelines." In: *5th International Workshop on Process Tomography (IWPT-5)*, 2014, 2014-09-16 - 2014-09-18, Jeju, South Korea.